MICROCOPY RESOLUTION TEST CHART

NATIONAL BUREAU OF STANDARDS-1963-A

AFOSR·TR· 87-0400

CLUSTERING AND ORDERING IN III-V ALLOYS

SEMICONDUCTOR RESEARCH LABORATORY

Washington University

Saint Louis, Missouri 63130

2 March 1987

AD-A179 767

DTIC
ELECTE
APR 2 4 1987
D

1 June 1982 to 31 December 1986

FINAL SCIENTIFIC REPORT NO. WU/SRL-59583A-12

Air Force Office of Scientific Research

Building 410

Bolling Air Force Base, DC20332

Grant No. AFOSR-82-0231

The United States Government is authorized to reproduce and distribute this report

for Governmental purposes.

87   4

Unclassified

SECURITY CLASSIFICATION OF THIS PAGE *(When Data Entered)*

REPORT DOCUMENTATION PAGE	READ INSTRUCTIONS BEFORE COMPLETING FORM
1. REPORT NUMBER AFOSR-TR- 87-0400 2. GOVT ACCESSION NO. *AD-AM 767*	3. RECIPIENT'S CATALOG NUMBER
4. TITLE *(and Subtitle)* Clustering and Ordering in III-V Alloys	5. TYPE OF REPORT & PERIOD COVERED Final 1 June 82-31 Dec. 1986
	6. PERFORMING ORG. REPORT NUMBER WU/SRL 59583A-12
7. AUTHOR(s) C.M. Wolfe, M.W. Muller, P.A. Fedders, G.A. Davis, S. Julie Hsieh, K.A. Salzman, Elizabeth A. Patten, P. Roblin	8. CONTRACT OR GRANT NUMBER(s) AFOSR-82-0231
9. PERFORMING ORGANIZATION NAME AND ADDRESS Washington University Box 1127 St. Louis, MO 63130	10. PROGRAM ELEMENT, PROJECT, TASK AREA & WORK UNIT NUMBERS 61103F 2306/B1
11. CONTROLLING OFFICE NAME AND ADDRESS Air Force Office of Scientific Research Building 410 Bolling AFB, DC 20332 NE	12. REPORT DATE 2 March 1987
	13. NUMBER OF PAGES 58
14. MONITORING AGENCY NAME & ADDRESS*(if different from Controlling Office)* Same as 11)	15. SECURITY CLASS. *(of this report)* Unclassified
	15a. DECLASSIFICATION/DOWNGRADING SCHEDULE

16. DISTRIBUTION STATEMENT *(of this Report)*

The United States Government is authorized to reproduce and distribute this report for Governmental purposes.

17. DISTRIBUTION STATEMENT *(of the abstract entered in Block 20, if different from Report)*

18. SUPPLEMENTARY NOTES

19. KEY WORDS *(Continue on reverse side if necessary and identify by block number)*

ZnSnP$_2$, In$_x$Ga$_{1-x}$P, Al$_x$Ga$_{1-x}$As, GaAs, heterojunctions, interfacial energy gaps, alloy formation, long range ordering, primitive layered structure, aluminum gallium arsenides, zinc compounds, tin compounds, phosphorus compounds.

20. ABSTRACT *(Continue on reverse side if necessary and identify by block number)*

ZnSnP$_2$ is a potentially useful semiconductor which can have either the sphalerite structure or the chalcopyrite structure with no tetragonal distortion (c=2a). We have grown ZnSnP$_2$ on various orientations of GaAs by liquid phase epitaxy and found that the best growth occurs on {110} surfaces. Double-crystal x-ray diffraction measurements indicate that these {110} layers have a lattice constant of 5.6507Å, while {111}As layers grown under

DD $_{1\ JAN\ 73}^{FORM}$ 1473   EDITION OF 1 NOV 65 IS OBSOLETE

Unclassified

SECURITY CLASSIFICATION OF THIS PAGE *(When Data Entered)*

20. Abstract (Continued)

identical conditions have a lattice constant of 5.6532Å, which
matches GaAs to within $\pm 2 \times 10^{-4}$ Å. Back reflection Laue patterns
show that the {110} layers are chalcopyrite, while the {111}As
layers are sphalerite. The Laue patterns also indicate that the
{110} epitaxy is mixed with the c-axis out of the growth plane.
A possible explanation for these results is that the {110}GaAs
surfaces in liquid phase epitaxy reconstruct into chalcopyrite-like
chains in the [001] direction, while the {111}As surfaces do not.
This would promote the formation of chalcopyrite $ZnSnP_2$ with anti-
phase boundaries on {110} surfaces.

   Using back reflection Laue measurements we have examined the
substrate orientation dependence of antiphase domain boundaries
for $ZnSnP_2 (c=2a)$ grown on GaAs by liquid phase epitaxy. These
results together with those of other workers indicate that {211}
substrates are best for the growth of chalcopyrite layers with c=2a,
while {100} substrates are best for those chalcopyrites with c<2a.
The suppression of antiphase domain boundaries can be related to
improved electrical properties for the chalcopyrite layers. In
general, crystal orientations with large c-axis components parallel
to the growth plane tend to be suppressed. This suggests that
differences in lateral growth rate from nuclei with different
orientations, rather than site preference, is a dominant factor in
the suppression of antiphase domain boundaries.

   Misordering defects which occur in the growth of chalcopyrite/
sphalerite systems have been investigated through the LPE growth
of $ZnSnP_2$ on GaAs. X-ray diffraction measurements reveal the
presence of misordering defects associated with multiple tetragonal
orientations in the epitaxy. Growth on {211} oriented substrates
reveals the lowest concentrations of orientation-related defects
while growth on vicinal {110} oriented substrates indicates the
strongest cation site differentiation required to produce long-range
ordering. The use of critically misoriented {110} substrates is
proposed for the growth of highly ordered chalcopyrite layers on
sphalerite substrates.

   The mixing enthalpy of ternary tetrahedral semiconductor
alloys is fairly well described by regular solution theory, with
a thermodynamic interaction parameter that is sensitive to the
lattice spacing of the binary constituents. We derive an estimate
of the interaction parameter from a model which ascribes the mixing
enthalpy to bond distortions associated with the alloy formation,
and relates these to the macroscopic elastic properties of the crystal.
Numerical estimates are given for the 18 alloys with cations Al,
Ga, In and anions P, As, Sb and are compared with experimental
values and alternative models. To within a single adjustable
parameter, the predictions agree with experiment and are consistent
with those of the delta lattice parameter (DLP) model. A further
calculation of the elastic energy associated with composition
fluctuations (clustering) in these alloys indicates that this energy
is sufficient to suppress clustering above the critical mixing
temperature.

20. Abstract (Continued)

Spatial composition fluctuations in semiconductor alloys, $A_xB_{1-x}C$ involve elastic energy when the lattice parameters of AC and BC differ. Therefore, the fluctuations are expected to be reduced below those exhibited by a purely random distribution of the constituent ions. We estimate the extent of the reduction, and relate it to recent observations of Raman linewidths and line shapes in $Ga_xIn_{1-x}As$ and $Ga_xAl_{1-x}As$.

Below band-gap photovoltaic response with a half-power point at 1.31eV is observed in p-type $In_{1-x}Ga_xP$ on n-type GaAs hetero-junctions with {111} interfaces. This response is apparently due to photon-assisted tunneling of carriers across the interfacial energy gap, which is smaller than the energy gaps of the constituent materials. The same mechanism can be employed in other hetero-junctions with appropriate energy-band lineups to obtain longer wavelength infrared response.

Below bandgap emission and absorption are observed in p-$ZnSnP_2$ on n-GaAs heterojunctions. The band lineup of this heterostructure system suggests that the below bandgap transition is between the valence bands of GaAs and the conduction band of $ZnSnP_2$ at the interface. The predicted value for the interfacial gap of $E_I=1.27eV$ compares with an experimental value of 1.31eV

Advances in technology have made possible the fabrication of rapidly varying heterostructures which hold the promise of important applications. We develop a set of approximate treatments of electron states in a variety of layered heterostructures. The approximations are all based on the concept of one-band generalized Wannier functions. Following a discussion of the validity of this representation, we apply it to an evaluation of the bound states in a narrow quantum well in GaAs, which clearly demonstrates the mixing of main and satellite valley states as well as the contribution of evanescent states, and of the states of a superlattice in a model structure of up to 20 quantum wells. As a final example we discuss the appli-cation of generalized Wannier functions to the matching of electronic states at a heterojunction between two model band structures with different effective masses, and compare the formalism with alterna-tive approaches to this problem.

Recent III-V alloy formation models indicate that negative charge transfer energy can overcome positive bond distortion energy to stabilize long-range order or compound formation. Although a report of a layered ordering in $Al_xGa_{1-x}As$ tends to confirm this result, we have as yet obtained no convincing evidence for such ordering in $In_xGa_{1-x}P$. Compound formation in these alloys may be critically dependent on growth temperature and kinetic factors.

TABLE OF CONTENTS

1. INTRODUCTION

Although there is substantial interest in III-V semiconductor alloys for electronic and optoelectronic devices, relatively little is known about the distribution of atoms in these materials or the effects of non-random distributions on device performance. In many of these alloys, however, non-random distributions of atoms are expected to be important from thermodynamic considerations. This is particularly true at the low temperatures commonly used for epitaxial growth. The available evidence suggests that short-range clustering of like atoms or short-range ordering of unlike atoms can produce device problems such as excess noise and leakage current, premature voltage breakdown, and lower carrier mobilities. Long-range ordering of unlike atoms, however, could potentially yield III-V ternary compounds with properties superior to their parent alloys. In epitaxial growth, substrate effects such as lattice match and non-equivalent sublattice sites are expected to have a strong influence on these phenomena. Also, two of the important III-V alloys, $Ga_xIn_{1-x}P$ and $Ga_xIn_{1-x}As$, can be epitaxially grown matched to GaAs and InP, respectively, at compositions near the point of greatest ordering probability. The objective of this work is to investigate various aspects of clustering and ordering in III-V alloys, including the interfacial properties of the materials.

2. Liquid Phase Epitaxial Growth of ZnSnP₂ on GaAs

G. A. Davis and C. M. Wolfe*

Semiconductor Research Laboratory, Washington University, St. Louis, Missouri 63130

ABSTRACT

ZnSnP₂ is a potentially useful semiconductor which can have either the sphalerite structure or the chalcopyrite structure with no tetragonal distortion (c = 2a). We have grown ZnSnP₂ on various orientations of GaAs by liquid phase epitaxy and found that the best growth occurs on {110} surfaces. Double-crystal x-ray diffraction measurements indicate that these {110} layers have a lattice constant of 5.6507Å, while {111} As layers grown under identical conditions have a lattice constant of 5.6532Å, which matches GaAs to within ±2 × 10⁻⁴Å. Back reflection Laue patterns show that the {110} layers are chalcopyrite, while the {111} As layers are sphalerite. The Laue patterns also indicate that the {110} epitaxy is mixed with the c-axis out of the growth plane. A possible explanation for these results is that the {110} GaAs surfaces in liquid phase epitaxy reconstruct into chalcopyrite-like chains in the [001] direction, while the {111} As surfaces do not. This would promote the formation of chalcopyrite ZnSnP₂ with antiphase boundaries on {110} surfaces.

ZnSnP₂ is an interesting semiconductor for the study of chalcopyrite growth on sphalerite GaAs. The primary reason for studying this system is the similarity between the structures of GaAs and ZnSnP₂ (1). The a to a mismatch of ZnSnP₂ on GaAs is small which allows for single crystal liquid phase growth. In addition, ZnSnP₂ exhibits no tetragonal distortion so the c to 2a mismatch is the same as the a to a mismatch. Thus, ZnSnP₂ grown on any substrate orientation will not incorporate any c to 2a mismatch. Since most chalcopyrites exhibit some tetragonal distortion, epitaxial growth is generally restricted to {100} oriented substrates to avoid c to 2a mismatch.

ZnSnP₂ is also of interest because solution-grown platelets exhibit both chalcopyrite and disordered sphalerite phases apparently having the same lattice constant (1, 2). The sphalerite phase dominates in platelets grown using large cooling rates ($\simeq$ 50°C/hr), while the chalcopyrite phase dominates for smaller cooling rates ($\simeq$ 5°C/hr). The existence of these two phases allows us to evaluate the growth conditions leading to chalcopyrite growth and provides insight for other chalcopyrite-on-sphalerite systems.

Growth Procedure

Liquid phase epitaxial growth of ZnSnP₂ on GaAs was performed in the open tube system shown schematically in Fig. 1. The starting materials used in this system were 99.999+% pure Zn and Sn and SnP₃ which was synthesized from 99.999+% pure Sn and red P₄ in a sealed tube process (3). The graphite boat shown in Fig. 1 was designed for growth of materials for which there is little phase diagram information. During homogenization of the growth melt, excess SnP₃ floats to the top and maintains a saturated solution as phosphorus evaporates into the gas stream. During growth, the homogeneous solution contained in the slider is positioned over the substrate and the temperature of the furnace is reduced linearly. Since little phosphorus loss to the gas stream was observed for the growth conditions used, the composition of the melt was adjusted so that there was little or no excess SnP₃ in the melt after saturation. The equivalent melt compositions used for various growth temperatures are shown in the partial phase diagram of Fig. 2. In all growth runs, the amounts of Zn, Sn, and SnP₃ were adjusted to give an equivalent ZnSnP₂ concentration in Sn with no excess Zn or P.

The cooling rates used in these growth experiments ranged from 1° to 5°C/hr. Cooling rates greater than 5°C/hr were not investigated due to the tendency of ZnSnP₂ to grow in the sphalerite phase at these rates. A homogenization period of 2 hr and growth periods of 6-18 hr were used. The homogenization or initial

growth temperature ranged from 530° to 640°C. A hydrogen flow rate of 30 ml/min was maintained in the furnace tube during homogenization and growth for all experiments.

The GaAs substrates were carefully prepared by lapping and chemical-mechanical polishing both the front and back surfaces. After scribing and breaking the substrates to the proper dimensions for the boat (0.25 × 0.25 in.), they were cleaned in boiling trichloroethylene, acetone, and methyl alcohol. A 5:1:1 or 10:1:1 H₂SO₄:H₂O₂:H₂O chemical etch was used
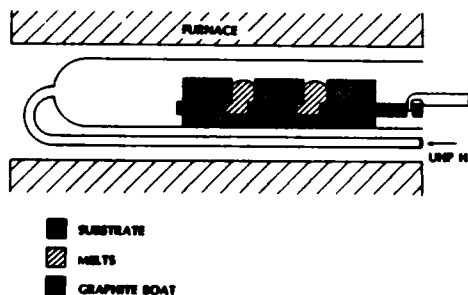

Fig. 1. Schematic illustration of the LPE boat used to grow ZnSnP₂ on GaAs.
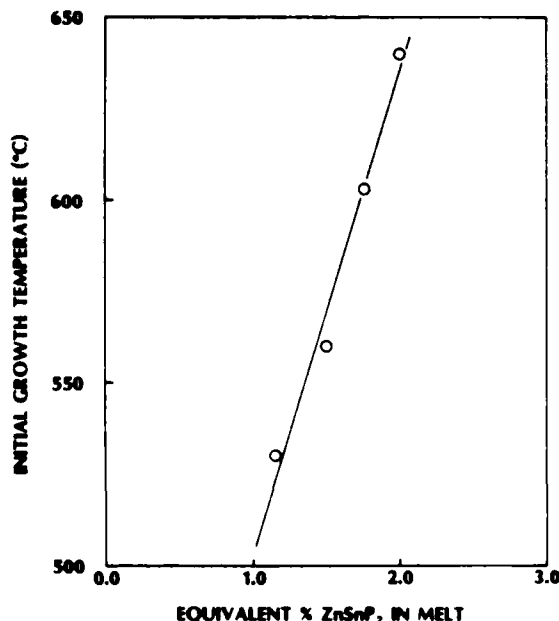

Fig. 2. Initial growth temperature as a function of ZnSnP₂ concentration for saturated or slightly supersaturated solutions.

prior to loading each substrate into the boat. This etch removed at least 10 μm of material from the growth surface. The 10:1:1 etch used in later experiments caused less rounding of the surface and produced more uniform growth.

Layer Morphology

Initial growth experiments were performed on {100}, {110}, {111}, and {211} oriented Cr-doped substrates to determine the optimum orientation for growth. Typical layers grown on some of these orientations are shown in Fig. 3, 4, and 5.

{100}, {211} Ga, {211} As, and {111} Ga oriented substrates produced growth which was quite rough and unsuitable for electrical measurements. Growth on {111} As oriented substrates had rough interfaces but uniform surfaces with very good morphologies. This is consistent with observations of predominant {111} facets in solution grown platelets (1) and with experiments in which we have observed low growth rates in the <111> directions. Layers grown on {110} oriented substrates revealed much smoother interfaces but had surfaces with more structure and tended to be of nonuniform thickness. Numerous growth experiments were performed on {111} As oriented substrates to reduce the amount of interfacial roughness, but little improvement was noted. In later experiments performed using {110} oriented substrates, we concentrated on improving the uniformity of the layers and eliminating large growth structures. By changing the final etch and adjusting the growth parameters, substantial improvements in the {110} oriented growth were noted.

For {111} As oriented substrates, the best growth was obtained using an initial growth temperature of 560°C with a cooling rate of 1°C/hr The melts for these growth runs had an equivalent ZnSnP₂ concentration of 1.4-1.5% with one gram of Sn used per run. For initial growth temperatures below 530°C, no layers could be grown, while for initial temperatures above 600°C, the morphologies and electrical characteristics of the layers degraded. The grown layers were generally 3-15 μm thick except for those grown at high temperatures, which were up to 30 μm thick.
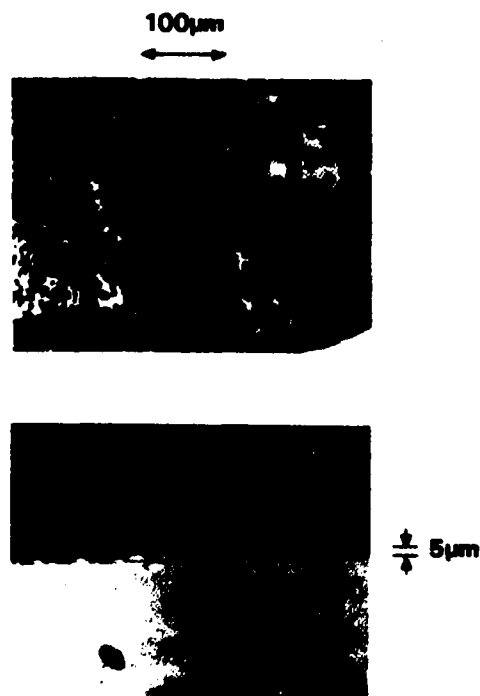
Fig. 3. (a, top) Surface and (b, bottom) cross-sectional views of typical ZnSnP₂ growth on {100} oriented GaAs.
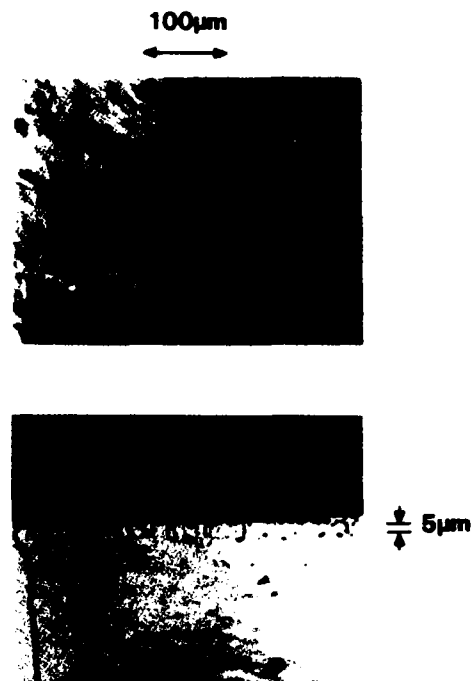
Fig. 4. (a, top) Surface and (b, bottom) cross-sectional views of typical ZnSnP₂ layers grown on {111} As oriented GaAs. The structure of the surface view was enhanced using a Nomarski interferometer.
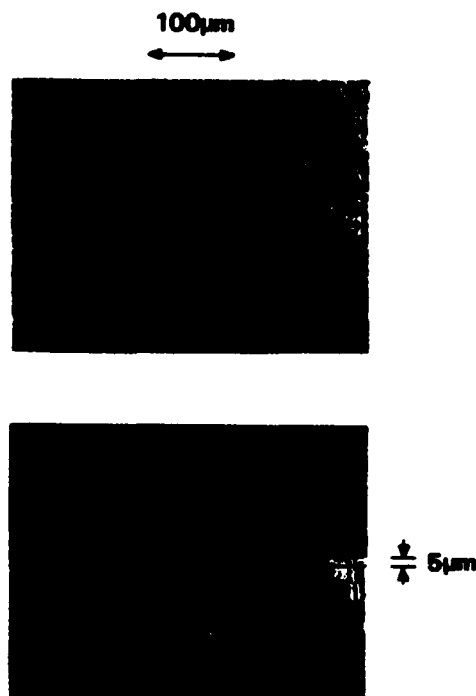
Fig. 5. (a, top) Surface and (b, bottom) cross-sectional views of a typical ZnSnP₂ layer grown on {110} oriented GaAs.

The conditions producing good growth on {110} oriented substrates are more restrictive than those for {111} As growth. For {110} oriented growth, the optimum initial growth temperature was 570°C. The layer quality degraded rapidly for initial growth temperatures less than 560° or greater than 580°C. The melt composition used was 1.4-1.5% ZnSnP₂ with one gram of Sn used per run. Good growth was obtained with cooling rates between 2.5°-5°C/hr. No layers were grown on {110} oriented substrates for cooling

-4-

1410   *J. Electrochem. Soc.:* SOLID-STATE SCIENCE AND TECHNOLOGY   *June 1983*

rates less than 2.5°C/hr. All layers grown on {110} oriented substrates were less than 5 μm thick.

X-Ray Diffraction Measurements

X-ray diffraction measurements were made on the layers grown on {111} As and {110} oriented GaAs using a double crystal diffractometer aligned for the GaAs 333 reflection for Cu Kα radiation. Peak widths at half-peak intensity (FWHM) of 8.7 and 10.6 sec of arc were reproducibly obtained with the {111} and {110} GaAs used for growth substrates, respectively.[1] Some results of these measurements are shown in Fig. 6, 7, and 8.

Most of the {111} As samples revealed a single broadened GaAs peak with some slight background reflection as seen in Fig. 6. This suggests that this epitaxial material lattice matches GaAs to within 2×10^{-4}A (4×10^{-3}%) based on an 8-7 sec resolution. The FWHM peak widths for these layers were 45 to 85 sec. The low intensity background reflection may be due to the rough interfaces of these layers or interfacial strain.

Some of the thinner {111} As layers revealed a secondary peak at about one tenth the intensity of the main peak separated by 4.9 min of arc as seen in Fig. 7. These layers were 3 μm thick and were grown using a 5°C/hr cooling rate. Typically, these {111} As layers had smoother interfaces than those grown with smaller cooling rates, and no broad background intensity was observed. The lattice constant associated with the secondary peak in Fig. 7 is 5.645A which is 0.1% smaller than the 5.651A lattice constant observed by other workers (1, 2) on solution-grown platelets. The FWHM widths of the main peaks were 20-30 sec, and those of the secondary peaks were around 2 min. The observation of secondary peaks from thin layers and broad background reflection from thick layers suggests that there is interfacial strain in these structures.[2]

A typical scan of the 333 reflection from a layer grown on {110} oriented GaAs is shown in Fig. 8. This scan shows two approximately equal intensity peaks, which are separated by 90 sec. All layers grown

[1] The 333 reflection from a (111) oriented Ge analyzer was used in all rocking curves presented. This causes some peak spreading due to the different lattice constants of the analyzer and sample crystals. The theoretical peak width for the 333 reflection using either Ge or GaAs (111) oriented analyzer and sample crystals is 4.7 sec of arc. [M. A. G. Halliwell, J. B. Childs, and S. O'Hara, in "Gallium Arsenide and Related Compound," C. Hilsum, Editor, p. 98, The Institute of Physics, London (1973).]

[2] The existence of strain in these structures is evidenced by the broadening of the reflection peak. While strain in a layer can obscure the rocking curve analysis, the presence of primarily one peak indicates a lattice match. [W. J. Bartels and H. Veenvliet, in "Gallium Arsenide and Related Compounds." C. M. Wolfe, Editor, p. 229, The Institute of Physics, London (1979).]
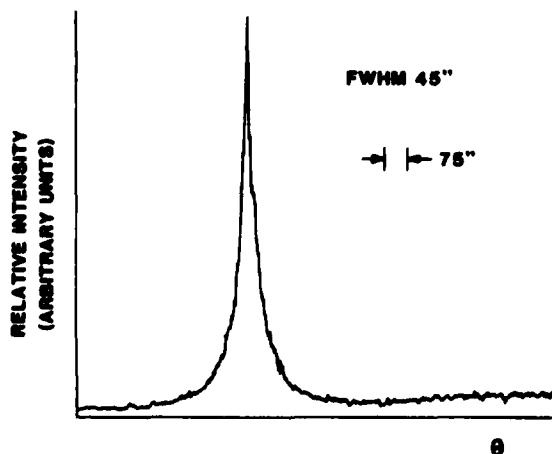
Fig. 6. A typical x-ray diffraction scan of the 333 reflection from ZnSnP₂ grown on {111} As oriented GaAs.
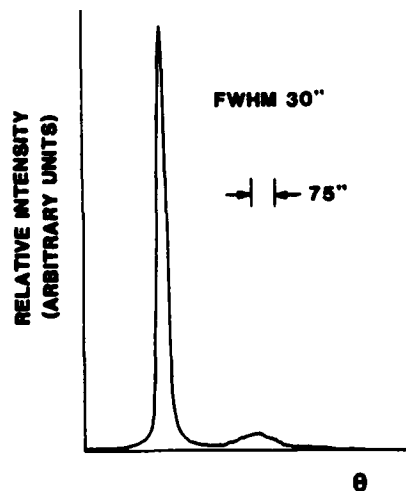
Fig. 7. A diffraction scan of the 333 reflection from ZnSnP₂ grown on {111} As oriented GaAs grown with a 5°C/hr cooling rate.
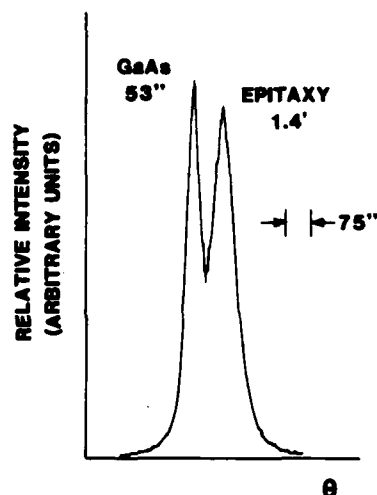
Fig. 8. A typical x-ray diffraction scan from ZnSnP₂ grown on {110} oriented GaAs.

on {110} oriented material revealed these two peaks with the epitaxial layer peak intensity scaling with the layer thickness. The lattice constant of the layers calculated from these data is 5.6507A $\pm 3 \times 10^{-4}$A based on a 5.6532A GaAs lattice constant (4) which is in excellent agreement with the platelet data.

Back Reflection Laue Patterns

Because of the differences between the diffraction measurements for {111} As and {110} oriented growth, back reflection Laue photographs of the layers were made to determine any differences in crystal structure. Typical photographs are shown in Fig. 9. In all photographs, the samples were aligned so that a <110> axis of the substrate was directed along the incident x-ray beam. A copper source was used for these exposures and the sample-to-film distance was approximately 4 cm.

Figure 9a is a photograph of an 8 μm ZnSnP₂ layer grown on {111} As oriented GaAs whose diffraction scan was similar to that shown in Fig. 6. Exposures of this layer contain no additional diffraction spots compared with exposures of GaAs. Hence, this ZnSnP₂ layer has grown with the sphalerite structure. A gnomonic projection of the sphalerite reflections observed in these photographs is shown in Fig. 10a. Figure 9b is a photograph of a 4 μm layer grown on
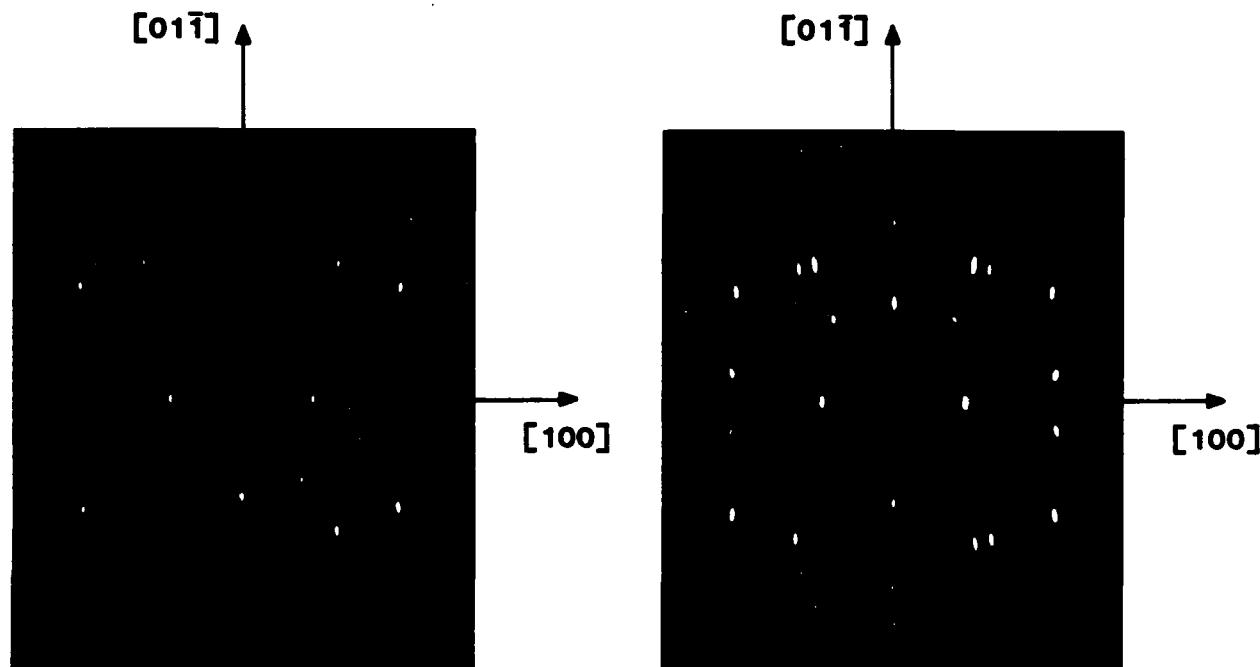
Fig. 9. Back reflection Laue photographs of ZnSnP₂ layers grown on (a, left) {111} As oriented GaAs and (b, right) {110} oriented GaAs.

{110} oriented GaAs. The diffraction scan for this ZnSnP₂ layer is shown in Fig. 8. The Laue photograph in Fig. 9b shows a number of diffraction spots which are not present in the GaAs exposure. These additional spots are due to a higher degree of ordering in the ZnSnP₂ layer and cannot be attributed to the slightly different lattice constant of the layer. The intense additional spots which are evident in this exposure are from high index chalcopyrite 167 and 259 planes, which are listed in catalogs of powder diffraction patterns. These diffraction spots are evident despite their small structure factor because they meet the first-order Bragg condition for a wavelength of 1.542A, i.e., at the high intensity Kα peak of the Cu x-ray spectrum. These observations indicate that the {110} oriented growth has the chalcopyrite structure. A gnomonic projection of the chalcopyrite reflections is shown in Fig. 10b.

Epitaxial Orientation

The manner in which the chalcopyrite structure of the ZnSnP₂ layer is oriented with respect to the sphalerite structure of the GaAs substrate is also of interest. Due to the tetragonal structure of the epitaxial layer, there are three ways in which it may orient relative to the substrate sphalerite structure. This is illustrated schematically in Fig. 11 where three chalcopyrite conventional (cubic) unit cells are shown at three different orientations on a {110} sphalerite surface. In this figure, the subscript "c" refers to chalcopyrite axes. The different relative orientations are with the [001]c axis oriented along the [100], [010], or [001] axes of the sphalerite structure. Other researchers (5) involved with chalcopyrite/sphalerite epitaxy have observed both unique epitaxy where only one relative orientation is present and

Fig. 10. Gnomonic projections of the (a) sphalerite reflections of Fig. 9(a) and (b) chalcopyrite reflections of Fig. 9(b). Larger circles represent larger reflected intensity.

-6-

1412   *J. Electrochem. Soc.*: SOLID-STATE SCIENCE AND TECHNOLOGY   *June 1983*
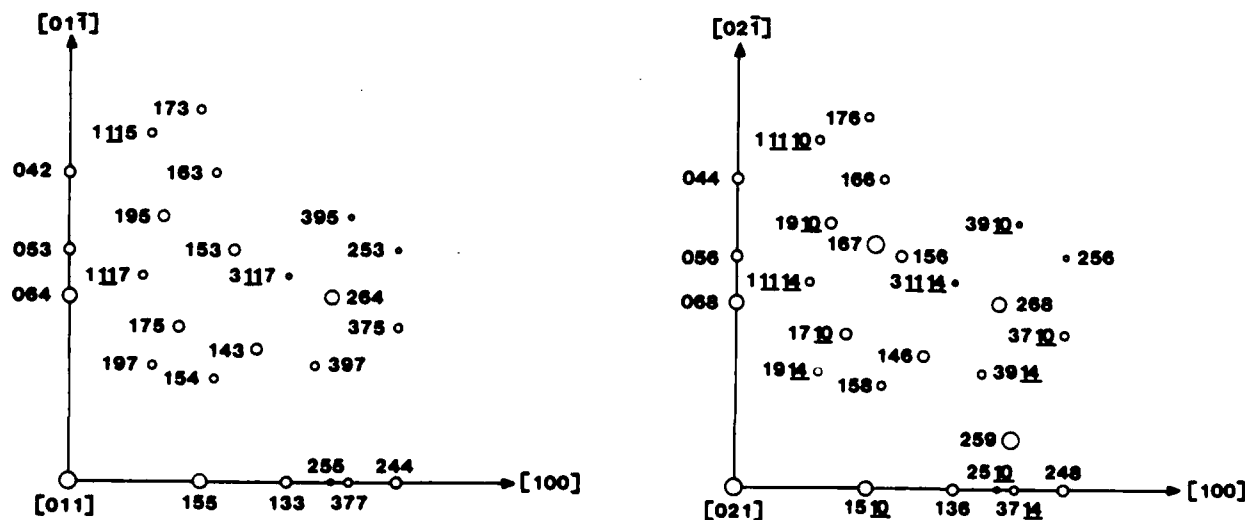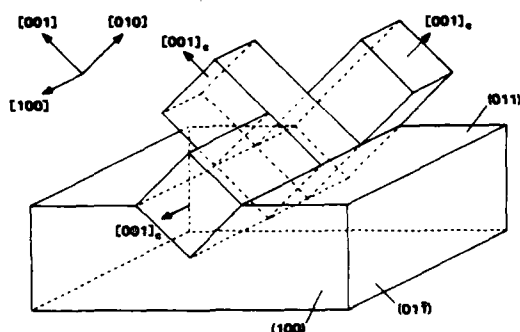

Fig. 11. Schematic illustration of the relative orientation of the chalcopyrite conventional unit cells on a {110} sphalerite surface.

mixed epitaxy where more than one relative orientation is present.

Because $ZnSnP_2$ exhibits no tetragonal distortion, the uniqueness of the epitaxy cannot be determined from the diffraction scans of the 333/336c reflections. The chalcopyrite Laue spots, however, indicate that the epitaxy is mixed with the [001]c axis out of the growth surface.

Hall and Resistivity Measurements

Van Der Pauw resistivity and Hall measurements were made on the {111} As and {110} layers. All layers measured were found to be p-type. Layers grown on {111} As oriented substrates have carrier concentrations of 1×10^{18}-1×10^{21} cm^{-3} and calculated mobilities of 10-70 cm^2/Vsec. The resistivity of these layers ranged from 2.5×10^{-4}-1.2×10^{-1} Ωcm. Layers grown on {110} oriented substrates have carrier concentrations of 3×10^{19}-5×10^{19} cm^{-3} with calculated mobilities of 15-40 cm^2/Vsec and resistivities of 4×10^{-3}-2×10^{-2} Ωcm. No strong correlations were observed between these data and the growth conditions of the layers.

Surface Effects

From the results discussed above, it is evident that the growth surface plays an important role in determining the crystal structure of $ZnSnP_2$ grown on GaAs substrates. A similar observation was made by Kroemer *et al.* (6) for GaAs grown on Ge substrates. For GaAs on Ge, the {110} orientation was found to be the optimum growth orientation for high quality GaAs layers. Kroemer *et al.* postulated that the {110} Ge surface is superior because of the formation of well structured As-like and Ga-like sites. They based this conclusion on Harrison's (7) model for the reconstruction of this nonpolar surface. Such a reconstructed Ge surface should suppress antiphase boundary formation in GaAs producing layers with superior properties.

An analogous effect may be responsible for the growth of the two $ZnSnP_2$ phases on different GaAs substrate orientations: The reconstructed {110} GaAs surfaces in liquid phase epitaxy may contain Ga sites which appear to be Zn-like or Sn-like, while the {111} As surfaces may not. In this manner, the {110} surfaces would promote chalcopyrite growth with antiphase boundaries. For instance, the {110} surfaces might reconstruct into linear chalcopyrite-like surface chains in the [001] direction which are out of phase with neighboring chains. This would promote

the chalcopyrite phase with antiphase boundaries, and could explain the somewhat degraded electrical properties of our chalcopyrite layers in comparison to the sphalerite layers. If this is the case then growing on misoriented substrates could increase the lateral growth velocity and inhibit antiphase boundary formation. Another possibility is that misoriented substrates may produce a surface which reconstructs to give longer range chalcopyrite-like regions which are free of antiphase boundaries.

Although Harrison (7) considered the reconstruction of polar surfaces such as GaAs, he did not separate the metallic or nonmetallic sublattices into further sublattices of dissimilar sites since such considerations were secondary to the scope of his work. Considering the experimental results discussed in this paper, a study of such reconstruction may be warranted.

Conclusions

We have developed a procedure for growing $ZnSnP_2$ layers on GaAs in an open tube liquid phase epitaxial system. After a preliminary study of $ZnSnP_2$ growth on various GaAs substrate orientations, the growth procedures were refined for growth on {111} As and {110} oriented substrates. $ZnSnP_2$ grown on {111} As oriented substrates with cooling rates smaller than 5°C/hr was sphalerite and lattice matched GaAs. $ZnSnP_2$ grown on {110} oriented substrates with cooling rates between 2.5°-5°C/hr was mixed orientation chalcopyrite with a lattice constant of 5.6507A, in agreement with data on solution-grown platelets. All layers grown were p-type with carrier concentrations of 1×10^{18}-1×10^{21} cm^{-3} and mobilities of 10-70 cm^2/Vsec. Antiphase boundaries, which are present in such mixed orientation epitaxy, may be responsible for the inferior electrical characteristics of the chalcopyrite layers.

REFERENCES

1. J. L. Shay and J. H. Wernick, "Ternary Chalcopyrite Semiconductors: Growth, Electronic Properties, and Applications," Pergamon Press, Elmsford, NY (1975).
2. A. A. Vaipolin, N. A. Goryunova, L. I. Keschinskii, G. V. Loshakova, and E. O. Osmanov, *Phys. Status Solidi*, **29**, 435 (1968).
3. G. A. Davis, Master's Thesis, Washington University, St. Louis, MO (1981).
4. E. D. Pierron, D. L. Parker, and J. B. McNeely, *Acta Crystallogr.*, **21**, 290 (1966).
5. J. E. Andrews, H. H. Stadelmaier, M. A. Littlejohn, and J. Comas, *This Journal*, **128**, 1563 (1981).
6. H. Kroemer, K. J. Polasko, and S. C. Wright, *Appl. Phys. Lett.*, **36**, 763 (1980).
7. W. A. Harrison, *Surf. Sci.*, **55**, 1 (1976).

3. ANTIPHASE DOMAIN BOUNDARY SUPPRESSION IN CHALCOPYRITE-ON-SPHALERITE EPITAXY

G.A. DAVIS *, M.W. MULLER and C.M. WOLFE

Semiconductor Research Laboratory, Washington University, St. Louis, Missouri 63130, USA

Using back reflection Laue measurements we have examined the substrate orientation dependence of antiphase domain boundaries for $ZnSnP_2$ ($c = 2a$) grown on GaAs by liquid phase epitaxy. These results together with those of other workers indicate that {211} substrates are best for the growth of chalcopyrite layers with $c = 2a$, while {100} substrates are best for those chalcopyrites with $c < 2a$. The suppression of antiphase domain boundaries can be related to improved electrical properties for the chalcopyrite layers. In general, crystal orientations with large c-axis components parallel to the growth plane tend to be suppressed. This suggests that differences in lateral growth rate from nuclei with different orientations, rather than site preference, is a dominant factor in the suppression of antiphase domain boundaries.

1. Introduction

The II–IV–V_2 chalcopyrites have a number of interesting properties [1] with potential device applications. In particular, the development of techniques by which these materials can be epitaxially grown on III–V sphalerite or IV diamond substrates can result in heterojunctions which combine nonlinear optical properties with light emission, detection, or signal processing capabilities. One of the problems in achieving these heterojunctions, however, is that the chalcopyrite crystal structure is tetragonal, whereas the sphalerite and diamond structures are cubic.

The chalcopyrite structure (space group I$\bar{4}$2d) is tetragonal because the II and IV cation sites are non-equivalent, while the corresponding sites in the cubic sphalerite and diamond structures are equivalent. Because of the lower symmetry of the tetragonal structure, many of the chalcopyrites exhibit a shortened c-axis ($c/a < 2$ for the tetragonal superlattice) while others do not. Consequently, in chalcopyrite-on-sphalerite or chalcopyrite-on-diamond epitaxy, there is no unique

* Current address: Varian Associates, 611 Hansen Way, Palo Alto, California 94303, USA.

direction for the c-axis, and antiphase domain boundaries are produced between regions with different c-axis orientations. Through their strains and contribution to scattering these antiphase domain boundaries are expected to degrade the transport properties and stability of the material, and to present problems in device fabrication.

The problem of antiphase domain boundary formation has received some attention in the recent literature. Kroemer et al. [2] have examined the conditions under which it should be possible to achieve sphalerite-on-diamond epitaxy without antiphase domain boundary formation. Considering the results of Harrison et al. [3], they point out that there are good reasons to expect substrate orientation to be important in the suppression of antiphase domain boundaries. For example, the {110} diamond surfaces could coherently reconstruct in such a way as to produce cation-like and anion-like sites.

Wright et al. [4] found that antiphase domain boundaries are suppressed when sphalerite GaP is grown on a {211} surface of Si. They explain this result by demonstrating that the {211} diamond surface can consist of microscopic steps which exhibit cation-like and anion-like sites without reconstruction. These results are also directly appli-

cable to the reduction of antiphase domain boundaries associated with cation–anion site interchange in chalcopyrite-on-diamond epitaxy. They are not applicable, however, to the suppression of antiphase domain boundaries associated with cation–cation site interchange which produces regions with different c-axis orientations.

Andrews et al. [5] have examined antiphase domain formation for $ZnSiAs_2$ epitaxially grown on {100} and {111} surfaces of GaAs and Ge. In this work they were able to determine growth conditions under which the chalcopyrite c-axis grew uniquely normal to the {100} surfaces. Thus, antiphase domain boundaries were suppressed for this orientation. For nominal {111} substrates, however, their results indicated that, of the three possible c-axis orientations, the preferred orientation was the c-axis closest to the surface normal.

Since $ZnSiAs_2$ is one of the $II–IV–V_2$ chalcopyrites which exhibits a foreshortened c-axis, the question arises as to whether it is foreshortening or the tetragonal atomic arrangement which produces the unique c-axis orientation on {100} substrates. As Andrews et al. [5] point out, to answer this question it is necessary to investigate antiphase domain formation in a chalcopyrite material with $c/a = 2$ such as $ZnSnP_2$.

In the present paper we examine antiphase domains in $ZnSnP_2$ grown on {100}, {110}, misoriented {110}, {111}, and {211} surfaces of GaAs. This heterojunction system is well suited for such a study for the following reasons: (1) The GaAs substrate should suppress antiphase domain boundaries associated with cation–anion interchange, leaving only those associated with nonequivalent cations. (2) As indicated above, there is no foreshortening in $ZnSnP_2$ ($c = 2a$) so that different substrate orientations can be examined with relative ease. (3) The small lattice mismatch of 0.44% between $ZnSnP_2$ (5.6507 Å) and GaAs (5.6532 Å) [6] minimizes lattice strain and makes epitaxial growth easier.

2. Growth procedure

An open tube liquid phase epitaxial system was used for the growth of $ZnSnP_2$ on GaAs in this work. The details of the system have been previously discussed [6]. The growth solutions were composed of Zn, Sn and SnP_3 synthesized in a sealed tube process with a 1.20% equivalent $ZnSnP_2$ concentration in Sn. This provided slightly supersaturated solutions at the homogenization and initial growth temperature of $570.0 \pm 1.0°C$, and maintained melt saturation during a 2 h homogenization period. Growth was initiated by sliding the solution over the substrate and cooling the system linearly at 3.5 to 4.5°C/h for 5 to 16 h. These conditions produced optimum quality growth for all orientations examined.

The GaAs substrate surfaces were prepared as follows: Each as-received wafer was lapped and chemical-mechanically polished using a 1% Br–CH_3OH solution until both surfaces were uniform and free of gross damage. Such damage was usually evident after a 20 s etch in the Br–CH_3OH solution. After scribing and breaking each wafer into substrates of the proper dimensions for the LPE boat, the substrates were cleaned in boiling trichloroethylene, acetone and methyl alcohol. Each substrate was etched for 2 min in a 10:1:1 $H_2SO_4:H_2O_2:H_2O$ solution, 10 min after initial mixing, and rinsed thoroughly in deionized H_2O just prior to loading the furnace.

The misoriented {110} substrates were prepared individually after scribing and breaking the wafers into the proper sized pieces. Each {110} substrate was mounted on a 2° angle lapping block and lapped and polished as above. The substrate was then remounted face down on a 0° lapping block and the lapping and polishing procedure was repeated. The resultant substrates had parallel polished faces at an angle of $2.0 \pm 0.2°$ from the initial {110} surfaces. These substrates were subsequently cleaned and etched as indicated above.

The {110} substrates were misoriented in two orthogonal directions: towards a perpendicular ⟨110⟩ and towards a perpendicular ⟨001⟩ direction. The direction of misorientation was determined from the perpendicular cleavage planes of the wafers: those misoriented towards a perpendicular cleavage plane are misoriented towards a perpendicular ⟨110⟩ direction; those misoriented along a perpendicular cleavage plane are misori-

ented towards a perpendicular $\langle 001 \rangle$ direction. For brevity these surfaces will be denoted $\{110\}/\langle 110 \rangle$ and $\{110\}/\langle 001 \rangle$, respectively.

3. Layer morphology

Surface and cross-sectional views of a typical $ZnSnP_2$ layer grown on a $\{100\}$ GaAs substrate are shown in fig. 3 of ref. [6]. This layer and subsequent $\{100\}$ layers had smooth interfaces but rough surfaces containing pits which often extended to the substrate. Although we tried many times, we were not able to improve the $\{100\}$ morphology.

A typical $\{110\}$ layer is shown in fig. 5 of ref.

[6]. This $ZnSnP_2$ layer and other $\{110\}$ layers grown later had smooth interfaces, surfaces with some structure, and tended to be somewhat non-uniform in thickness.

Typical morphology for $\{111\}$ layers is shown in fig. 4 of ref. [6]. This layer and subsequent $\{111\}$ layers had very rough interfaces and smooth surfaces. Back reflection Laue photographs demonstrated that these layers were sphalerite [6]. However, we found, subsequently, from electron microprobe analysis that all of our $\{111\}$ layers were $(GaP)_{2x}(ZnSnP_2)_{1-x}$ alloys, with the Ga supplied by dissolution of the substrate. Although these are interesting results, they are beyond the scope of the present work.

Surface and cross-sectional views of typical
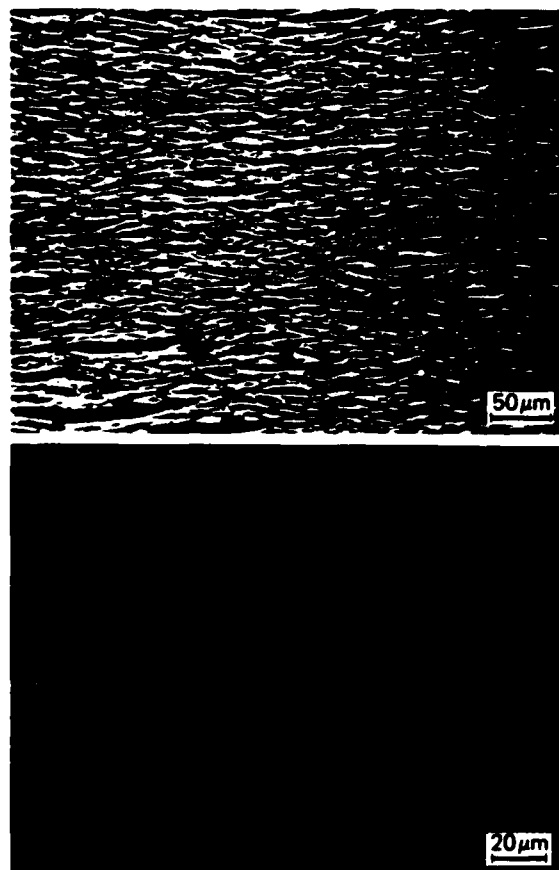
Fig. 1. Surface and cross-sectional views of $ZnSnP_2$ grown on GaAs misoriented 2° off the $\{110\}$ towards a perpendicular $\langle 100 \rangle$.
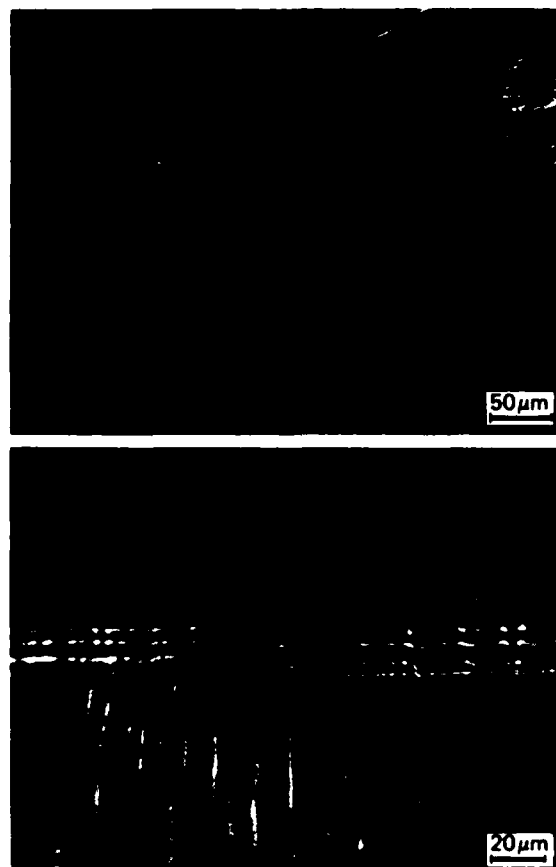
Fig. 2. Surface and cross-sectional views of $ZnSnP_2$ grown on GaAs misoriented 2° off the $\{110\}$ towards a perpendicular $\langle 110 \rangle$.

G.A. Davis et al. / Antiphase domain boundary suppression
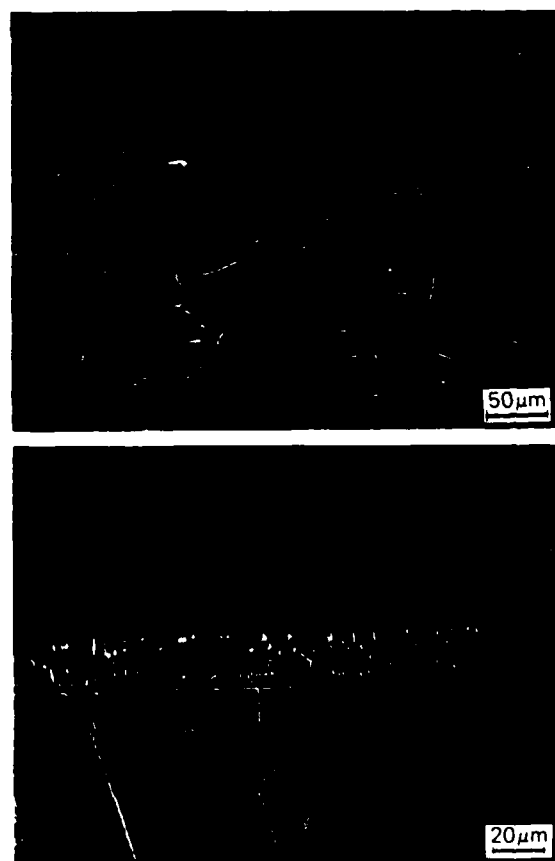
Fig. 3. Surface and cross-sectional views of ZnSnP₂ grown on {211}As GaAs.
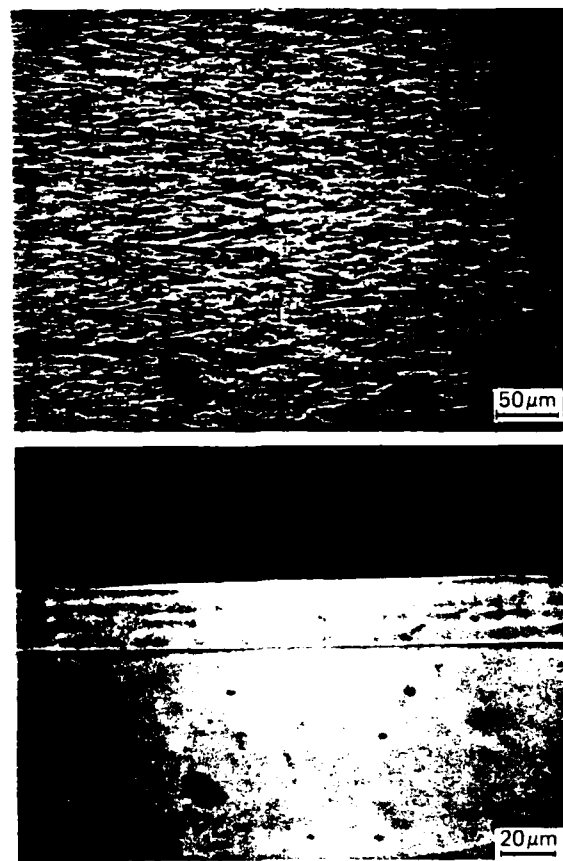
Fig. 4. Surface and cross-sectional views of ZnSnP₂ on {211}Ga GaAs.

misoriented $\{110\}/\langle001\rangle$ ZnSnP₂ are shown in fig. 1. These layers are 5 to 7 μm thick for 16 h growth times with smooth interfaces and moderately smooth surfaces exhibiting some structure. This morphology is quite similar to that achieved with $\{110\}$ growth except for somewhat more surface structure.

Growth on $\{110\}/\langle110\rangle$ surfaces showed marked improvement over growth on $\{110\}$ and $\{110\}/\langle001\rangle$ surfaces. A typical $\{110\}/\langle110\rangle$ ZnSnP₂ layer is shown in fig. 2. These layers are 20 to 25 μm thick for 16 h growth times with smooth interfaces and surfaces.

ZnSnP₂ layers grown on $\langle211\rangle$As and $\langle211\rangle$Ga oriented GaAs are shown in figs. 3 and 4, respectively. Growth on the $\{211\}$As orientation is 20 to 25 μm thick for a 16 h growth time with smooth interfaces and fairly smooth surfaces containing some structure. The $\{211\}$Ga growth is also 20 to 25 μm thick for a 16 h growth time with smooth interfaces and surfaces exhibiting minimal structure. It is interesting to note that the cross-sectional view of fig. 4 does not show the rippling observed in the other cross-sectional view suggesting this growth has improved crystallinity. While $\{211\}$Ga growth is the most sensitive to changes in the growth conditions, it can be reproducibly obtained.

4. Structural measurements

To examine the structure of the epitaxial $ZnSnP_2$ and determine the relative orientations of the tetragonal axis of the chalcopyrite layer with respect to the cubic axes of the sphalerite substrate, back reflection Laue photographs were taken. A determination of the tetragonal axis orientation relative to the cubic axes is fundamental to this work since the existence of only one relative orientation is a necessary (but not sufficient) condition for the elimination of antiphase boundaries. The technique used was adapted from our previous observations of allowed reflections from the chalcopyrite structure for {110} growth [6].

The experimental arrangement for the photographs is illustrated schematically in fig. 5. In all Laue photographs the $ZnSnP_2$–GaAs heterostructures were oriented so that the Cu X-rays were incident along one of the ⟨110⟩ directions of the sphalerite substrate. If the sample is oriented so that this corresponds to the [021] chalcopyrite direction, then four additional diffracted spots – the 259, 167, $\bar{2}$59, and $\bar{1}$67 diffractions – will be

Fig. 6. Laue photograph of $ZnSnP_2$ grown on nominal {110} GaAs with primary X-ray beam along surface normal.

Fig. 5. Schematic of allowed chalcopyrite reflections.

evident in the photographs. It can be seen from fig. 5 that a tetragonal axis in the [001] direction will produce these four additional spots on one side of the photograph. If the chalcopyrite layer is oriented with its tetragonal axis along the [010] axis of fig. 5, then the reflections would be observed on the other side of the photograph. Thus, with one such Laue photograph we observe whether two of the three possible tetragonal axis orientations (c-axes) are present in the $ZnSnP_2$ layer. The third possible relative orientation of the c-axis can be observed by using a different ⟨110⟩ direction for the primary X-ray beam. For the case shown in fig. 5, one could observe chalcopyrite growth with the c-axis in the [100] direction by taking Laue photographs using primary X-rays in the [110] or [101] directions.

With this procedure back reflection Laue patterns were recorded for a large number of $ZnSnP_2$ layers grown on {100}, {110}, {110}/⟨110⟩, {110}/⟨001⟩, and {211} GaAs substrates. (As indicated above, the {111} layers were not
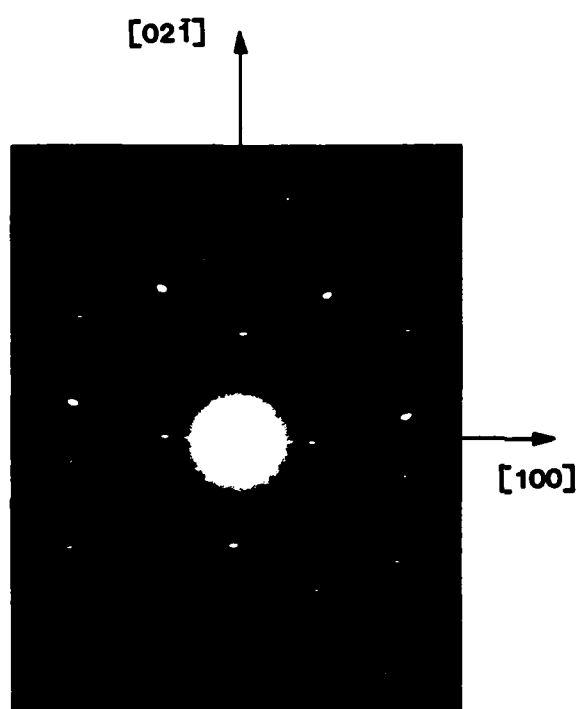
Fig. 7. Laue photograph of ZnSnP$_2$ grown on {110}/⟨110⟩ GaAs with primary X-ray beam in [110] direction 2° off the surface normal.
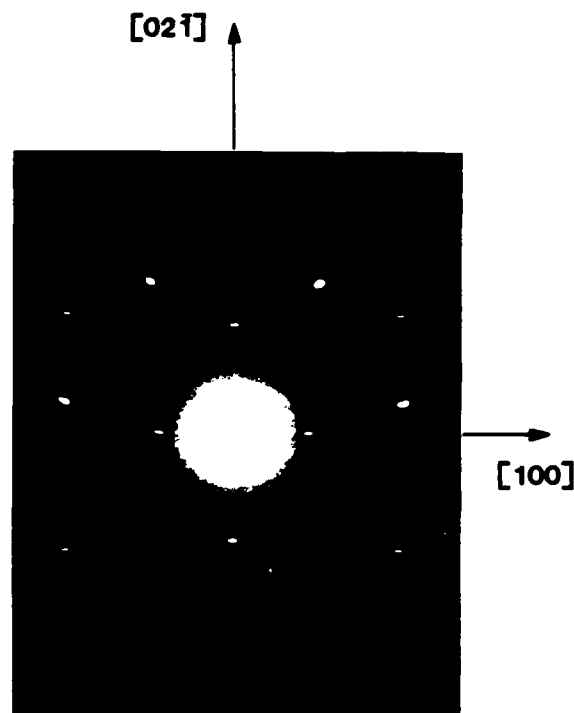
Fig. 8. Laue photograph of ZnSnP$_2$ grown on (112) GaAs with primary X-ray beam in [101] direction.

ZnSnP$_2$.) Fig. 6 is a typical photograph for the {110} growth and it reveals eight uniform chalcopyrite spots. This photograph was taken with the primary X-ray beam along the surface normal and indicates that {110} growth contains equal amounts of two *c*-axis orientations.

Fig. 7 is a photograph of a ZnSnP$_2$ layer grown on {110}/⟨110⟩ GaAs. The direction of the primary beam in this case was the [110] axis 2° from the surface normal. This photograph contains four high intensity chalcopyrite spots associated with one *c*-axis orientation as well as four low intensity chalcopyrite spots (opposite the former spots) associated with a less abundant second *c*-axis orientation.

A typical Laue pattern for layers grown on {211} substrates is shown in fig. 8. For a surface normal of [112] the primary X-ray beam was in the [101] direction. This photograph shows the four asymmetric spots observed when only one *c*-axis

orientation is present in the epitaxial layer. The absence of other orientations was confirmed by photographs with the primary beam in the other ⟨110⟩ directions. (In one direction only sphalerite spots are observed.)
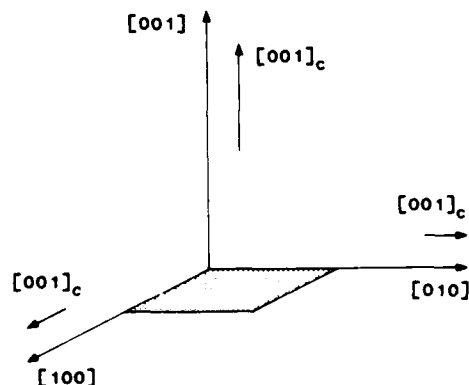
Fig. 9. Schematic illustration of the relative orientations of ZnSnP$_2$ grown on (100) GaAs.
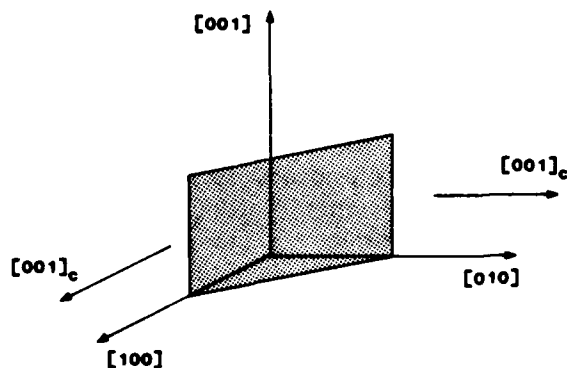
Fig. 10. Schematic illustration of the observed relative orientations of ZnSnP$_2$ grown on {110} GaAs.

Fig. 12. Schematic illustration of the relative orientation of ZnSnP$_2$ grown on (211) GaAs.

The results of these Laue measurements for all of the ZnSnP$_2$ layers are summarized schematically in figs. 9 to 12. In these figures the shaded planes indicate the growth surfaces and the arrows along the axes of the cubic unit cell indicate the relative abundance of the three possible chalcopyrite c-axis orientations. The arrows are denoted $[001]_c$ to indicate the chalcopyrite tetragonal axis. The lengths of the arrows illustrate the relative abundance of each orientation.

As indicated in fig. 9, all three possible c-axis orientations are observed in {100} growth with the c-axis normal to the surface most abundant.

Fig. 10 shows the relative c-axis orientations observed in {110} growth. In this case the epi-

taxial layers contained equal amounts of material with tetragonal axes in the [100] and [010] directions but none in the [001] direction.

There was no detectable difference between the Laue photographs for {110}/⟨001⟩ growth and that shown in fig. 6 for {110} growth. Photographs of {110}/⟨110⟩ growth, however, revealed a significant increase in the abundance of material with the c-axis in the [010] direction and a decrease in the amount with the c-axis in the [100] direction. This is shown in fig. 11. In some layers grown on the {110}/⟨110⟩ surfaces, the smaller relative c-axis orientation was not observed. Variations in the relative abundance of the two c-axis orientations may be due to unintentional misorientation of the substrates during preparation.

The {211}As and {211}Ga growth revealed the best results in that only one c-axis orientation was observed. This is illustrated in fig. 12 which shows the observed relative orientation of the tetragonal axis along the [001] direction for a (112) surface. This habit was observed in all {211} growth, regardless of morphology.

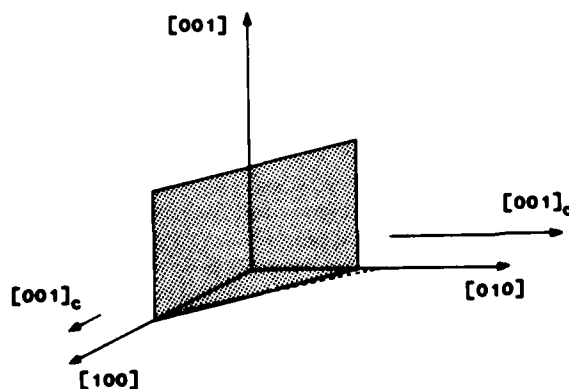Fig. 11. Schematic illustration of the relative orientations of ZnSnP$_2$ grown on (110) GaAs misoriented 2° towards a perpendicular ⟨110⟩.

5. Compositional analysis
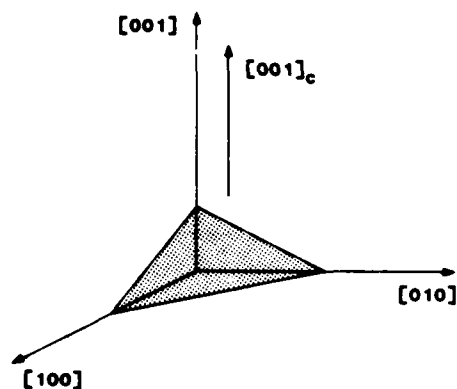
To determine the composition of the epitaxial layers, electron microprobe analysis was performed for each substrate orientation. With the exception of the {111} layers, all were stoichiometric ZnSnP$_2$ within the accuracy of the analysis

which was about 1%. The analysis indicated a slight tendency to incorporate Ga from the GaAs substrate into the layers near the interface with the Ga level being less than 1 mol%. No As was found in any of these layers.

6. Electrical measurements

Most of the ZnSnP$_2$ layers were grown on semi-insulating GaAs substrates to facilitate electrical characterization. Van der Pauw measurements were then performed on the various orientations, except for the {100} samples which had poor morphology, and the carrier concentrations and mobilities were calculated with a simple one-band model.

The layers grown on {110} and {110}/⟨001⟩ substrates, which were composed of material with two c-axis orientations of roughly equal abundance, had hole concentrations of 3 to 5×10^{19} cm^{-3} and mobilities of 15 to 40 cm^2/V·s. The layers grown on {110}/⟨110⟩ substrates, with one of the two c-axis orientations suppressed, and those grown on {211} substrates, with only one c-axis, had hole concentrations of 2 to 5×10^{18} cm^{-3} and mobilities of 20 to 45 cm^2/V·s. Thus, the suppression of antiphase domain boundaries apparently yields improved electrical transport properties.

7. Conclusions

A comparison of our results for ZnSnP$_2$ ($c = 2a$) grown on GaAs to those of Andrews et al. [5] for ZnSiAs$_2$ ($c < 2a$) grown on GaAs indicates certain orientation preferences for the suppression of antiphase domain boundaries in chalcopyrite-on-sphalerite epitaxy. For the chalcopyrite compounds with $c = 2a$, {211} substrates are apparently the best, while for those with $c < 2a$, {100} substrates are better for the suppression of antiphase domain boundaries. Here, of course, we are referring to antiphase domain boundaries associated with material having different c-axes. There may still be antiphase domains which conserve the c-axis, such as those which are produced by rotation of 90° about the c-axis.

Our results and those of Andrews et al. [5]

indicate that antiphase domains with the largest c-axis components in the growth plane tend to be suppressed. The misoriented {110} experiments demonstrate this rather convincingly. From fig. 10 it can be seen that tilting a (110) surface towards the perpendicular [001] direction does not change the relative components of [100] and [010] c-axis orientations in the growth plane, while from fig. 11 tilting a (110) towards the perpendicular [$\bar{1}$10] does.

Although we do not understand the reasons for the orientation dependence of antiphase domain boundary suppression, it appears to be more than site preference. Slight surface misorientations do not affect the results, so surface reconstruction is probably not a factor. Also, considering the results for {211} substrates, there is no obvious reason why this orientation would distinguish between cation sites in a manner which would minic the chalcopyrite structure. Although there may be some energetically favorable site preference, it seems more likely that, somehow, the high lateral growth velocity suppresses the formation of antiphase domains.

References

[1] J.L. Shay and J.H. Wernick, Ternary Chalcopyrite Semiconductors (Pergamon, Oxford, 1975).

[2] H. Kroemer, K.J. Polasko and S.L. Wright, Appl. Phys. Letters 36 (1980) 763.

[3] W.A. Harrison, E.A. Kraut, J.R. Waldrop and R.W. Grant, Phys. Rev. B18 (1978) 4402.

[4] S.L. Wright, M. Inada and H. Kroemer, J. Vacuum Sci. Technol. 21 (1982) 534.

[5] J.E. Andrews, H.H. Stadelmaier, M.A. Littlejohn and J. Comas, J. Electrochem. Soc. 128 (1981) 1563.

[6] G.A. Davis and C.M. Wolfe, J. Electrochem. Soc. 130 (1983) 1408.

4. CHALCOPYRITE-SPHALERITE HETEROEPITAXIAL GROWTH

G.A. DAVIS
Semiconductor Research Laboratory, Washington University, St. Louis, MO 63130

ABSTRACT

Misordering defects which occur in the growth of chalcopyrite/sphalerite systems have been investigated through the LPE growth of $ZnSnP_2$ on GaAs. X-ray diffraction measurements reveal the presence of misordering defects associated with multiple tetragonal orientations in the epitaxy. Growth on {211} oriented substrates reveals the lowest concentrations of orientation-related defects while growth on vicinal {110} oriented substrates indicates the strongest cation site differentiation required to produce long-range ordering. The use of critically misoriented {110} substrates is proposed for the growth of highly ordered chalcopyrite layers on sphalerite substrates.

INTRODUCTION

The chalcopyrite-phase semiconducting compounds have generated much interest in the past for application of their unique optical and electronic transport properties [1]. Much of this interest has moderated recently in light of the substantial difficulties encountered in the growth of large high-quality crystals suitable for device processing: solution-grown and vapor-grown platelets, from which most of the data concerning the chalcopyrites has been determined, contain significant impurity concentrations in addition to being inconsistent with current planar processing techniques. Epitaxial growth of the chalcopyrites on their sphalerite analogs has resulted in layers containing large concentrations of defects which severely degrade the properties of these materials. Pending the development of procedures capable of producing low defect concentration epitaxial layers, these materials will remain technologically insignificant. The objective of this work is to study the nature of chalcopyrite/sphalerite epitaxy in order to develop growth conditions which suppress defect formation.

DEFECT CONSIDERATIONS

Defects are formed in the growth of mixed epitaxial systems when the substrate exhibits a lower degree of ordering than that exhibited by the epitaxial material. As a consequence, the substrate can not ensure proper long-range ordering of the epitaxial constituents and misordering defects result.

This type of defect was initially discussed by Holt [2] for the sphalerite/diamond-structure system. In this system the defects are in the form of boundaries across which there exists a cation/anion site interchange (incoherence) and are called antiphase domain boundaries (ADBs). The nature and suppression of ADBs have been extensively studied in the GaP/Si, GaAs/Ge and GaAs/Si systems [3-6] for applications to sphalerite/diamond-structure device integration. ADB suppression has been pursued through the use of diamond-structure substrates which promote cation/anion site differentiation consistent with the sphalerite structure. Such site differentiation may be encouraged through reconstruction of the substrate surface [3,7] into dissimilar cation-like and anion-like sites or through dissimilar bond coordination of the sites [4]. This latter method has resulted in MBE GaP free of ADBs for growth on {211} oriented Si substrates. Single domain OMVPE GaAs grown on {100} oriented Si substrates demonstrates

the additional facility of highly constraining growth conditions in eliminating ADBs. Sphalerite-phase ordering is not supported by reconstruction or bond coordination for the {100} orientation and there are additional complications associated with charge accumulation and dipole formation at such a polar interface [8]. It is noted that these electrostatic complications may be relieved through exchange of anions and cations across the heterointerface.

The situation one encounters in chalcopyrite/sphalerite growth is somewhat more complicated due to the number of constituents involved and the complexity of the cation sublattices. Presumably there will be no defects generated from cation/anion ambiguity since the well ordered anion sublattice of the substrate is consistent with that of the epitaxial material. Hence we will only be concerned with defects arising from misordering of the cation sublattices. We may distinguish between two types of defects in this system; (1) antiphase domain boundaries being those defects caused by a simple translation of the epitaxial structure which results in cation incoherence, and (2) orientation domain boundaries (ODBs) being those defects at the boundaries between regions having different tetragonal orientations. These are illustrated in Figure 1 for hypothetical growth on {100} oriented sphalerite substrates. ODBs are easily inferred from

(a)   (b)
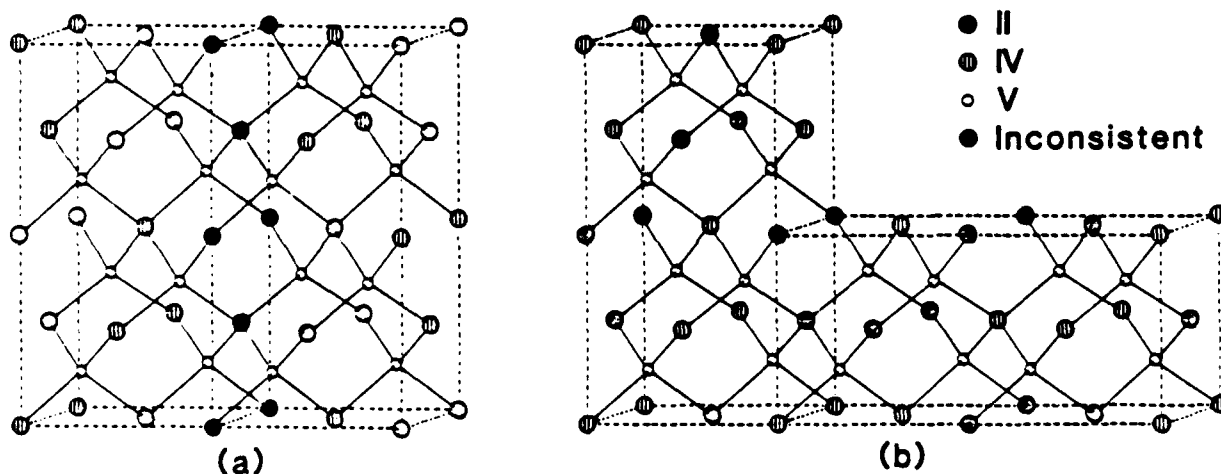
Figure 1 (a) Antiphase domain boundary and (b) Orientation domain boundary for hypothetical {100} orientation growth. The conventional cell has been shifted in the right side of (a) for clarity.

simple diffraction measurements and their existence indicates ambiguous or inconsistent cation ordering at the heterointerface. Since different tetragonal orientations present different atomic structures at the hetero-interface, the predominance of one tetragonal orientation indicates preferential cation coordination which is at least short-ranged. The approach to eliminating these defects is identical to that used to eliminate ADBs in the sphalerite/diamond-structure systems: by ensuring proper cation site differentiation at the heterointerface both ADBs and ODBs will be eliminated. The problems encountered are also identical and one must be cautious to select non-polar (with respect to the cations) surfaces for growth or ensure adequate redistribution at the heterointerface to alleviate charge accumulation and dipole formation. It is noted that the bond coordination approach can not be utilized in this system (for planar growth surfaces) since all substrate cations are identically coordinated.

EXPERIMENTAL

The LPE growth and X-ray diffraction characterization of ZnsnP$_2$ on GaAs [9,10] was used for these defect suppression studies. ZnSnP$_2$ is of only minor interest for device applications due to the small cation electronegativity difference and consequent weak anisotropy it exhibits. It is of primary interest to this study, however, due to this lack of cation distinction and proclivity to disorder.

The LPE growth procedure was implemented in an open tube system utilizing a standard horizontal sliding boat. The growth solutions were comprised of Sn, Zn, and SnP$_3$ with an equivalent composition of 1.20% ZnSnP$_2$ in Sn providing a saturated solution at the 570°C initial growth temperature. Cooling rates of 3.5-4.5°C/hr for 5-16 hrs produced epitaxial layers 4-30μm thick depending upon substrate orientation. The growth process was self-limiting for those orientations yielding thin layers, notably the {100}, {110}, and {111} orientations, due to spontaneous nucleation in the melt. {100}, {110}, misoriented {110}, {111}, and {211} substrate orientations were used in this study. Photomicrographs of a superior epitaxial layer are shown in Figure 2.

(a)   **(b)**
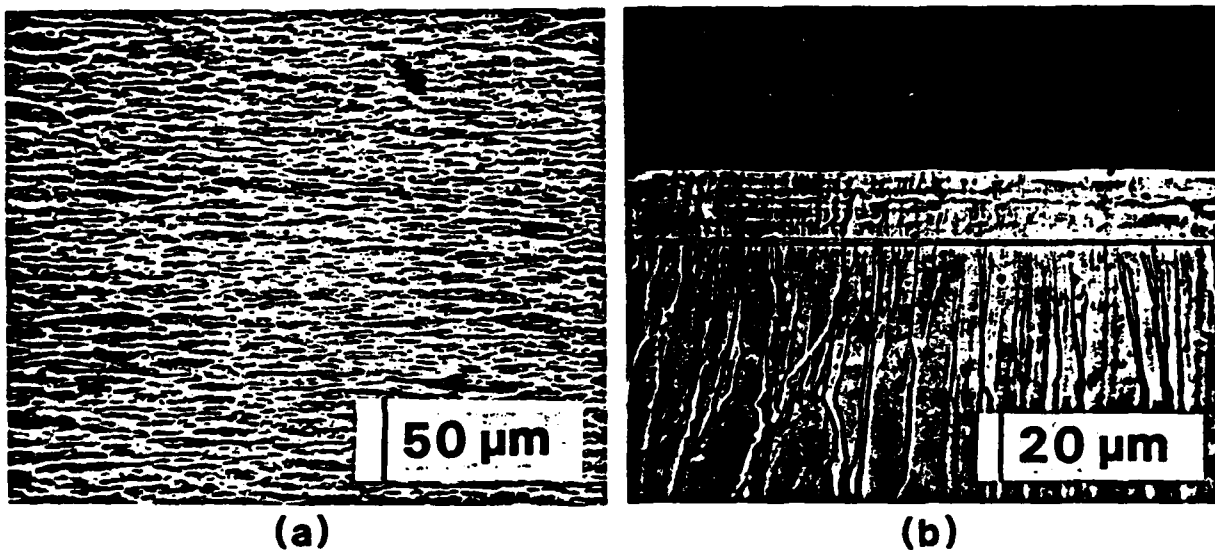
Figure 2 (a) Surface and (b) Dilineated cross-sectional views of a ZnSnP$_2$ layer grown on a misoriented {110} GaAs substrate.

Back-reflection Laue photographs were used to determine the relative abundance of the three possible tetragonal orientations and hence the existence of ODBs. In these photographs the samples were oriented such that the 0.5 mm Cu-target primary X-ray beam was directed along a <110> direction with a sample-to-film distance of 4 cm (35% of the long dimension of the photographs). Epitaxial material having a <021> direction along the primary beam produces four asymmetric reflections in addition to the sphalerite reflections. These reflections, the 259, 25$\bar{9}$, 167, and 16$\bar{7}$, are easily observed despite their small structure factors since they meet the first order Bragg condition for the Kα peak of the Cu X-ray spectrum. A typical photograph revealing one relative orientation of the tetragonal axis is shown in Figure 3. Through photographing two orthogonal <110> directions, the relative abundance of the three possible tetragonal orientations may be determined.
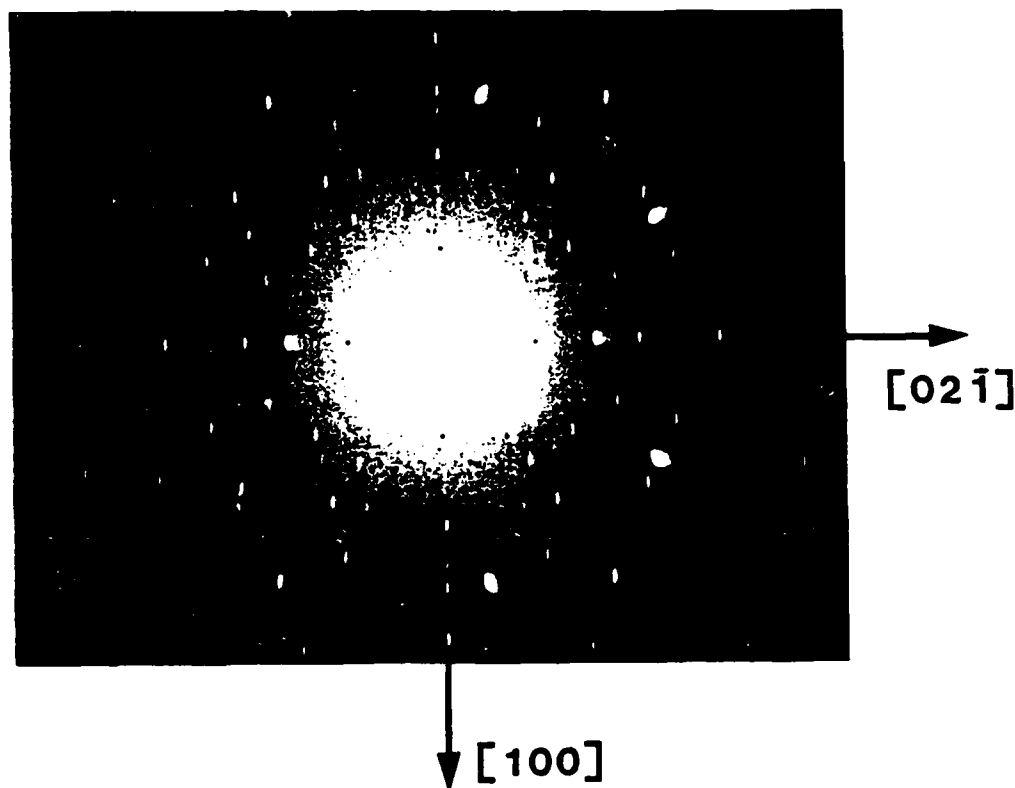
Figure 3 Laue photograph of ZnSnP$_2$ grown on a misoriented {110} GaAs substrate. The four asymmetric high-intensity refractions, allowed for the chalcopyrite structure, indicate a single tetragonal orientation having the [021] direction normal to the surface.

DISCUSSION

The observed abundance of the tetragonal orientations is illustrated in Figure 4 for growth on {100}, {211}, {110}, and misoriented {110} substrates. In this figure the shaded planes indicate the substrate surfaces and the arrows along the conventional axes of the substrate lattice indicate the relative abundance of material with the tetragonal axis oriented along the indicated direction. Epitaxial layers grown on {111} oriented substrates are sphalerite-phase alloys of ZnSnP$_2$ and GaP attributed to an instability of this orientation under the growth conditions. The {100} orientation growth exhibits all possible tetragonal orientations with the surface normal orientation being slightly more abundant, as illustrated in Figure 4 (a). This growth habit suggests that cation site differentiation is sufficiently weak so that no tetragonal orientation dominates and hence no long-range ordering is supported. In terms of suppressing ODBs, the use of {211} oriented substrates yields the best results with epitaxial layers consistently exhibiting only one tetragonal orientation, as illustrated in Figure 4 (b). While this growth habit indicates preferential localized cation coordination, it is not clear whether ordered cation distinction extends across the substrate surface as is necessary to eliminate ADBs and produce single domain growth. Layers grown on {110} oriented substrates reveal only two of the tetragonal orientations, with a complete absence of material oriented with its tetragonal axis in the surface plane, as illustrated in Figure 4 (c). The equal abundance of the two out-of-surface
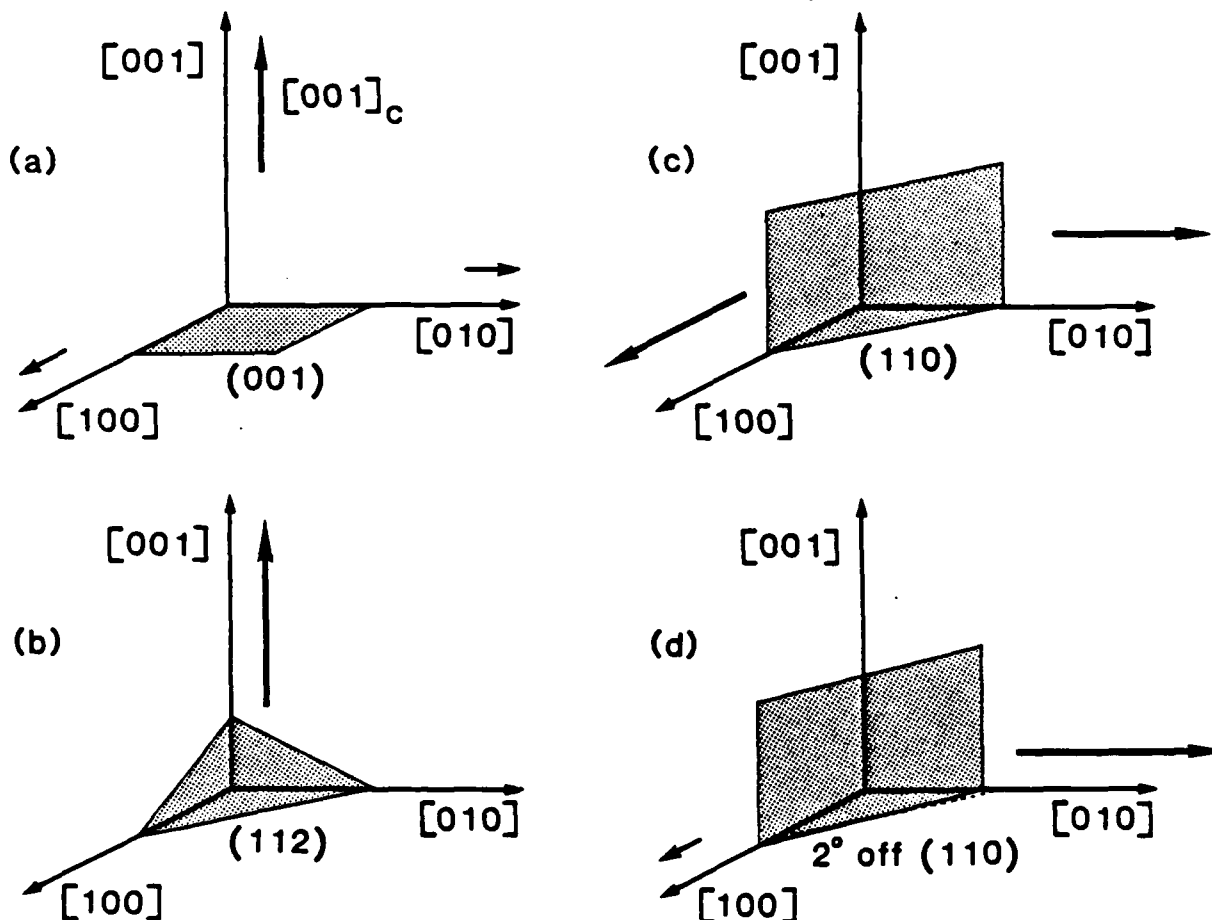
Figure 4 Observed abundance of tetragonal orientations of (a) {100}, (b) {112}, (c) {110}, and (d) misoriented {110} substrates. The shaded planes indicate the substrate surfaces.

orientations is observed in all Laue photographs and suggests that the single crystalline grains are significantly smaller than the area of the primary X-ray beam. The prohibitively large strain and electrostatic energies associated with such a large concentration of ODBs ($>>2\times10^3$cm^2) suggest that the cation site differentiation of this orientation is substantial. Subsequent experiments utilizing substrates misoriented 2° off of a {110} towards a perpendicular <110> reveal a reduction of one of the two tetragonal orientations observed in nominal {110} growth, as illustrated in Figure 4 (d). In these layers the in-surface orientation is not observed. Also, some Laue photographs reveal only one tetragonal orientation, indicating an increase in the grain size. Through the use of substrates critically misoriented in this manner, it may be possible to induce long-range chalcopyrite-phase ordering.

One possible explanation of the {110} orientation results is the existence of a marked preference for one cation species to occupy all available cation sites at the heterointerface. Such a site preference is somewhat compatible with the two out-of-surface orientations which contain alternating large II-V and IV-V regions, and incompatible with the in-surface orientation which contains alternating cations at the surface. One would anticipate such a preference of one species over another based on the different bond strengths of these cations at the heterointerface. This behavior is apparently observed in the ordering of Al$_x$Ga$_{1-x}$As into a monolayer superlattice structure when grown on {110} oriented substrates [11],

wherein the cation electronegativity difference is extremely small. Such a planar cation preference would produce defect-free growth on {021} oriented substrates as illustrated in Figure 5. The corresponding {011} chalcopyrite orientation exhibits alternating II-V and IV-V layers not exhibited by the other corresponding orientations. As with {100} sphalerite/diamond-structure growth, this configuration is electrostatically prohibitive unless there is an exchange of constituents across the heterointerface.
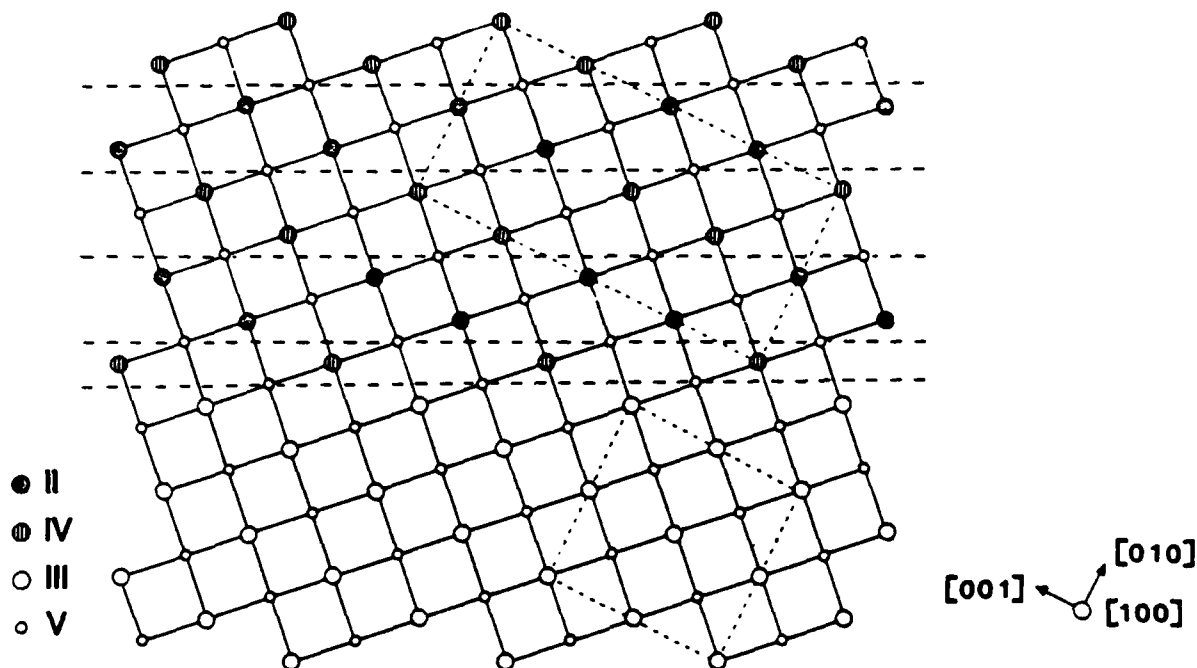
Figure 5   (011) Oriented chalcopyrite structure on (021) oriented sphalerite substrate illustrating the layered nature of this orientation. The conventional cells of the substrate and epitaxy are denoted by fine dashed lines.

Finally, it is interesting to note the correlation between the degree of disordering and the self-limiting thichnesses of the epitaxial layers. Those orientations which reveal a high degree of disordering, the {100}, {110}, and {111}, are typically on the order of 5μm thick while those which reveal a low degree of disordering, the {211} and misoriented {110} are significantly thicker, being on the order of 30μm thick. This behavior indicates a misordering-related impediment to the continued growth at the sample surface due, for instance, to electrostatic contributions which prohibit the incorporation of cations in the regions of misorientation defects.

CONCLUSIONS

The suppression of misordering defects has been studied through the LPE growth of $ZnSnP_2$ on GaAs. While growth on the {211} orientations exhibits the lowest concentration of ODBs, the use of vicinal {110} substrates appears to be the most promising for the elimination of both ADBs and ODBs due to their strong cation differentiation. In particular, the use of {021} oriented substrates may promote long-range ordering based on the results of vicinal {110} growth experiments. A further investigation on the concentration and form of misordering defects through the use of

imaging diffraction techniques would clearly be useful to complete
this study. The application of constraining growth conditions, avail-
able in growth procedures other than LPE, may be of additional utility.

REFERENCES

1. J.L. Shay and J.H. Wernick, Ternary Chalcopyrite Semiconductors:
    Growth, Electronic Properties, and Applications, (Pergamon Press,
    Oxford, 1975).

2. D.B. Holt, J. Phys. Chem. Solids 30, 1297 (1969).

3. Herbert Kroemer, Kenneth J. Polasko, and Steve C. Wright, Appl.
    Phys. Lett. 36, 763 (1980).

4. Steven L. Wright, Masanori Inada, and Herbert Kroemer, J. Vac.
    Sci. Technol. 21, 534 (1982).

5. N.-H. Cho, B.C. DeCooman, C.B. Carter, R. Fletcher, and D.K.
    Wagner, Appl. Phys. Lett. 47, 879 (1985).

6. Masahiro Akiyama, Yoshihiro Kawarada, and Katsuzo Kaminishi,
    Jap. J. Appl. Phys. 23, L843 (1984).

7. Walter A. Harrison, Surface Sci. 55, 1 (1976).

8. W.A. Harrison, E.A. Kraut, J.R. Waldrop, and R.W. Grant, Phys.
    Rev. B18, 4402 (1978).

9. G.A. Davis and C.M. Wolfe, J. Electrochem. Soc. 130, 1408 (1983).

10. G.A. Davis, M.W. Muller, and C.M. wolfe, J. Cryst. Growth 69,
    141 (1984).

11. T.S. Kuan, T.F. Kuech, W.I. Wang, and E.L. Wilkie, Phys. Rev.
    Lett. 54, 201 (1985).

5.   MIXING ENTHALPY AND COMPOSITION FLUCTUATIONS IN TERNARY III–V SEMICONDUCTOR ALLOYS†

P. A. FEDDERS and M. W. MULLER
Washington University, St. Louis, MO 63130, U.S.A.

Abstract—The mixing enthalpy of ternary tetrahedral semiconductor alloys is fairly well described by regular solution theory, with a thermodynamic interaction parameter that is sensitive to the lattice spacing of the binary constituents. We derive an estimate of the interaction parameter from a model which ascribes the mixing enthalpy to bond distortions associated with the alloy formation, and relates these to the macroscopic elastic properties of the crystal. Numerical estimates are given for the 18 alloys with cations Al, Ga, In and anions P, As, Sb and are compared with experimental values and alternative models. To within a single adjustable parameter, the predictions agree with experiment and are consistent with those of the delta lattice parameter (DLP) model. A further calculation of the elastic energy associated with composition fluctuations (clustering) in these alloys indicates that this energy is sufficient to suppress clustering above the critical mixing temperature.

1. INTRODUCTION

The calculation of phase diagrams and of other thermodynamic properties of tetrahedral ternary III–V semiconductor alloys of the form $A_xB_{1-x}C$ (or AC_xD_{1-x}) using regular solution theory has proved to be a useful and reasonably accurate approximation. Several of the ternary alloys with cations Al, Ga, In and anions P, As, Sb have important present or potential applications in electronic technology. These eighteen alloys are mixtures of binary compounds with, in general, different lattice parameters. The lattice parameters of the binary compounds are different when the AC and BC bond lengths are different, and the lattice parameter of the alloy then differs from both. The lattice parameters of all the ternary alloys that can be formed from the ions listed except those involving the cation pair Al, Ga are sensitive to composition. One then may take the view that the bonds are distorted or rearranged in forming the alloy. The energy associated with the bond distortion can be estimated from the macroscopic elastic properties of the crystals. We discuss the contribution of this energy to the enthalpy of mixing and its effect on clustering and spinodal decomposition. We suggest that it is a major or dominant factor in both phenomena.

2. MIXING ENTHALPY

In regular solution theory the molar enthalpy of mixing of a binary solution is given by

$$\Delta H_m = x(1 - x)\Omega \qquad (1)$$

where Ω is the interaction parameter and where x and $1 - x$ are the fractions of the components making up the solution. In terms of a picture of pairwise interaction energies, the interaction parameter is

$$\Omega = 6N_0\epsilon \qquad (2)$$

where $6N_0$ is the number of interacting pairs on the fcc sublattice and

$$\epsilon = 2\epsilon_{AB} - \epsilon_{AA} - \epsilon_{BB} \qquad (3)$$

is the excess of the AA and BB bond energies between like ions over the AB bond energy of unlike ions. In the ternary alloys under discussion these second nearest neighbor interactions are thought to be rather small, consistent with the small experimental values of the interaction parameter.

Stringfellow, using the covalent bonding ideas of Phillips and Van Vechten[1], has introduced the delta lattice parameter model[2] which provides values of the interaction parameter of all the alloys in terms of a single adjustable parameter. The agreement between the DLP theory and experiment is remarkably good for a theory with a single adjustable parameter. The model takes a less specific approach than the identification of eqns (2) and (3) of the interaction parameter with the sum of binary bond energies, and assumes that the energy is a more global property of the semiconductor that depends only on the lattice parameter of the crystal. The idea is that the bonding energy is proportional to the band gap which, in turn, is proportional to a power of the lattice parameter. This is similar to but distinct from Van Vechtens proposal[3] that Ω is produced by the reduction of the band gaps due to the disorder associated with alloying. The DLP model leads to an approximate value for Ω of

$$\Omega_s = (35/8) K\Delta^2 d^{-4.5} \qquad (4)$$

P. A. FEDDERS and M. W. MULLER

where $\Delta = a - b$, $\bar{d} = 1/2(a + b)$, with a and b the lattice parameters of AC and BC respectively. The quantity K is obtained by a least squares fit to the experimental data and is equal to 1.15×10^7 cal/mole $\text{Å}^{2.5}$. The excellent fit to the experimental data depends largely on the Δ^2 dependence of Ω.

We wish to show here that if part or all of Ω is interpreted as being associated with strain or lattice parameter mismatch, then it is readily shown that this contribution exhibits the same Δ^2 dependence.

It is observed that the average lattice spacing of the alloys closely follows Vegard's law

$$d_0 = xa + (1 - x)b. \tag{5}$$

Since the difference between the lattice parameters a and b of the binary compounds corresponds to the different AC and BC bond lengths, the bonds must be distorted or rearranged to form the alloy. If a and b do not differ too widely, the energy of the rearranged configuration must be of second order in $a - d_0$ and $b - d_0$. Thus the contribution to the enthalpy of formation of the alloy is

$$\Delta H_m = \frac{\lambda}{\bar{d}}(x(d_0 - a)^2 + (1 - x)(d_0 - b)^2), \tag{6}$$

where λ is an adjustable parameter. With d_0 from eqn

(5) this becomes

$$\Delta H_m = x(1 - x)\lambda \left(\frac{\Delta}{\bar{d}}\right)^2 \tag{7}$$

with the same Δ^2 dependence as the DLP model.

Since we are viewing the effect as an elastic distortion, we can obtain a crude numerical estimate for λ from the macroscopic elastic properties of the crystal. At one extreme one can assume a strict virtual crystal model of the alloy, which would identify the bond distortion energy with that of on isotropic compression or dilatation. At $x = 1/2$, the principal strains are given by $1/2\Delta$ and the elastic energy per unit volume is

$$W = 1/2B \left(\frac{3}{2}\frac{\Delta}{\bar{d}}\right)^2 \tag{8}$$

yielding

$$\lambda = \frac{9}{2}BV, \quad \Omega' = \lambda \left(\frac{\Delta}{\bar{d}}\right)^2 \tag{9}$$

where B is the bulk modulus and V is the molar volume of the alloy with $x = 1/2$. Table 1 lists Ω, and Ω' for the ternary compounds under discussion.

Equation (9), which contains no adjustable parameters, yields higher interaction parameter values than

Table 1. Experimental and calculated values of the interaction parameter. Bulk moduli by interpolation between binary compound values from Refs. [8] and [9]; interaction parameters (in k cal/mole) in columns 3, 4, and 5 quoted from Stringfellow, Ref. [2] (small differences in the calculated values in column 4 because we use fewer significant numbers than Ref. [2] for $\Delta/\bar{d}$)

Alloy	$\frac{\Delta}{\bar{d}}$	$B \times 10^{-11}$ dyne cm^{-2}	Ω exp	Ω calc DLP	$\frac{1.74 \times 10^6}{(\Delta/\bar{d})^{2.45}}$	Ω'	$\Omega'' = 0.226\Omega'$
AlGaP	0.002	8.73				0	0
AlInP	0.072	7.93				12100	2740
GaInP	0.074	8.05	3500, 3250	3630	2940	13000	2940
AlGaAs	0.002	7.60	0	0	0	0	0
AlInAs	0.068	6.81	2500	2814	2370	10500	2370
GaInAs	0.070	6.67	1650, 3000, 2000	2815	2510	10700	2420
AlGaSb	0.008	5.79	0	23	8	140	30
AlInSb	0.054	5.34	600	1456	1400	6400	1450
GaInSb	0.062	5.21	1475, 1900	1846	1830	8100	1830
AlPAs	0.036	8.17				3000	680
AlPSb	0.117	7.26				31600	7140
AlAsSb	0.081	6.83				15300	3460
GaPAs	0.036	8.16	400, 1000	985	446	2900	660
GaPSb	0.104	7.25				21300	4810
GaAsSb	0.075	6.56	4500, 4000	3355	3090	12200	2760
InPAs	0.032	6.57	400	585	436	2300	520
InPSb	0.099	6.01				22600	5110
InAsSb	0.067	5.32	2900, 2250	2289	2330	9600	2170

the DLP theory. A much better fit to the experimental data is obtained if the prediction of eqn (9) is reduced by a factor of about 4.4, resulting in the column labeled Ω'' in Table 1. Indeed, the entries in that column fit the observed values as closely as String-fellow's[2] "best fit" 2.45 power law. Moreover a plausible case can be argued for a reduction of the estimate by a factor of this order.

It has been demonstrated recently[4] that although the average lattice parameter closely follows Vegard's law, the AC and BC bond lengths do not take the common nearest neighbor value of the virtual crystal but remain much closer, by a factor of 4 or 5, to their lengths in the binary compounds. If it is assumed that the stretching and compression of nearest neighbor bonds is the only distortion, this reduces the estimate of λ by the square of this factor, of order 20. This, however, almost certainly underestimates the effect of the distortion, since the conservation of nearest neighbor bond lengths requires a distortion of the bond angles and of second neighbor bond lengths and angles.

In addition, the fact that the AC and BC bond lengths tend to remain constant (to about 80%) independent of alloy composition, necessarily implies that the A and B atoms in the alloy are much more correlated than in a random solution. These strong correlations could well be due to the strong elastic forces. Neither our theory nor any other theory currently takes this into account properly. Thus within the scope of our model, Table 1 furnishes strong evidence that this quasi-elastic energy is a significant, and perhaps a dominant part of the enthalpy of mixing.

3. CLUSTERING

A binary mixture whose enthalpy of mixing is positive has a tendency to separate into its components. This tendency manifests itself in the form of spinodal decomposition and the development of a miscibility gap below a critical mixing temperature and in the form of clustering on a microscopic scale above this temperature. In the alloys under discussion here, this tendency is most readily interpreted in terms of preferential pairwise interactions as expressed by eqns (2) and (3), but it does not depend on this interpretation. Jones, Porod, and Ferry[5] have recently examined the degree of clustering that may be expected to occur above the critical temperature of mixing as a function of the interaction parameter interpreted in this manner, of the temperature, and of the mole fraction x. We extend this calculation to include an elastic energy which is large enough to overcome the clustering tendency.

Since the lattice parameters of the alloys follow Vegard's law, the ions of the alloy at least *on the average* occupy positions on a virtual crystal lattice with the lattice parameter of eqn (5). Note that this statement is not in conflict with the observation cited above[4] that the bond lengths need not follow Vegard's law.

Clustering produces a fluctuation from the average composition, while the region of the cluster must occupy the volume prescribed by the average virtual crystal lattice. Thus the region of the cluster is strained. The energy associated with the strain tends to reduce the degree of clustering, but we shall see that it does not eliminate a miscibility gap below the critical mixing temperature. The effect is similar to the "lattice latching"[6] and stabilization against decomposition[7] associated with the mismatch strains of heteroepitaxy. In the present instance we deal with the strains arising from fluctuations in a homogeneous medium. In either case, the existence of a strained region presupposes the existence of the crystal lattice to be matched by the continuing growth. In epitaxy, this lattice is furnished by the substrate. In homogeneous growth it depends on the formation of a nucleus, which at a given composition can only form at temperatures above the spinodal decomposition curve. This is the reason why the strain energy affects clustering but not the miscibility gap.

Let the average composition of an alloy be $A_{x_0}B_{1-x_0}C$ and the local composition $A_x B_{1-x}C$. Then the lattice parameter is

$$d_0 = x_0 a + (1 - x_0)b. \tag{10}$$

If the crystal were permitted to relax everywhere, the local lattice parameter would be

$$d = xa + (1 - x)b. \tag{11}$$

However, the compatibility constraint imposes a local strain

$$\delta = d - d_0 = (x - x_0)(a - b) \equiv \zeta\Delta, \tag{12}$$

the second equality defining the composition fluctuation ζ.

The energy density of the strain can be computed as in eqn (8) and is

$$W = (9/2)B\zeta^2\left(\frac{\Delta}{d}\right)^2 \tag{13}$$

per unit volume.

Unlike eqn (8) for the elastic contribution to the mixing enthalpy, eqn (12) should not be a significant overestimate of the strain energy. In the present application we are computing the energy of actual compressions and dilatations in terms of measured elastic constants and the nature of the bond distortions accompanying the strain is irrelevant. Therefore, if the mixing enthalpy is dominated by the bond distortion effects discussed in Section 2, then it is evident that the strain energy of composition fluctuations is more than adequate to overcome the clustering tendency.

A similar argument can be made if the clustering is ascribed to preferential pairwise interactions. The

-25-

molar bond energy density of the ternary alloy, taking into account the 4 nearest and 12 next nearest neighbor interactions is

$$E = N_0(4\epsilon_A x + 4\epsilon_B(1 - x)$$

$$= 6\epsilon_{AA}x^2 + 12\epsilon_{AB}x(1 - x) + 6\epsilon_{BB}(1 - x)^2), \quad (14)$$

where ϵ_A and ϵ_B are the AC and BC interaction energies. The contribution to the bond energy density of a composition fluctuation ζ is $E(x_0 + \zeta) - E(x_0) = \eta$, given by

$$\eta = N_0((4\epsilon_A - 4\epsilon_B + 12\epsilon_{AB} - 12\epsilon_{BB} - 12x_0\epsilon)\zeta - 6\epsilon\zeta^2)$$
$$(15)$$

with ϵ as defined in eqn (3).

In a crystal of a given composition, the contribution to the interaction energy linear in the fluctuations must by definition average to zero. Therefore only the term in ζ^2 need be considered from the purpose of minimizing the free energy. But from eqn (2) this term is just

$$\eta = -\Omega\zeta^2, \quad (16)$$

so that the net molar energy of the fluctuations, from eqns (13) and (16), is

$$WV + \eta = (\Omega' - \Omega)\zeta^2 \quad (17)$$

averaged over the crystal.

Equation (17) yields a positive (or zero) fluctuation energy for each of the ternary alloys we are considering, indicating that clustering is suppressed by the strain energy.

4. CONCLUSION

The view is represented in our model that the formation of a tetrahedral semiconductor alloy is accompanied by bond distortion, and that an estimate of the electronic energy of this distortion can be obtained from the macroscopic elastic properties of the crystal. Superficially this view appears distinct from the basis of the DLP model, which is deduced from the empirical lattice parameter dependence of the optical bandgap and from Van Vechtens proposal. But the bandgap itself, as pointed out by Phillips and Van Vechten[1], is a measure of the covalent bonding energy. The elastic constants of a crystal depend as directly on the bonding energy as its optical and dielectric properties. Therefore it is perhaps not too surprising that models derived from optical and from elastic crystal parameters should yield predictions of similar form for the thermodynamic properties. The merit we may claim for the present model is that it contributes a new and convenient experimental approach to the thermodynamic quantities and that it may yield a fruitful theoretical insight.

REFERENCES

1. Phillips J. C. and Van Vechten J. A., *Phys. Rev.* B2, 2147 (1970).
2. Stringfellow G. B., *J. Phys. Chem. Solids* 34, 1749 (1973); *J. Crystal Growth* 27, 21 (1974).
3. Van Vechten J. A., *Handbook on Semiconductors* (Edited by S. P. Keller), Vol. 3, Chap. 1, Sec. 3, p. 52. North-Holland, Amsterdam (1980).
4. Mikkelsen J. Jr. and Boyce J. B., *Phys. Rev. Lett.* 49, 1412 (1982).
5. Jones K. A.; Porod W. and Ferry D. K., *J. Phys. Chem. Solids* 44, 107 (1983).
6. Stringfellow G. B., *J. Appl. Phys.* 43, 3455 (1972).
7. Stringfellow G. B., *J. Appl. Phys.* 54, 404 (1983).
8. Martinez G., *Handbook on Semiconductors* (Edited by M. Balkanski), Vol. 2. North Holland, Amsterdam (1980).
9. Wiley J. D., *Semiconductors and Semimetals* (Edited by R. K. Willardson and A. C. Beer), Vol. 10. Academic Press, New York (1975).

6. Composition correlations in ternary semiconductor alloys

M. W. Muller

Department of Electrical Engineering and Semiconductor Research Laboratory,
Washington University, Saint Louis, Missouri 63130

(Received 2 July 1984)

Spatial composition fluctuations in semiconductor alloys $A_xB_{1-x}C$ involve elastic energy when the lattice parameters of AC and BC differ. Therefore, the fluctuations are expected to be reduced below those exhibited by a purely random distribution of the constituent ions. We estimate the extent of the reduction, and relate it to recent observations of Raman linewidths and line shapes in $Ga_xIn_{1-x}As$ and $Ga_xAl_{1-x}As$.

Ternary tetrahedrally coordinated semiconductor alloys $A_xB_{1-x}C$ or AC_xD_{1-x}, where A and B are group III (or II) elements, and C and D group V (or VI) elements can for many purposes be described as binary mixtures whose component particles reside (approximately) on the sites of an fcc lattice. Specifically, thermodynamic parameters such as mixing enthalpy[1] and spinodal curves[2] conform fairly well to the rules describing regular solutions.

The key quantity of regular solution theory is the interaction parameter Ω, which can be interpreted in terms of pair interaction energies; thus

$$\Omega = \tfrac{1}{2}N_0Z(2E_{AB}-E_{AA}-E_{BB}) ,$$

where N_0 is Avogadro's number, Z the coordination number (12 for fcc), and E_{ij} are the (negative) pair interaction energies. A negative value of Ω indicates a tendency to ordering (compound formation), a positive value a tendency to decomposition. All the observed interaction parameters of the alloy group with $A,B = $ Al,Ga,In; (Zn,Cd,Hg) $C,D = $ P,As,Sb; (Se,Te) are positive or zero. Thus, one expects—and observes—miscibility gaps and spinodal decomposition below a critical mixing temperature characteristic of each alloy.

The observed interaction parameters are found to be proportional to the square of the lattice parameter difference between the pure compounds that constitute the alloy. This dependence has been interpreted, in the so-called delta-lattice-parameter (DLP) model in terms of the lattice parameter dependence of the average band gap,[3] and more recently, especially after details of the composition dependence of bond lengths in $Ga_{1-x}In_xAs$ were revealed by extended x-ray absorption fine structure (EXAFS) measurements,[4] in terms of the bond distortions associated with the formation of the alloy. By relating the bond distortion energies to the macroscopic elastic constants of the crystals, a good case could be made for ascribing most or all of the observed mixing enthalpy to this cause.[5,6]

A positive mixing enthalpy would normally produce clustering of like particles above the critical mixing temperature, and an estimate of the degree of clustering to be expected was published recently.[7] For the model that was used in this calculation, the origin of the positive interaction parameter is irrelevant. It has been pointed out, however, that in the type of "lattice gas" that represents these alloys, with a composition-dependent lattice parameter, if an alloy crystal is formed at all, elastic interactions will suppress the clustering.[5] It was also suggested that these elastic interactions were likely to produce an ordering tendency, that is to say,

that local composition fluctuations might be reduced below the level to be expected of a purely random distribution of the constituents. What follows is a simple thermodynamic model for the composition correlations induced by the elastic energy.

The lattice parameters of these alloys follow Vegard's law quite accurately. Any deviation from a linear dependence of lattice parameter on composition (bowing) is small enough to be quite negligible for the purpose of this argument. Consider a region of the alloy large enough to be regarded as macroscopic. If the composition of this region deviates from the average composition of the alloy, but must be accommodated in the volume of the virtual lattice that "belongs to it," it will suffer compression or dilatation.

The energy associated with the strain is readily computed.[5] Let the average composition of the alloy be $A_{x_0}B_{1-x_0}C$ and the local composition $A_xB_{1-x}C$. Then the lattice parameter is

$$d_0 = x_0a + (1-x_0)b , \tag{1}$$

where a is the lattice parameter of AC and b the lattice parameter of BC. If the crystal were permitted to relax everywhere, the local lattice parameter would be

$$d = xa + (1-x)b ; \tag{2}$$

however, the compatibility constraint imposes a local strain

$$\delta = d - d_0 = (x-x_0)(a-b) = \Delta x(a-b) , \tag{3}$$

with an associated energy density (per unit volume)

$$W(\Delta x)^2 = 18B\left|\frac{a-b}{a+b}\right|^2(\Delta x)^2 , \tag{4}$$

where B is the bulk modulus of the crystal.

Equation (4) is based on isotropic compression or dilatation; an analogous expression can be obtained for a planar strain. In that form the elastic energy is thought to be responsible for the "lattice latching" observed in heteroepitaxy,[8] the growth of a single lattice-matched alloy composition over a range of melt compositions. It also accounts for the successful heteroepitaxial growth of alloy compositions unstable in the bulk at the growth temperature.

It has been shown[5] that a reasonable fit to the interaction parameters of the III-V alloys considered here is given by the semiempirical formula

$$W' = 0.226 \times 18B\left|\frac{a-b}{a+B}\right|^2 \tag{5}$$

making a contribution to the mixing enthalpy per mole of

$$\Delta H = W'x(1-x)V \ , \tag{6}$$

where V is the molar volume of the alloy.

The entropy of mixing is approximately

$$S = \ln\left|\frac{N_A!N_B!}{N_{AA}!N_{BB}!(N_{AB}!)^2}\right| \ , \tag{7}$$

where the N_i are numbers of ions and the N_{ij} numbers of second neighbor pairs. Per mole this is

$$S \simeq R\,[\,x\ln x + (1-x)\ln(1-x) - x^2\ln(x^2)$$

$$-(1-x)^2\ln(1-x)^2 - 2x(1-x)\ln x(1-x)\,] \ . \tag{8}$$

Using Eqs. (4), (6), and (8) in the thermodynamic formula[9] for macroscopic fluctuations of concentration on an assembly of N sites with total Gibbs free energy G

$$\langle(\Delta x)^2\rangle = \frac{kT}{(\partial^2 G/\partial x^2)_{T,P,N}} \ , \tag{9}$$

we find

$$\langle(\Delta x)^2\rangle = \frac{1}{N}x(1-x)\left[1 + \frac{2(W-W')V}{RT}x(1-x)\right]^{-1} \ . \tag{10a}$$

or, in terms of the critical mixing temperature T_c given by $2RT_c = W'V = 0.226WV$

$$\langle(\Delta x)^2\rangle = \frac{1}{N}\left\{\frac{x(1-x)}{1+13.7(T_c/T)x(1-x)}\right\} \ . \tag{10b}$$

One may guess conservatively that the disorder grown into a crystal corresponds roughly to a value frozen in at the growth temperature. Thus, if we compare a lattice-matched alloy such as $Ga_{0.5}Al_{0.5}As$ with $T_c \simeq 0$ with the mismatched alloy $In_{0.5}Ga_{0.5}As$ with $T_c \sim 600$ K grown epitaxially at $T \sim 900$ K, we expect, from Eq. (10a) or (10b) to find a relative reduction of the mean-square concentration fluctuations in the mismatched alloy by a factor ~ 0.3. The reduction would be expected to be more significant, depending on cooling rate and on the growth parameters, if appreciable solid-state diffusion takes place after growth.

Some qualitative experimental support for this prediction is to be found in linewidths and line shapes observed by Parayanthal and Pollak[10] in Raman scattering from $Al_xGa_{1-x}As$ and $In_xGa_{1-x}As$. In this work it was found that the broadening and asymmetry of the Raman line was more pronounced in the lattice-matched alloy $Al_xGa_{1-x}As$ than in the mismatched $In_xGa_{1-x}As$.

A "spatial correlation" model has been successfully used to interpret the effect of microcrystalline,[11] and implantation damage[12] disorder on Raman linewidths and line shapes. This model replaces the phonons of the infinite ordered crystal with phonons localized within "correlation regions" whose size is a measure of the partial ordering in the imperfect crystal. As a result, the $q=0$ momentum selection rule of the perfect crystal is relaxed, and phonons in a region of the Brillouin zone corresponding to the correlation length participate in the scattering. Experimental values of the correlation length are deduced by fitting the observed

linewidths and line shapes, assuming a Gaussian size distribution of the correlation regions, generally in reasonable agreement with the estimated sizes of crystallites[11] or undamaged regions.[12]

Substitutional disorder in an alloy similarly breaks the crystal's translational symmetry and, hence, the $q=0$ selection rule for Raman scattering. Since the perturbation is the phonon modulation of the dielectric tensor, the effective size of the scattering regions is given by the correlation length of this tensor's spatial fluctuations.[13] No theoretical prediction has so far been made for this quantity, but Parayanthal and Pollack[10] were able to fit their observed Raman lines with a spatial correlation model in which the correlation length is simply a phenomenological parameter determined from the experimental data. For their epitaxially grown alloys, this parameter ranges from about 8 to above 30 lattice parameters.

Of the two alloy series for which results are given, $Ga_xAl_{1-x}As$ has, within experimental accuracy, zero mixing enthalpy, and the cations should constitute a perfect lattice gas on their fcc sublattice. Their concentration fluctuations, which may be taken as measure of the disorder, then are given by Eqs. (10) with $T_c = 0$. The Raman lines bear this out qualitatively, in the sense that the linewidths and asymmetries are greatest for samples with x near 0.5.

The broadening of the Raman lines even in the completely random alloy $Ga_xAl_{1-x}As$ is modest as compared with the spectrum of amorphous materials, and the spatial correlation model is successful in the interpretation of the line shapes. This suggests that one might assign the role of the defects that disrupt the phonon modes to fairly large fluctuations from the average composition. The correlation or coherence length can then be related to the statistics of large fluctuations.

In a random binary alloy, the probability distribution of ions is binomial. With a coordination number $Z = 12$, the distribution of even the nearest-neighbor shell is fairly well represented by a Gaussian, and the probability of occurrence of a deviation $\geq \xi$ is approximated by

$$P(\xi) = \mathrm{erfc}(\zeta) \ , \tag{11}$$

where $\zeta = \xi/[2\langle(\Delta x)^2\rangle]^{1/2}$.

In order to arrive at an order of magnitude estimate of the correlation length, we take the size of the defect to comprise one cation shell of Z ions. If a deviation of relative magnitude ξ is to occur in a region containing NZ cations, we should have $NZP(\xi) = 1$, and, therefore, the average distance between such defects, which we take to be the correlation length, is

$$L = N^{1/3}a = [Z\,\mathrm{erfc}(\xi)]^{-1/3}a \ , \tag{12}$$

where a is the lattice parameter. Equation (12) yields values consistent with the estimates based on the Raman spectra if ξ is about two standard deviations. Using the average value of L for the GaAs-like mode in $Ga_xAl_{1-x}As$ for the four samples with x near 0.5, we find $\xi = 1.88$.

Equations (10) and (12) also provide a comparison of the correlation lengths in $Ga_xIn_{1-x}As$ and $Ga_xAl_{1-x}As$. Because of the suppression of concentration fluctuations, we expect the scattering centers associated with wide fluctuations to be rarer, increasing the correlation length. Using the factor 0.3 estimated from Eq. (10) for the reduction in

the mean square fluctuation in Eq. (12), we find

$$\frac{L_{Ga_{0.5}In_{0.5}As}}{L_{Ga_{0.5}Al_{0.5}As}} \simeq 12 \ . \tag{13}$$

This factor is larger than the numbers deduced from the Raman spectra by Parayanthal and Pollak, suggesting that additional phonon scattering processes are active.

The reduction in randomness discussed here is expected to have other experimentally testable consequences, which will be considered elsewhere.

[1] G. B. Stringfellow, J. Phys. Chem. Solids 33, 665 (1972).
[2] G. B. Stringfellow, J. Appl. Phys. 54, 404 (1983).
[3] G. B. Stringfellow, J. Cryst. Growth 27, 21 (1974); J. C. Phillips and J. A. VanVechten, Phys. Rev. B 2, 2147 (1970).
[4] J. C. Mikkelsen, Jr. and J. B. Boyce, Phys. Rev. Lett. 49, 1412 (1982).
[5] P. A. Fedders and M. W. Muller, J. Phys. Chem. Solids 45, 685 (1984).
[6] J. C. Mikkelsen, Jr. (private communication).
[7] K. A. Jones, W. Porod, and D. K. Ferry, J. Phys. Chem. Solids 44, 107 (1983).
[8] G. B. Stringfellow, J. Appl. Phys. 43, 3455 (1972).
[9] A. Münster, in Fluctuation Phenomena in Solids, edited by R. E. Burgess (Academic, New York, 1965), p. 184.
[10] P. Parayanthal and F. H. Pollak, Phys. Rev. Lett. 52, 1822 (1984).
[11] H. Richter, Z. P. Wang, and L. Ley, Solid State Commun. 39, 625 (1981).
[12] K. K. Tiong, P. M. Amirtharay, F. H. Pollak, and D. E. Aspnes, Appl. Phys. Lett. 44, 122 (1984).
[13] R. Shuker and R. W. Gammon, Phys. Rev. Lett. 25, 222 (1970).

7. Below band-gap photoresponse of In$_{1-x}$Ga$_x$P-GaAs heterojunctions

S. Julie Hsieh, Elizabeth A. Patten, and C. M. Wolfe
Semiconductor Research Laboratory, Washington University, St. Louis, Missouri 63130

Below band-gap photovoltaic response with a half-power point at 1.31 eV is observed in p-type In$_{1-x}$Ga$_x$P on n-type GaAs heterojunctions with {111} interfaces. This response is apparently due to photon-assisted tunneling of carriers across the interfacial energy gap, which is smaller than the energy gaps of the constituent materials. The same mechanism can be employed in other heterojunctions with appropriate energy-band lineups to obtain longer wavelength infrared response.

Several schemes have been used in intrinsic infrared photodetectors to obtain response below the band gap of the constituent semiconductors. One of these methods is to form an alloy between two compounds which have conduction and valence bands of opposite symmetry, such as PbTe and SnTe.[1] Since the conduction and valence bands must interchange at some alloy composition, they move toward one another producing alloy band gaps smaller than the end-

points. Another method uses electroabsorption (photon-assisted tunneling) to shift the absorption edge to longer wavelengths.[2] This has been employed in reverse-biased GaAs[1] and Ga$_{1-x}$Al$_x$As devices.[3] A recently proposed scheme is to form an alloy between two materials with different crystal structures. In the region where the alloy undergoes a phase change from one structure to another, the absorption edge is lowered presumably due to antisite disorder. This behavior has been observed in (GaAs)$_{1-x}$Ge$_{2x}$ alloys.[5] In the present work we discuss and present experimental evidence for what appears to be another method of obtaining longer wavelength response.

The scheme is essentially the inverse of a photon emission process previously described.[6] It employs the electric field at the interface of a heterojunction to tunnel charge carriers across an interfacial energy gap smaller than the energy gaps of the semiconductors on either side. Photoresponse is obtained by the photoexcitation of electrons from the valence band of one material to virtual states, and then electron tunneling into the conduction band of the other material. Conversely, electrons from the valence band of one material can tunnel into virtual states and then be photoexcited into the conduction band of the other material. The latter process is equivalent to hole tunneling, and both are illustrated schematically in Fig. 1. The formalism for these physical processes is that of band-to-band electroabsorption in a nonuniform electric field which has been previously examined in some detail.[3,4,7]

One of the heterojunction systems which exhibits the required energy band lineup is In$_{1-x}$Ga$_x$P-GaAs. An abrupt heterojunction model for this system is shown in Fig. 1. Several of the parameters of the model vary from sample to sample and were determined in the following ways: the energy gap of GaAs was measured by photoconductivity on high-purity epitaxial samples to be 1.39 eV. The energy gap of In$_{1-x}$Ga$_x$P was determined from its dependence on lattice constant,[8] where the latter was obtained by double-crystal x-ray diffraction scans. On this basis the energy gap of the lattice-matched alloy In$_{0.49}$Ga$_{0.51}$P was 1.90 eV. The separations between the electrochemical potential energy, ζ, and the band edges were determined from Hall measurements:
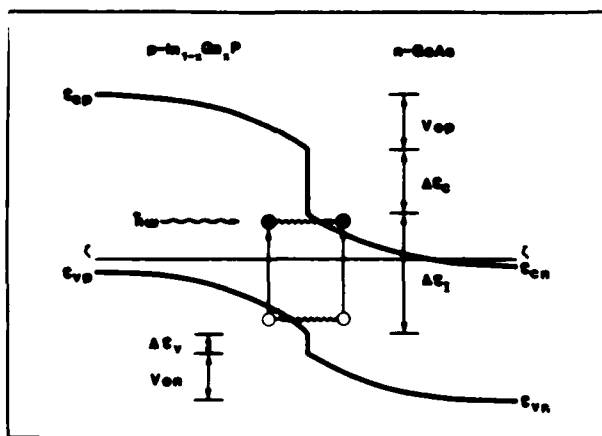
first on the GaAs substrates and then on In$_{1-x}$Ga$_x$P layers grown on semi-insulating GaAs by liquid phase epitaxy under the same conditions as those grown on n^+ substrates. The built-in potential and the band bending on either side were obtained from capacitance-voltage measurements. From these measurements all the parameters of the model, including $\Delta\epsilon_v$, $\Delta\epsilon_c$, and $\Delta\epsilon_I$, were determined experimentally.

For a lattice-matched heterojunction with a nominal {111} interface, the band offsets were $\Delta\epsilon_v = 0.08$ eV, $\Delta\epsilon_c = 0.59$ eV, and $\Delta\epsilon_I = 1.31$ eV. Although these results are consistently obtained experimentally, it should be pointed out that they are not close to the expected theoretical values. Using a dielectric model,[9] for example, we calculate ionization energies for GaAs and In$_{0.49}$Ga$_{0.51}$P of 5.68 eV and 5.91 eV, respectively. These ionization energies and the experimental energy gaps yield band offsets of $\Delta\epsilon_v = -0.23$ eV, $\Delta\epsilon_c = 0.28$ eV, and $\Delta\epsilon_I$ equals the band gap of GaAs. Thus, below band-gap photoresponse is not predicted from this dielectric model. Although there is probably no reason to expect good agreement between theory and experiment, we have some preliminary evidence that the valence-band offset is in the predicted direction for In$_{1-x}$Ga$_x$P-GaAs heterojunctions with nominally charge-neutral[10] {211} interfaces. Thus, at least part of the difference in band lineups may be due to dipoles associated with the residual charge at {111} interfaces.

Figure 2 shows the room-temperature photovoltaic response for a {111} heterojunction at 0 and -0.5 V applied bias. (These diodes were rather leaky and exhibited substantially increased noise at higher reverse voltages.) For these measurements the device was biased with a constant-voltage power supply and light was incident on a cleaved surface perpendicular to the heterojunction interface. The salient features are a below band-gap peak with a half-power point at 1.31 eV which increases substantially with reverse bias as expected for tunneling. The 1.31-eV half-power point is equal to the value obtained for the interfacial energy gap, $\Delta\epsilon_I$. This exact agreement, however, should not be taken seriously. Also, in the heterojunction the In$_{1-x}$Ga$_x$P epitaxial layer was doped to produce 2.5×10^{17} cm^{-3} holes, while the GaAs substrate has 1.4×10^{18} cm^{-3} electrons. Thus,

FIG. 1. Abrupt heterojunction model for In$_{1-x}$Ga$_x$P-GaAs indicating schematically the photon-assisted tunneling processes for electrons on the p side and holes on the n side.
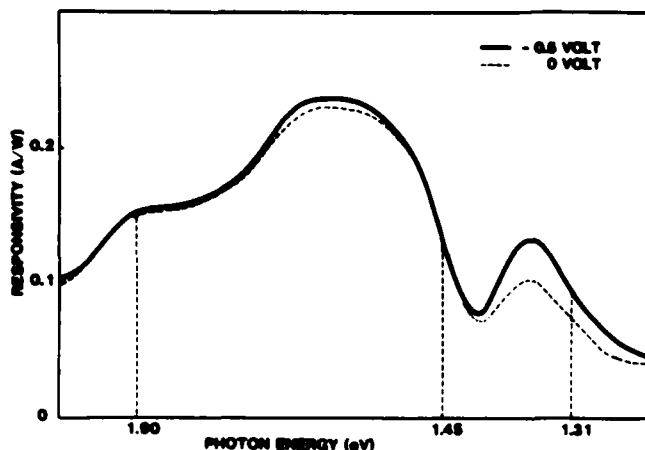

FIG. 2. Responsivity as a function of photon energy for the heterojunction of Fig. 1 showing below band-gap response at two bias voltages.

most of the potential was in the $In_{1-x}Ga_xP$ where it should enhance the lower effective mass and higher probability electron tunneling. The GaAs absorption edge is apparently shifted to higher than band-gap energy due to the high electron concentration.[11]

To test the concept that the below band-gap response is associated with tunneling across the interfacial energy gap, several other experiments were performed. When the doping of the p-type $In_{1-x}Ga_xP$ was increased from 2.5×10^{17} to 6.0×10^{18} cm^{-3} on the same n-type GaAs substrates, the below band-gap response was greatly reduced. Increased doping on the p side is expected to reduce electron tunneling. Since large effective mass hole tunneling from the n side is much less probable, the smaller below band-gap response is consistent with a tunneling mechanism. To eliminate the possibility that the below band-gap response was due to impurity transitions in the space-charge region on either side of the interface, photoconductivity measurements were performed on the epitaxial layer and on the substrate. These measurements indicated no below band-gap photoresponse at the same energy due to impurities. Except for the coincidence of the response energy with $\Delta\epsilon_1$, we cannot, however, rule out the possibility of impurity transitions at the interface itself.

In conclusion, we have observed below band-gap photovoltaic response in $In_{1-x}Ga_xP$-GaAs p-n heterojunctions which is apparently due to photon-assisted tunneling across the interfacial energy gap between the two materials. Although the observed response for {111} interfaces at 1.31 eV is not at a particularly useful wavelength, it should be possible to apply the same idea for infrared detectors at longer wavelengths. We are currently investigating the possibility of obtaining smaller interfacial energy gaps in the $In_{1-x}Ga_xP$-GaAs system by examining interfaces with different orientations. Other lattice-matched heterojunction systems, of course, should also be examined. Our results indicate, however, that heterojunctions with the required band lineups cannot be predicted with great reliability.

[1] J. O. Dimmock, I. Melngailis, and A. J. Strauss, Phys. Rev. Lett. 16, 1193 (1966).

[2] W. Franz, Z. Naturforsch A 13, 484 (1958); L. V. Keldysh, Sov. Phys. JETP 7, 788 (1958).

[3] G. E. Stillman, C. M. Wolfe, J. A. Rossi, and J. P. Donnelly, Appl. Phys. Lett. 11, 671 (1974).

[4] J. C. Dyment, F. P. Kapron, and A. J. Springthorpe, *Institute of Physics Conference Series No. 24* (Institute of Physics, London, 1975), p. 200.

[5] Kathie E. Newman and John D. Dow, Phys. Rev. B 27, 7495 (1983).

[6] H. Kroemer and G. Griffiths, IEEE Electron Device Lett. 4, 20 (1983).

[7] See G. E. Stillman and C. M. Wolfe, in *Semiconductors and Semimetals*, edited by R. K. Willardson and A. C. Beer (Academic, New York, 1977), Vol. 12, p. 291.

[8] G. B. Stringfellow, P. F. Lindquist, and R. A. Burmeister, J. Electron. Mater. 1, 437 (1972).

[9] J. A. Van Vechten, Phys. Rev. 187, 1007 (1969).

[10] W. A. Harrison, E. A. Kraut, J. R. Waldrop, and R. W. Grant, Phys. Rev. B 18, 4402 (1978).

[11] E. Burstein, Phys. Rev. 93, 632 (1954); T. S. Moss, Proc. Phys. Soc. (London) B 76, 775 (1954).

8. Below Bandgap Emission and Absorption in ZnSnP₂/GaAs Heterojunctions

E. A. PATTEN, G. A. DAVIS, S. J. HSIEH, AND C. M. WOLFE, FELLOW, IEEE

Abstract—Below bandgap emission and absorption are observed in p-ZnSnP₂ on n-GaAs heterojunctions. The band lineup of this heterostructure system suggests that the below bandgap transition is between the valence bands of GaAs and the conduction band of ZnSnP₂ at the interface. The predicted value for the interfacial gap of $E_I = 1.27$ eV compares with an experimental value of 1.31 eV.

I. INTRODUCTION

THERE IS CONSIDERABLE current interest in III–V compound and alloy heterostructures because of the capability they provide for tailoring energy bands in lattice-matched materials systems. This capability, however, can be increased substantially by including lattice-matched heterostructures between chalcopyrite II–IV–VI₂ compounds and alloys [1] and the above sphalerite materials. In this letter we present experimental evidence on and discuss the use of p-ZnSnP₂ on n-GaAs heterojunctions to emit and detect radiation below the bandgaps of the constituent semiconductors.

The band diagram for ZnSnP₂/GaAs in forward bias is shown in Fig. 1. This heterojunction has an energy-band lineup, which, as discussed previously [2], may provide a source of below bandgap emission. The mechanism, indicated in Fig. 1, involves the tunneling of electrons across the interfacial region either to or from virtual states in the gap. This enables long-wavelength radiative recombination of the confined electrons and holes in adjacent wells on the two sides of the interface. Although the band diagram in Fig. 1 is for a forward-biased heterojunction, the equilibrium configuration is very similar only with deeper wells and wider space-charge regions. Therefore, long-wavelength absorption also appears possible involving the inverse of the process just described [3].

Photovoltaic, photoconductivity, Hall, I–V, and CV measurements were performed to determine the necessary band parameters to construct an interfacial band diagram. This construction yielded a value for the interfacial energy E_I. The photovoltaic and emission experiments revealed a below bandgap peak which is compared with the theoretical value of E_I. Other significant aspects of the data as they pertain to the model are discussed.
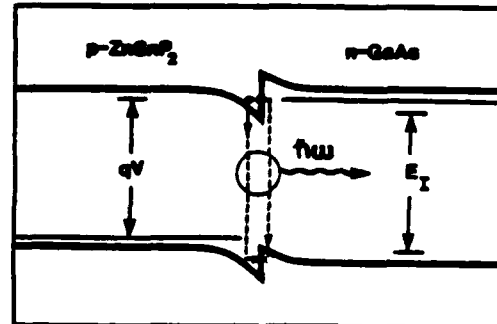
Fig. 1. Abrupt ZnSnP₂/GaAs heterojunction in forward bias with mechanism for tunneling-assisted radiative recombination indicated.

II. DEVICE FABRICATION

The heterostructures used in this investigation consisted of liquid-phase epitaxial (LPE) layers of ZnSnP₂ grown on {211} Ga–GaAs with a lattice mismatch of less than 0.44 percent. The details of the growth process were reported earlier [4]. The {211} orientation of the GaAs substrate was chosen since it has been shown to suppress antiphase domain boundaries associated with different c-axis orientations in the chalcopyrite ZnSnP₂ layer [5]. The devices were defined with standard photolithographic techniques and mesa-etched with Br-methanol to an area of 2×10^{-3} cm².

The GaAs substrates used were n⁺($\approx 10^{18}$ cm⁻³), and the ZnSnP₂ was grown p⁺($\approx 10^{19}$ cm⁻³), according to Hall measurements on ZnSnP₂ layers grown on semi-insulating (SI) GaAs. There was some evidence of Zn diffusion into the GaAs substrates. Delineation etches of ZnSnP₂ layers grown on SI substrates revealed both a growth interface and a diffusion front of about 1 μm into the substrate. When the ZnSnP₂ growth was performed on n⁺-GaAs, however, the diffusion of Zn was not large enough to convert the GaAs to p-type, as evidenced by a single line visible at the interface. In a similar manner, electron microprobe analysis indicated outdiffusion of Ga (but not As) into less than 1 μm of the ZnSnP₂ with no type conversion.

III. RESULTS AND DISCUSSION

The bandgaps of the two materials were obtained through photoconductivity and photovoltaic measurements. The value for the n⁺-GaAs bandgap was determined to be 1.42 eV. The ZnSnP₂ bandgap of 1.45 eV was determined from differential analysis of photoconductivity data for layers grown on SI GaAs. This method was used since a clear peak for ZnSnP₂ was not apparent in the photovoltaic spectra on

Fig. 2. Room-temperature absorption and emission spectra of a ZnSnP₂/GaAs heterojunction. Absorption spectrum is measured at zero bias whereas the emission is measured at 10-A·cm⁻² current density.

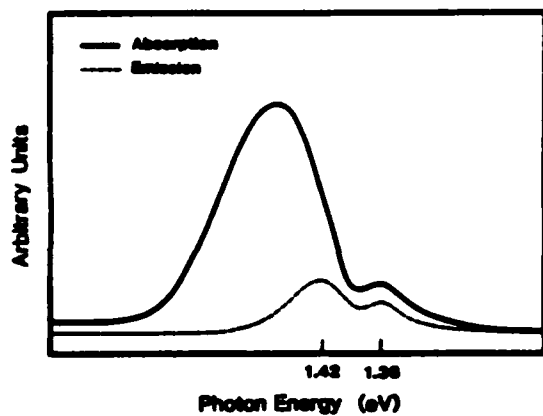Fig. 3. Emission spectra for forward-biased ZnSnP₂/GaAs heterojunction at 10, 10, 30, and 40-A·cm⁻² constant current density.

n⁺-GaAs. The value of 1.45 eV for ZnSnP₂ is consistent with previous measurements [6].

CV measurements were performed to obtain a value for the built-in potential V_0. This method uses a linear extrapolation of C^{-2} versus V to zero. The largest value of V_0 obtained in this manner was 1.75 V. We used this value in the analysis that follows since the measured V_0 should decrease when interface charge (of either sign) is present. The true V_0 can only be obtained by correcting for the interface charge.

To compare with this experimental value, a theoretical estimate of the built-in potential can be determined from the ionization energies, the energy gaps, and the relative positions of the electrochemical potential in the two materials. Using a dielectric model [7], we calculated an ionization energy of 5.91 eV for ZnSnP₂ and used an experimental ionization energy of 5.50 eV for GaAs [8]. In determining the densities of states, we took $m_e^* = 0.0665\, m_0$ for GaAs [9] and $m_h^* = 0.39\, m_0$ for ZnSnP₂ [6]. The carrier concentrations were $n = 8 \times 10^{17}$ cm⁻³ for the GaAs substrate and $p = 5 \times 10^{19}$ cm⁻³ for the ZnSnP₂. Using the band parameters from these numbers yields a built-in potential of 1.74 V. The close agreement between this and the experimental value of 1.75 V, however, should not be taken too seriously. The above parameters also allow us to calculate a value for the interfacial energy E_I, which designates the energy difference between the bottom of the electron well and the top of the hole well. The above numbers yield a value of $E_I = 1.27$ eV.

To compare the above calculated value of E_I with our experimental value, consider the results shown in Fig. 2. The higher solid curve is the photovoltaic response (or absorption) of the heterojunction. The lower dashed curve is the emission spectrum of the heterojunction in forward bias at a constant current density of 10 A·cm⁻². The higher energy emission peak has its maximum at the energy of the half power point of the higher energy absorption peak. From their energies, these peaks appear to be the emission and absorption peaks for GaAs. For a band-to-band transition one expects this kind of relation between the absorption and emission peaks.

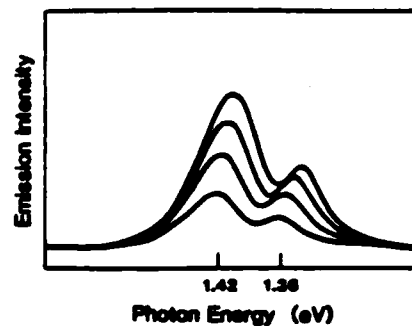The other set of peaks at lower energy have their maxima

at approximately the same value. This would be expected for transitions between the wells shown in Fig. 1. Usually one extracts the absorption edge from an absorption peak by using the half power point energy. For the absorption and emission peaks associated with the interfacial gap, one might extrapolate the steep part of the tail down to the zero line since neither significant absorption nor emission is expected below E_I using our model. The emission peak extrapolates to approximately 1.31 eV and absorption peak to about 1.30 eV. These values are in reasonable agreement with our theoretically predicted value of 1.27 eV.

An obvious concern in analyzing the data is the possibility that the low energy peak may not be due to the mechanism we have described but rather to transitions involving impurity levels in the gap. The energy coincidence of the emission and absorption peaks contradicts an impurity level interpretation, since a shift in these energies when impurities are involved is usually observed due to the Franck–Condon principle [10].

Also of interest in both spectra is the absence of an observable ZnSnP₂ peak. In the emission mode, minority carriers are injected into both sides of the heterojunction and participate in the various recombination processes. The supply of recombining species is much more plentiful on the GaAs side due to the much larger majority carrier concentration of the ZnSnP₂. Therefore, it is reasonable that the GaAs emission may be the only band-to-band transition observable. In the absorption mode, the space-charge region on the GaAs side is much larger than that on the ZnSnP₂ side. Since only this portion of the device contributes to the absorption signal, again it is reasonable to only see the GaAs peak.

Finally, in Fig. 3 we see the emission spectra shift to longer wavelengths with increasing current through the device. The spectra shown are for 10-, 20-, 30-, and 40-A·cm⁻² constant current density. This shift is most likely due to device heating. Double-crystal X-ray diffraction measurements indicate no difference in thermal expansion between ZnSnP₂ and GaAs from room temperature to about 150°C. Since the lattice constants on both sides of the interface expand together at the same rate, we expect to see the two emission peaks move at about the same rate with respect to current, as in Fig. 3.

IV. CONCLUSIONS

The results on below bandgap emission in ZnSnP₂/GaAs heterojunctions tend to confirm previous expectations [2] that

heterostructures with this type of "staggered" band lineup have potential application as photon emitters. The absorption results are also consistent with the below bandgap absorption recently observed [3] in $In_{1-x}Ga_xP/GaAs$ heterojunctions with similar band lineups. In addition, our results show that chalcopyrite-on-sphalerite heterostructures with reasonably good interfacial properties can be attained.

REFERENCES

[1] J. L. Shay and J. H. Wernick, *Ternary Chalcopyrite Semiconductors.* Oxford: Pergamon Press, 1975.

[2] H. Kroemer, "Staggered-lineup heterojunctions as sources of tunable below-gap radiation: Operating principle and semiconductor selection," *IEEE Electron Device Lett.*, vol. EDL-4, pp. 20–22, 1983.

[3] S. J. Hsieh, E. A. Patten, and C. M. Wolfe, "Below bandgap photoresponse of $In_{1-x}Ga_xP$–GaAs heterojunctions," *Appl. Phys. Lett.*, to be published.

[4] G. A. Davis and C. M. Wolfe, "Liquid phase epitaxial growth of ZnSaP₂ on GaAs," *J. Electrochem. Soc.*, vol. 130, pp. 1408–1412, June 1983.

[5] G. A. Davis, M. W. Muller, and C. M. Wolfe, "Antiphase domain boundary suppression in chalcopyrite on sphalerite epitaxy," *J. Crystal Growth*, to be published.

[6] N. A. Groyunova, M. L. Belle, L. B. Zlatkin, G. V. Loshakova, A. S. Poplavnoi, and V. A. Chaldyshev, "Optimal properties and band structure of ZaSaP₂," *Sov. Phys.-Semicond.*, vol. 2, pp. 1126–1132, 1969.

[7] J. A. Van Vechten, "Quantum dielectric theory of electronegativity in covalent systems. II. Ionization potentials and interband transition energies," *Phys. Rev.*, vol. 187, pp. 1007–1012, 1969.

[8] G. W. Gobeli and F. G. Allen, "Photoelectric properties of cleaved GaAs, GaSb, InAs, and InSb surfaces: comparison with Si and Ge," *Phys. Rev.*, vol. 137, p. A245, 1965.

[9] G. E. Stillman, C. M. Wolfe, and J. O. Dimmock, "Magnetospectroscopy of shallow donors in GaAs," *Solid-State Commun.*, vol. 7, pp. 921–925, 1969.

[10] J. Franck, "Elementary processes of photochemical reactions," *Trans. Faraday Soc.*, vol. 21, p. 536, 1925; E. U. Condon, "Nuclear motions associated with electron transitions in diatomic molecules," *Phys. Rev.*, vol. 32, pp. 858–866, 1928.

9. Spatially varying band structures

P. Roblin

Department of Electrical Engineering, The Ohio State University, Columbus, Ohio 43210

M. W. Muller

Department of Electrical Engineering, Washington University, St. Louis, Missouri 63130

(Received 13 May 1985)

Advances in technology have made possible the fabrication of rapidly varying heterostructures which hold the promise of important applications. We develop a set of approximate treatments of electron states in a variety of layered heterostructures. The approximations are all based on the concept of one-band generalized Wannier functions. Following a discussion of the validity of this representation, we apply it to an evaluation of the bound states in a narrow quantum well in GaAs, which clearly demonstrates the mixing of main and satellite valley states as well as the contribution of evanescent states, and of the states of a superlattice in a model structure of up to 20 quantum wells. As a final example we discuss the application of generalized Wannier functions to the matching of electronic states at a heterojunction between two model band structures with different effective masses, and compare the formalism with alternative approaches to this problem.

With the development of special growth techniques such as molecular beam epitaxy (MBE) and metal organic chemical vapor deposition (MOCVD), tailor-made submicron semiconductor heterostructures can now be designed. An entirely new variety of structures, including quantum wells, superlattices, and modulation-doped structures, can be conceived and some have already led to successful device applications. Quantum wells are being investigated in semiconductor lasers[1] and resonant tunneling[2] for submillimeter radiation. Potential applications for superlattices include nonlinear optics in relation to optical switching (bistability),[3] the Bloch oscillator,[4] and the Zener oscillator[5] for submillimeter radiation. An important application of modulation doping[6] is the high electron mobility transistor, a low-noise microwave amplifier,[7] and a candidate for high-speed logic.[8]

These semiconductor heterostructures are made of successive semiconductor crystal layers grown on top of each other. Provided the lattice parameters are closely matched, the lattices of the semiconductors essentially cohere with a minimal perturbation. Due to the special growth techniques used, the spatial variation of the semiconductor materials and/or of the doping can be controlled so as to occur in a few lattice parameters.

The physical properties of the structures of these semiconductors are the object of extensive theoretical and experimental effort with respect to important potential device applications, some of which were mentioned above, but most of which, however, remain unrealized.

A fundamental property on which all these heterostructures rely is the spatial variation of the band gap and the conduction and valence band structures. In this paper, we shall be concerned with the development of a consistent and simplified picture of spatially varying band structures.

Band structures derive from the periodic nature of the crystal potential and are therefore mathematically well de-fined only for an infinite crystal. However, in practice, the concept of bands holds on a microscopic scale. This is exemplified by the use of band diagrams in classical device theory. The total classical Hamiltonian H can be written as

$$H(\mathbf{k},\mathbf{r}) = E(\mathbf{k}) - eV(\mathbf{r}) , \qquad (1)$$

where $E(\mathbf{k})$ is the conduction or valence band structure, e the electron charge, and $V(\mathbf{r})$ the electrostatic potential. The symbol $\mathbf{r}$ denotes the spatial location and $\mathbf{k}$ the Bloch wave vector or quasimomentum. In a band diagram, usually only the bottom of the conduction band and the top of the valence band are represented, which is equivalent to specifying $\mathbf{k}$.

Equation (1), together with the acceleration theorem,[9] constitute the semiclassical picture on the basis of which one can describe the ballistic motion of an electron or derive (using the Boltzmann transport equation) the standard device equations.[10] In the heterostructures discussed above, the spatial dimensions are made sufficiently small for the quantization of the electron states to be significant. One needs then to revert to the quantum-mechanical form of Eq. (1) where the quasimomentum is replaced by the operator

$$\mathbf{k} = -i\frac{\partial}{\partial \mathbf{r}} , \qquad (2)$$

and to solve the Schrödinger equation,

$$i\hbar\frac{\partial}{\partial t}\psi(t,\mathbf{r}) = H\psi(t,\mathbf{r}) .$$

Equation (1), together with (2), is often referred to as the Wannier theorem, the derivation of which can be found in textbooks on semiconductor theory.[11] The Wannier theorem relies on two basic assumptions. The first is the one-band approximation which holds if the perturbation potential $V(\mathbf{r})$ is not strong enough for band mixing

to occur or interband transition such as tunneling to take place. Secondly, the perturbation potential should vary slowly or smoothly with position so as to constrain the potential overlap matrix to a diagonal representation.

These assumptions are adequate for the classical representation in which the electrons are essentially free and can be represented by a wave packet $\Psi(r)$. For the submicron heterostructures of interest here, these assumptions do not hold, as the potential variations in modulation-doped or in spatially varying band-gap structures are both large and can occur in a few lattice parameters. In this paper we shall propose a concept of generalized band structures for which the Wannier theorem can be generalized and applied to submicron heterostructures.

First, we shall rederive the Wannier theorem in Sec. I, specializing it to one-dimensional structures. Since the submicron heterostructures grown by MBE or MOCVD are layered structures, a one-dimensional picture can be implemented, provided some assumptions are made. Such one-dimensional models are of heuristic interest as their simplicity promotes a better insight, and they are sometimes used in semiquantitative studies.

In Sec. II we discuss the extension of the Wannier theorem, using the generalized Wannier functions, and study in Sec. III two examples of heterostructures. These examples constitute both a test and a demonstration of applications of the generalized Wannier picture. Finally, we present in Sec. IV the application of the generalized Wannier picture to "true" heterostructures and discuss the generalization of the concept of bands to spatially varying band structures.

I. THE ONE-DIMENSIONAL WANNIER PICTURE

In this section we consider the problem of a crystal electron in an external one-dimensional potential U. The total Hamiltonian of the electron is given by

$$H = H_0 + U(\hat{d} \cdot r) ,$$

where H_0 is the unperturbed crystal Hamiltonian and $U(x)$ is the one-dimensional energy potential varying along an axis (the device axis) represented by the unit vector $\hat{d}$.

We assume the device axis to be parallel to the lattice vector. We only consider face-centered-cubic semiconductor lattices for which a lattice vector $R(n)$ can be written using the orthonormal basis of the Bravais lattice as $R(n) = An$, with n a set of integers (n_1, n_2, n_3), a^* the lattice parameter of the cubic lattice, and A the matrix

$$A = \frac{a^*}{2} \begin{bmatrix} 0 & 1 & 1 \\ 1 & 0 & 1 \\ 1 & 1 & 0 \end{bmatrix} .$$

We shall denote as a the modulus of the smallest lattice vector a parallel to $\hat{d}$; a is therefore the effective lattice parameter along the direction $\hat{d}$, and any lattice vector parallel to $\hat{d}$ is written $R = na$, with n an integer.

A reciprocal-lattice vector K is written in the same basis as $K(l) = Bl$, with l a set of integers (l_1, l_2, l_3) and B the matrix

$$B = \frac{2\pi}{a^*} \begin{bmatrix} -1 & 1 & 1 \\ 1 & -1 & 1 \\ 1 & 1 & -1 \end{bmatrix} ,$$

so that $AB = 2\pi$. It is easy to prove that for cubic lattices there always exists a reciprocal-lattice vector parallel to a given direct-lattice vector. This is equivalent to finding the constant c such that $K = cR$. A possible solution is $c = 8\pi/a^{*2}$, which leads to

$$l = \begin{bmatrix} 2 & 1 & 1 \\ 1 & 2 & 1 \\ 1 & 1 & 2 \end{bmatrix} n .$$

We shall denote q as the modulus of the smallest reciprocal-lattice vector q parallel to $\hat{d}$ so that any reciprocal vector parallel to $\hat{d}$ can be written $K = lq$, with l an integer. Since the lattice vector and the reciprocal-lattice vector satisfy the relation

$$R(n) \cdot K(l) = 2\pi n \cdot l ,$$

we have that q and a satisfy

$$a \cdot q = aq = 2\pi p ,$$

with p an integer. For the $\langle 100 \rangle$ direction $[R = a(1,0,0)]$, we have $n = (-1,1,1)$, and the smallest reciprocal vector is given by $l = (0,1,1)$, so that $a = a^*$ and $p = 2$.

In the extended zone scheme the Bloch-function solution $\phi(k,r)$ of

$$H_0 \phi(k) = E(k) \phi(k) \qquad (3)$$

is a periodic function of k along the device direction $\hat{d}$. We can introduce a one-dimensional quasimomentum k along the device direction $\hat{d}$ defined by

$$k(k) = k_\perp + k\hat{d} ,$$

with $k_\perp$ the transverse momentum perpendicular to the direction $\hat{d}$. It follows that a Bloch function along the direction $\hat{d}$ can be written as $\phi(k\hat{d} + k_\perp, r) = \phi(k)$, which is a periodic function of k with period q: $\phi(k + nq) = \phi(k)$ for n, an integer.

We can now define, along the direction $\hat{d}$, a one-dimensional Wannier function $w(m, r, k_\perp)$ as the spatial Fourier coefficient of the Bloch function $\phi(k)$,

$$w(m, r, k_\perp) = (1/\sqrt{q}) \int_{-q/2}^{q/2} \phi(k\hat{d} + k_\perp, r)$$
$$\times \exp(-ikm\, 2\pi/q) dk , \qquad (4)$$

and reciprocally we have

$$\phi(k\hat{d} + k_\perp, r) = (1/\sqrt{q}) \sum_m w(m, r, k_\perp) \exp(ikm\, 2\pi/q) .$$

From the orthogonality property of the Bloch functions and from Eq. (3), one easily verifies that these Wannier functions (WF's) form an orthogonal set

$$\langle w(n) | w(m) \rangle = \int_{-\infty}^{\infty} w(n, r, k_\perp)^* w(m, r, k_\perp) dx' = \delta_{nm} ,$$

P. ROBLIN AND M. W. MULLER

with $x' = \hat{d} \cdot r$, and satisfy the useful property

$$H_0 w(m, r, k_\perp) = \sum_n E(n - m) w(n, r, k_\perp) ,$$

with

$$E(n) = (1/q) \int_{-q/2}^{q/2} E(k_\perp + k\hat{d}) \exp(-ikn \, 2\pi/q) dk .$$

The $E(n)$ are recognized as the Fourier coefficients of the band structure along the line $k(k)$ parallel to the device axis.

For a sufficiently smooth and weak one-dimensional potential $U(\hat{d} \cdot r)$, no band mixing is expected and the transverse momentum is conserved. One can then expand the electron state in Wannier functions of the band considered with an envelope $f(n,t)$,

$$\Psi = \sum_n f(n,t) w(n, r, k_\perp) . \tag{5}$$

The weight function $|f(n,t)|^2$ is the probability of finding the electron at the lattice site n at time t. Replacing Ψ in the Schrödinger equation

$$H\Psi = i\hbar \frac{\partial}{\partial t} \Psi \tag{6}$$

by the expansion of Eq. (5), multiplying Eq. (6) by $w(n)^*$, and integrating over x', one obtains the Wannier recurrence equation

$$\sum_m [E(n - m) + U(n,m)] f(m,t) = i\hbar \frac{\partial}{\partial t} f(n,t) , \tag{7}$$

where $U(n,m)$ is the matrix element given by

$$U(n,m) = \langle w(n) | U | w(m) \rangle$$

$$= \int_{-\infty}^{\infty} w(n, r, k_\perp)^* U(\hat{d} \cdot r) w(m, r, k_\perp) dx' . \tag{8}$$

The one-band Wannier recurrence equation derived holds for sufficiently small perturbation potentials U. For Eq. (7) to be solved, both the band-structure Fourier coefficients and the matrix elements $U(n,m)$ are required.

As expressed by Eq. (8), the matrix elements are evaluated from the Wannier functions. Techniques for the evaluation of the Wannier functions have been developed by Kohn.[12] The evaluation of the WF for silicon has been recently reported by Kane and Kane;[13] however, the WF derived is a linear superposition of the WF's of the four valence bands. The evaluation of realistic WF's is a complicated matter, which we would like to avoid in the simple picture we intend to develop.

Some direct approximations can be derived from the properties of the WF's. In the case of simple bands, it is possible to select the phase of the Bloch functions so that the WF's are exponentially localized.[14] From both the orthogonality and the tight localization of the WF's, it follows that the matrix element of a smooth potential is accurately represented by the sampling of the potential at the lattice sites:

$$U(n,m) = U(x' = na/p)\delta_{nm} . \tag{9}$$

We shall discuss in Sec. III the extent to which these approximations can be used for sharply varying potentials.

Finally, an important property of the one-dimensional WF's which we did not address so far is their invariance under translation from one lattice site to another. Following the approach of Wannier,[15] we first write

$$\Psi(k, r - R) = (1/\sqrt{q}) \sum_m \exp(ikma/p) w(m, r - R, k_\perp) , \tag{10}$$

which using the translation property of the Bloch function, can be written

$$\Psi(k, r - R) = (1/\sqrt{q}) \sum_m \exp(-ik \cdot R) \exp(ikma/p)$$

$$\times w(m, r, k_\perp) .$$

For $R = n\mathbf{a}$, we have

$$k \cdot R = (k\hat{d} + k_\perp) \cdot R = k\hat{d} \cdot R = kna ,$$

and changing the index of summation we obtain

$$\Psi(k, r - R) = (1/\sqrt{q}) \sum_m \exp(ikma/p) w(m + np, r, k_\perp) . \tag{11}$$

Identifying the coefficients in the series (10) and (11), we finally get

$$w(m, r - n\mathbf{a}, k_\perp) = w(m + np, r, k_\perp) .$$

Considering the $\langle 100 \rangle$ direction for which $p = 2$, it follows that there exist two sets of WF's, each of which can be generated from two generic WF's by a lattice translation

$$w(2n, r) = w(0, r - n\mathbf{a}), \quad w(1 + 2n, r) = w(1, r - n\mathbf{a}) .$$

The number of WF's for a given direction is therefore given by p for the face-centered-cubic lattice considered. For our purpose it is convenient to picture these WF's as located at p sites along the lattice vector $\mathbf{a}$ associated with the direction $\hat{d}$. We can then write these WF's as

$$w(n, r, k_\perp) = w(x' - na/p, r_\perp, k_\perp) = w(x' - na/p) = w(n) ,$$

where a is the effective lattice parameter for the direction $\hat{d}$. The one-dimensional WF we have introduced is in fact a hybrid entity, since it corresponds to the Bloch state $k_\perp$ for the transverse coordinates $r_\perp$. The properties of the WF's of one-dimensional lattices cannot be assumed to apply directly to the one-dimensional WF we have defined. Therefore, problems concerning the reality of the WF and the simultaneous convergence of the WF's remain to be addressed. These studies are not trivial matters for three-dimensional crystals,[14] in particular for lattices without a center of inversion.

In our simplified treatment we shall assume the picture developed to be truly one-dimensional. The reality and exponential localization of the WF's in one-dimensional structures are discussed by Kohn.[16] More recent work by Zak[17] raises the one-dimensional Wannier picture to the status of a well-defined representation in quantum mechanics and introduces the canonical Wannier function with minimal position uncertainty and located in the zero cell of the Bravais lattice.

Zak also demonstrates that the position operator has a

discrete spectrum. This implies that the applied potentials are transformed by the one-band approximation into steplike potentials. This is due to the inability of the one-band approximation to deal with the perturbation of the inner crystal potential. However, as we shall see in the next section, most of the band mixing can be formally accounted for with the use of the generalized Wannier function. For stronger potentials it is further necessary to account for the polarization of the semiconductor.[18]

II. THE GENERALIZED WANNIER PICTURE

In this section we shall be concerned only with abrupt modulation-doped heterostructures or models of abrupt heterostructures for which the band gap is spatially varying while the band structure is assumed to be conserved.

The one-dimensional Wannier picture developed in the previous section is capable of handling fast spatial variation of the potential since the nondiagonal term of the matrix potential $V(n,m)$ can be accounted for. However, the formalism developed relies on the one-band approximation which strictly holds only for small potential perturbations. Its use for submicron heterostructures seems unjustifiable. Indeed, the band-edge variation in these structures is large and band mixing is expected.

One should then resort to a multiband expansion, and the envelope equation (7) now reads

$$i\hbar\frac{\partial}{\partial t}f(n,b)=\sum_m\left[E(n-m,b)f(m,b)+\sum_{b'}\langle w(n,b)|U(x)|w(m,b')\rangle f(m,b')\right],$$

where b is the band index.

It is, however, possible to avoid a multiband expansion if one introduces the concept of generalized bands. As was remarked by Zak,[17] "a band is a surprisingly stable entity under external perturbations." This might seem to be a paradoxical statement coming from Zak, who has been very critical of the use of the one-band approximation in general,[19] and in particular for the Stark effect.[20] In fact, the existence of bands under external perturbations does not rely on the one-band approximations. A band of energy is essentially a quasicontinuum of energy states. Such an entity seems to survive numerous mistreatments such as high impurity concentrations, alloying with random distribution of two atoms on a given sublattice in III-V compounds, even for abrupt heterojunctions. However, surface states or band tailing or even alloy and roughness scattering effects occur, and it might be more accurate to refer to these bands as generalized bands. Such bands in most cases can only be represented mathematically as resulting from the mixing of the bands of the unperturbed crystals. This is similar to the expansion of the pseudo-wave-function in terms of plane waves in the calculation of band structures using the pseudopotential method; the bands evaluated result from the mixing of the bands of the empty lattice.

A one-band formalism can then be developed if one uses the exact Wannier functions instead of the Wannier functions of the unperturbed lattice. It remains to be demonstrated that such Wannier functions exist. The Wannier functions as we introduced them [see Eq. (4)] are defined as Fourier coefficients of the Bloch functions which are periodic in k space. The quasimomentum is defined by the translation operator[15] only for periodical potentials. At a heterojunction, the periodicity is broken and no quasimomentum, Bloch functions, or Wannier functions can be defined, but one can attempt to generalize the entities, as the periodicity is essentially broken only at the junction. The most obvious approach is to generalize the Wannier functions which are strongly localized on each lattice site and therefore will be strongly perturbed only at the junction itself.

The existence of generalized Wannier functions (GWF's) has been theoretically established by Kohn and Onffroy[21] for one-dimensional structures. These Wannier functions can be labeled by their generalized band index; they account, however, for the presence of interface states in the forbidden band gap.[22] We shall denote these generalized Wannier functions as $a(n,x)$. They span the same function space as the eigenfunctions of the perturbed lattice for the same generalized band.

The index n will be taken here as the site index, although depending on the potential well there may be more than one or even no GWF's associated with the interface sites. The GWF's are localized about the lattice site (or the periodic potential minima). Rehr and Kohn have shown[23] that they can be exponentially localized. An essential property of the GWF's is that they form an orthonormal set

$$\langle a(n)|a(m)\rangle=\int_{-\infty}^{\infty}a(n,x)a(m,x)dx=\delta_{nm}.$$

The eigenfunctions are linear combinations of $a(n,x)$,

$$\Psi(x,E)=\sum_n f(n,E)a(n,x),$$

with $f(n,E)$ the solution of

$$Ef(n,E)=\sum_m H(n,m)f(m,E),\qquad(12)$$

where $H(n,m)$ is the Hamiltonian matrix element given by

$$H(n,m)=\langle a(n)|H|a(m)\rangle.$$

Here H is the total Hamiltonian of the heterojunction given by

$$H=H_0+U(x),$$

with H_0 the unperturbed crystal potential and $U(x)$ the heterojunction effective potential.

Equation (12) is similar to Eq. (7), except that we use the GWF instead of the unperturbed Wannier functions. The knowledge of the GWF weight $f(n,E)$ is sufficient in

P. ROBLIN AND M. W. MULLER

most applications and Eq. (12) can be solved if the matrix element $H(n,m)$ is known.

The derivation of the matrix element is the critical part of this method. One approach consists of first deriving the GWF's at each site. An important property of the GWF's demonstrated by Kohn and Onffroy states that for lattice sites far from the interface the GWF's approach the unperturbed WF exponentially in n,

$$a(n,x) \simeq w(x-na) \text{ for } |n| \gg 0 ,$$

assuming the interface at $n=0$. Only a few GWF's are found to be perturbed or to differ from the WF, as was reported by Gay and Smith.[22] It follows that a few lattice parameters away from the interface the Wannier picture developed in Sec. I holds and the only remaining unknown terms are the interface Hamiltonian matrix terms.

A variational method for the derivation of the GWF has been proposed by Kohn and Onffroy for one-dimensional potentials and was tested by Gay and Smith.[22] A three-dimensional treatment is required for the heterostructures of interest here. The derivation of the Wannier functions in three dimensions being quite involved,[13] the derivation of the more complicated GWF will not be considered as a practical approach. For our present purposes, we shall use for the Hamiltonian matrix simple approximations derived from the general properties of the Wannier functions discussed in Secs. I and II.

The essential result brought about by the GWF formalism is that as long as a generalized band of energy can be assumed, it is possible to lump all the band-mixing effects into the interface Hamiltonian matrix elements, whereas the wave function $f(n)$ remains given by an equivalent Hamiltonian recurrence equation.

III. TWO SIMPLE EXAMPLES

We shall now consider two simple applications of the Wannier picture. The first consists of the evaluation of the resonant states in a square quantum well 0.5 eV deep using GaAs band structure. One expects to observe the interaction of the upper-valley and central-valley states of GaAs for such a deep well.[24]

These band-structure data, kindly furnished by Professor Karl Hess of the University of Illinois, were given at a set of sampled points in the Brillouin zone. Using the

FIG. 2. Fourier coefficients of the Γ to X band structure of Fig. 1.

sampling theorem, we reconstituted the band structure. The band structure was in addition fitted at Γ to $0.068 m_0$. This consequently slightly altered the smoothness of the upper valley. The resulting band structure of GaAs along Δ is shown in Fig. 1. The amplitudes of the Fourier coefficients of the GaAs band structure along Δ are plotted in Fig. 2. We present in Fig. 3 the locus of the amplitude of the roots $\exp[jk_i(E)a]$ that solve the equation $E(k_i)=E$, where $E(k)$ is the band structure along Δ. One obtains 20 roots. Roots 1 and 2 correspond to Bloch wave functions of the central valley at Γ. Roots 3 and 4 correspond to the Bloch waves of the upper valley centered on X. The unexpected behavior at X of roots 5, 6, 7, and 8 is due to the fact that the upper-valley minimum does not occur exactly at X. The shift of the X minimum
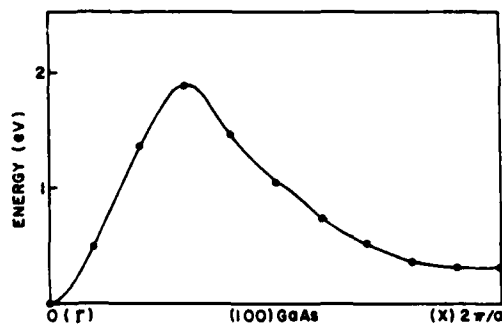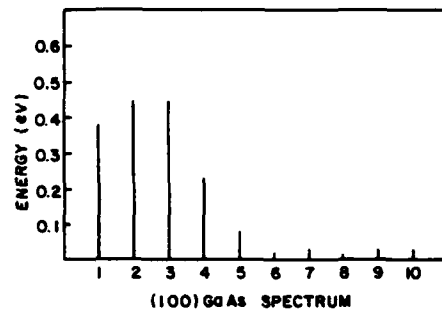

FIG. 1. GaAs band structure along Δ (dots: original sampled data; solid curve: reconstructed band structure with effective mass fitted at Γ to $0.068 m$).
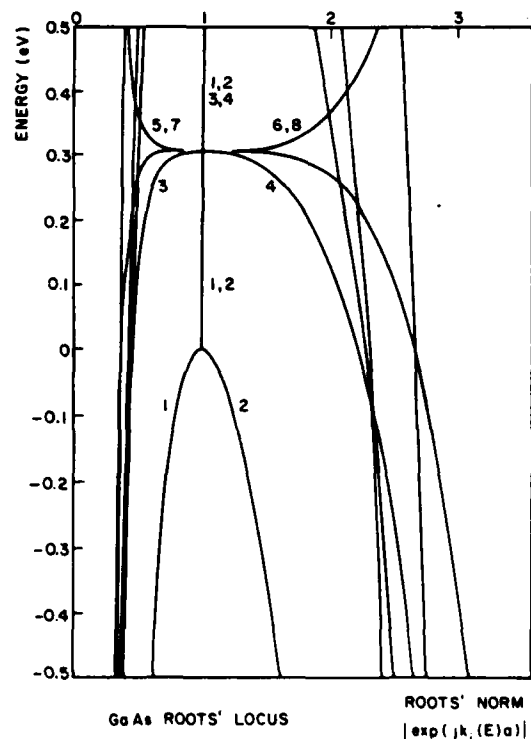

FIG. 3. Locus of the roots of GaAs band structure of Fig. 1 as a function of the energy.

is an artifact of the spectrum truncation. Since the band structure is slightly distorted, we do not expect these roots to contribute much. There are finally 12 remaining roots with a very high damping rate. These roots contribute only within the matching area. One observes in Fig. 3 the evanescent Bloch waves being transformed into propagating Bloch waves at Γ (0 eV) and X (0.3 eV).

The Wannier picture calls for the matrix element of the quantum well potential. For trial purposes we evaluated numerically (with the Gauss-Legendre integration technique) its matrix element using the WF's, the weakly localized WF's of the empty lattice

$$w(x - ma/p) = \left[\frac{p}{a}\right]^{1/2} \frac{\sin[(px/a - m)\pi]}{[(px/a - m)\pi]} \cdot$$

It is most enlightening to consider the diagonal terms plotted in Fig. 4 (with an arbitrary energy scale). One observes that these diagonal terms approximately follow the assumed square potential, even for such a narrow well. The energy difference (a few percent) is distributed in the nondiagonal terms and contributes somewhat to the matching. Using the complete matrix element, we found that sufficiently accurate results could be generated by directly reducing the matrix element to diagonal terms corresponding to the sampling of the assumed potential at the lattice site [see Eq. (9)].

We have developed an algorithm to solve the eigenvalue problem and have evaluated the locus of the resonant energy level of the square quantum well of depth 0.5 eV, as a function of the well width L. The result is plotted in Fig. 5 (open circles) and compared with the energy-level locus (solid curve) of the effective-mass approximation. It should be pointed out that in our picture the well width can only be varied by increments of a half-lattice parameter for the 100 direction.

We label the first, resonant state 1. For a wide potential well, both the WF and the continuum methods yield the same results, since the resonant level lies at low energy where the effective mass is quite accurate. For a narrower well, one observes a divergence of the two energy plots as the effective-mass approximation becomes inadequate at higher energy.

For a well smaller than five lattice parameters, the first resonant state occurs above 0.3 eV. This resonant state results, then, from a superposition of the central-valley Bloch wave and the upper-valley Bloch wave. Indeed, one observes the interference of the energy locus (labeled a) of
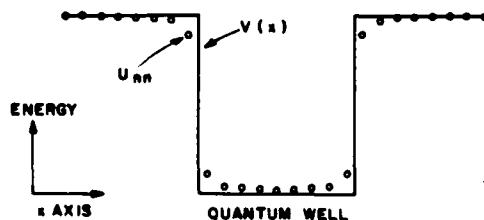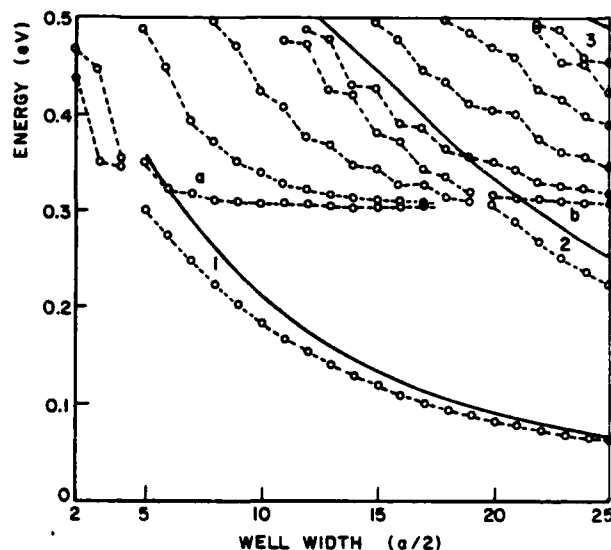

FIG. 5. Energy levels of a GaAs quantum well, as a function of the well width. The well depth is 0.5 eV.

the first resonant level of the upper valley with the energy locus 1 of the central valley. This destroys the smooth variation of these energy loci as they interact. The same phenomenon occurs also as the second and third resonant-level loci (denoted, respectively, 2 and 3) cross the X relative minimum (0.3 eV). A more thorough discussion of this interference effect has been recently reported by Chang and Ting.[24]

The phenomenon just described constitutes an example of what may be called a full band-structure effect which can be handled by the generalized Wannier picture. The algorithm developed can be used to study any type of variation of the band gap. As a second example, we consider the simple case of a superlattice made of square wells such as in the Kronig-Penney problem.[25] We assume a simple tight-binding band structure $E(k) = A(1 - \cos ka)$ with the effective mass at $k = 0$ selected to be $0.12m_0$. The well depth is 0.2 eV, the width and separation of the wells is chosen to be $10a$ so that the superlattice parameter is $20a$. This leads to two resonant levels in an individual well. In Fig. 6 we present the result for, successively, 1, 2, and 20 wells. The discrete band structure of the 20-well superlattice is plotted in Fig. 7 (open circles). This is to be compared to the band structure (solid curve) of the Kronig-Penney model in the effective-mass approximation.

FIG. 4. Diagonal matrix element of a quantum well $U(x)$, nine lattice parameters wide.
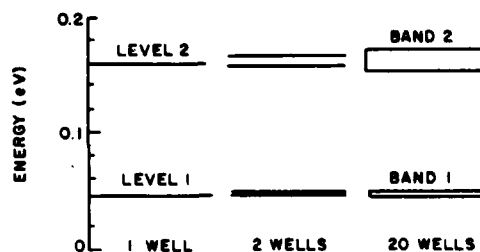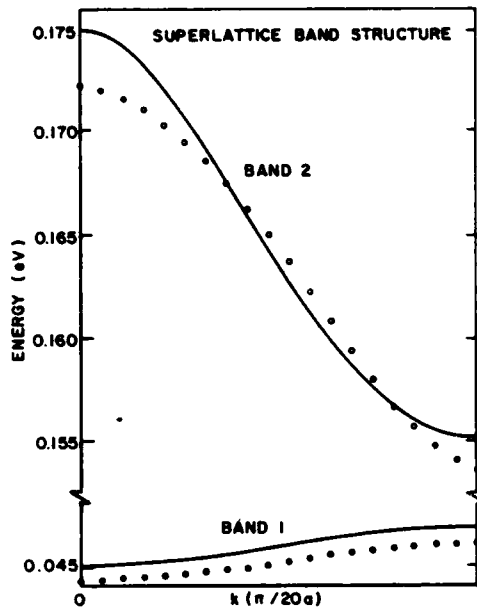

FIG. 6. Superlattice formation.

FIG. 7. Superlattice band structure (open circles: tight-binding superlattice of 20 quantum wells; solid curve: Kronig-Penney model).

The low-lying bands (band 1) have a similar shape but are separated by a shift of 1 meV. This small shift originates from the use of the approximate diagonal matrix element for the superlattice potential.

The upper bands (band 2), however, differ appreciably. Part of the difference is due to the deviation from parabolicity of the cosine band and results in a much higher conduction-band maximum for the effective-mass approximation. The remaining difference is essentially due to the finite character of the superlattice composed of only 20 wells.

More sophisticated structures can be studied with the algorithm developed, but this was not our purpose, as we intended to test the generalized Wannier picture using simple examples for which closed-form solutions are available.

IV. SPATIALLY VARYING BAND STRUCTURES

The Wannier picture developed above and its generalization so far do not apply to band structures varying with space. Let us point out right away that the idea of spatially varying band structures is an ill-defined concept, which can be made more rigorous within the framework of the generalized Wannier picture.

A one-dimensional approach will break down for the proper description of a spatially varying band structure, since the variation in the band structure occurs in the three-dimensional k space and therefore requires a three-dimensional matching of the Wannier envelope.

We shall, however, for simplicity partially retain the one-dimensional picture by assuming the spatially varying band structure to be given by

$$E(\mathbf{k},x)=E(k,x)+\frac{\hbar^2 k_\perp^2}{2m^*} ,$$

where m^* is a transverse effective mass which is not varying in space. Such a band structure does not correspond to any realizable interface but constitutes a convenient model. In this model we use the one-dimensional GWF formalism to solve for the eigenstates of this structure. A set of orthogonal GWF's noted $a(n,x)$ can be defined as in Sec. II. These GWF's can be exponentially localized at each lattice site n. For the case of an abrupt heterojunction, the GWF's $a(n,x)$ approach exponentially with n the WF's of semiconductors 1 and 2, for lattice sites far from the interface (at $n=0$). A few lattice sites away from the interface, inside semiconductor 1, a GWF closely resembles the WF of the unperturbed semiconductor 1; the orthogonality with the GWF's of semiconductor 2 across the interface essentially affects only the exponentially decaying tail of this GWF. Finally, one is again led to the generalized one-band formalism of Sec. II, with the GWF envelope given by the one-dimensional Wannier recurrence equation (7).

The derivation of the Hamiltonian matrix elements $H(n,m)$ is again critical to the analysis. We favor a direct evaluation of these elements, which remains to be devised. In its absence, alternative approaches can be conceived, and we shall demonstrate such an approach for a simple system.

First consider the trial Hamiltonian

$$H(n,m)=E(n-m,n)+U(n,m) ,$$

where $E(n-m,n)$ is the band-structure Fourier coefficient which is assumed to vary in space with the lattice site n. Such a Hamiltonian, which might be proposed for a smoothly spatially-varying band structure, is not correct as the Hamiltonian is no longer Hermitian:

$$H(n,m)\neq H^*(m,n) .$$

This arises as a consequence of using the intrinsically ill-defined concept of spatially dependent band structures. The GWF formalism is capable of accounting for the breakdown of the band structure. The Hermiticity is indeed compatible with

$$E(m-n,n)\neq E(n-m,n) ;$$

it follows that the related band structure at the lattice site n,

$$E(k,n)=\sum_l E(l,n)e^{ikla} ,$$

is now imaginary and therefore, as expected, has lost its usual physical meaning.

For an abrupt heterojunction, the use of GWF formalism is reduced to the derivation of matching rules. Indeed, away from the interface the Wannier picture of Sec. I holds and the only unknown terms are the interface Hamiltonian element $H(n,m)$.

Consider the tight-binding band structures given by

$$E_1(k,x)=A-A\cos(ka), \quad E_2(k,x)=B-B\cos(ka) ,$$

where the amplitudes A and B are, respectively, related to their effective mass by

$$A = \frac{\hbar^2}{m_1 a^2} \text{ and } B = \frac{\hbar^2}{m_2 a^2} \; .$$

For simplicity we evaluate the matrix element $H(n,m)$ using the unperturbed WF's on both sides of the junction. In the tight-binding approximation, the only remaining unknown is then the matrix element $H(i,i+1) = -C/2$, assuming the interface is located somewhere between the lattice site i and $i+1$. The resulting Hamiltonian is shown around the interface in Fig. 8 for $U(n,m)=0$.

The evaluation of C depends now on the particular matching theory upon which we choose to rely. There has been much published recently on the matching of wave functions across a heterojunction. The GWF picture proposes a general method which enables us to evaluate the wave function in heterostructures but calls for the knowledge of $H(n,m)$. In its absence we intend first to relate this method to other matching theories.

Popular techniques are the effective-mass matching (see Ref. 26 and the discussion by Kroemer and Qi-Gao Zhu,[27,28] matching developed from the $(k \cdot p)$ Kane model by Bastard,[29] and White, Margues, and Sham,[30,31] and from tight-binding arguments by White, Margues, and Sham[30] and Ando and Mori.[32] A review of the different methods is briefly given in White, Margues, and Sham.[30] We intend to give a more complete discussion of the matching problem in a forthcoming paper.

It follows from the work of Zhu and Kroemer[28] that the effective-mass matching is related for small energies to the geometrical average for the "ideal" heterostructure (type I, Ref. 28) considered here,

$$C = (AB)^{1/2} \; .$$

From Bastard's work,[29] we have C given by the average

$$C = (A+B)/2 \; .$$

Both expressions actually lead to the same results when the variation of effective mass is small across the heterojunction. In Fig. 9 we compare the effective-mass matching with the geometrical average matching for a quantum well. This quantum well is made of a layer of $Ga_{0.47}In_{0.53}As$ sandwiched between $Al_{0.48}In_{0.52}As$. The effective masses are, respectively, taken as 0.041 and $0.075 m_0$ for GaInAs and AlInAs. These effective masses

FIG. 9. Energy locus as a function of well width for $Ga_{0.47}In_{0.53}As/Al_{0.48}In_{0.5}As$ quantum well (open circles: results using Wannier algorithm with the geometrical average matching; solid curve: results using the effective mass matching). The well depth is 0.5 eV.

should be corrected for narrow wells, as the nonparabolicity is no longer negligible (see Welch, Wicks, and Eastman[33]). The discrete-energy locus is seen to agree with the continuous-energy locus based on the effective-mass formalism.

This result was established within the tight-binding approximation. A more refined scheme will extend the connection rules to include higher-order overlaps.

V. PERSPECTIVE

We have introduced a generalized one-dimensional Wannier picture. This formalism enables us to handle sharp variations in potential as long as the potential strength is sufficiently moderate for the concept of a generalized band to hold. The associated band-mixing effects are then lumped into a generalized one-band Hamiltonian matrix. In the absence of a knowledge of the GWF, one can often rely in practice on the direct sampling of the potential at each lattice site.

The generalized one-band picture applies directly to modulation-doped structures and can be used as a model of heterostructures by treating the band-gap variation as an effective potential. Another application not covered here and for which this model was in fact developed, concerned the study of devices such as the Zener superlattice oscillator, for which the periodicity in k space of the subband together with its spatial variation are fundamental to the device operation.[5] Finally, practical derivation of the energy levels and eigenfunctions can be performed for arbitrary potentials or heterostructure configurations using the same algorithm.

The one-dimensional generalized Wannier formalism can be used to model true heterostructures, although a rigorous treatment requires a three-dimensional GWF analysis. In the one-dimensional picture, the matching of the wave function across the interface is determined by the interface Hamiltonian matrix elements.

FIG. 8. Tight-binding Hamiltonian.

P. ROBLIN AND M. W. MULLER

The derivation of Wannier functions is in general a complex problem due to their orthogonality and the fact that they are not eigenfunctions of the Hamiltonian. The best procedure would be to evaluate the generalized Fourier coefficients of the generalized band structure directly, just as the band structure is evaluated directly in pseudopotential calculations using variational techniques.

An alternative approach is to derive the interface Hamiltonian matrix directly from the enforcement of physical constraints. Such an approach was undertaken by Zhu and Kroemer[28] and Ando and Mori[32] for maximized matching (ideal heterojunction) using current continuity. We shall report, in a forthcoming paper, on the extension of these matching theories to a higher energy range (non-effective-mass case) and for the inclusion of higher-order overlap (non-tight-binding cases) for both type I and type II semiconductors (see Ref. 28).

The concept of generalized bands described here is largely intuitive and has been used so far as such. The introduction of the generalized Wannier functions brings support to the concept. One interesting feature of the generalized Wannier picture is that it accounts consistently for the concept of spatially varying band structure. The generalized Wannier picture appears then as an intermediate method situated between the direct study at the lattice level [e.g., linear combination of atomic orbitals (LCAO) techniques] and the techniques based on the effective-mass approximation.

We believe that useful insights can be drawn from this ability of the GWF formalism to handle the concept of band structure, through the use of the band-structure Fourier coefficients together with their spatial dependence on the lattice sites. The band structure appears as a physical entity established in a few lattice parameters. We found that five to ten lattice sites were sufficient for a close representation of a band structure along $\langle 100 \rangle$. This is in qualitative agreement with the Wannier functions evaluated by Kane and Kane.[13] Energy bands calculated from these Wannier functions were accurate to 0.1 eV when the Wannier-function overlaps were evaluated to twelfth neighbors (459 individual bonds). The spatial establishment of a small effective mass requires a larger number of sites since a larger number of Wannier-function overlaps or band-structure Fourier coefficients is required to fit a small effective mass while accurately reproducing the remainder of the band structure.

ACKNOWLEDGMENTS

[1]N. Holonyak, Jr., R. M. Kolbas, R. D. Dupuis, and P. D. Dapkus, IEEE J. Quantum Electron. QE-16, 170 (1980).

[2]T. C. L. Sollner, W. D. Goodhue, P. E. Tannenwa, and C. D. Parker, Appl. Phys. Lett. 43, 588 (1983).

[3]D. A. B. Miller, D. S. Chemla, D. J. Eilenber, and P. W. Smith, Appl. Phys. Lett. 41, 679 (1982).

[4]L. Esaki and R. Tsu, IBM J. Res. Dev. Jan., p. 61 (1970).

[5]P. Roblin, Ph.D. thesis, Washington University, 1984.

[6]H. L. Stormer, J. Phys. Soc. Jpn. 49, 1013 (1980).

[7]N. T. Linh, M. Laviron, P. Delescluse, P. N. Tung, D. Delagebeaudeuf, F. Diamond, and J. Chevrier, in Proceedings of the 9th IEEE Cornell Biennial Conference, 1983 (unpublished).

[8]P. M. Solomon and Hadis Morkoç, IEEE Trans. Electron Devices ED-31, No. 8 (1984).

[9]J. Callaway, Quantum Theory of the Solid State B (Academic, New York, 1974).

[10]J. E. Carroll, Hot Electron Microwave Generators (American Elsevier, New York, 1970).

[11]J. M. Ziman, Principles of the Theory of Solids (Cambridge University Press, Cambridge, Mass., 1979).

[12]W. Kohn, Phys. Rev. B 7, 4388 (1972).

[13]E. O. Kane and A. B. Kane, Phys. Rev. B 17, 2691 (1978).

[14]J. Des Cloizeaux, Phys. Rev. 135, A698 (1964).

[15]G. H. Wannier, Rev. Mod. Phys. 34, 645 (1962).

[16]W. Kohn, Phys. Rev. 115, 809 (1959).

[17]J. Zak, Phys. Rev. B 20, 2228 (1979).

[18]P. Roblin and M. W. Muller, J. Phys. C 16, 4547 (1983).

[19]J. Zak, in Solid State Physics, edited by F. Seitz, D. Turnbull, and H. Ehrenreich (Academic, New York, 1972).

[20]J. Avron, L. Gunther, and J. Zak, Solid State Commun. 17, 189 (1975).

[21]W. Kohn and J. R. Onffroy, Phys. Rev. B 8, 2485 (1973).

[22]J. G. Gay and J. R. Smith, Phys. Rev. B 11, 4906 (1975).

[23]J. J. Rehr and W. Kohn, Phys. Rev. B 10, 448 (1974).

[24]Yia-Chung Chang and D. Z.-Y. Ting, J. Vac. Sci. Technol. B 1, 435 (1983).

[25]R. de L. Kronig and W. G. Penney, Proc. R. Soc. London 130, 499 (1930).

[26]R. A. Smith, Wave Mechanics of Crystalline Solids (Wiley, New York, 1961), Chap. 4.

[27]H. Kroemer and Qi-Gao Zhu, J. Vac. Sci. Technol. 21, 551 (1982).

[28]Qi-Gao Zhu and Herbert Kroemer, Phys. Rev. B 27, 3519 (1983).

[29]G. Bastard, Phys. Rev. B 24, 5693 (1981).

[30]S. R. White, G. E. Margues, and L. J. Sham, J. Vac. Sci. Technol. 21, 544 (1982).

[31]S. R. White and L. J. Sham, Phys. Rev. Lett. 47, 879 (1981).

[32]T. Ando and S. Mori, Surf. Sci. 113, 124 (1982).

[33]D. F. Welch, G. W. Wicks, and L. F. Eastman, J. Appl. Phys. 55, 3176 (1984).

10. LONG RANGE ORDERING

For a semiconductor alloy, $A_x B_{1-x} C$, regular solution
theory indicates that the excess enthalpy or heat of mixing
is given by

$$\Delta H_m = x(1-x)\Omega,$$

where Ω is an interaction parameter which contains the physics
of the mixing process. For positive values of Ω we expect
to have cation clustering above and phase separation below
a critical temperature,

$$T_c = \frac{\Omega}{k4\ln 2} \ .$$

For negative values of Ω we expect a tendency toward cation
ordering above and compound formation below T_c.

10.1 RECENT ALLOY FORMATION MODELS

There have recently been several calculations of Ω for
III-V alloys based on the idea that most or all of the heat
of mixing is due to bond distortion. Fedders and Muller [1]
calculate Ω under the assumption that it is due to the changes
in the bond lengths, a and b, of the binary compounds, AC and
BC, required to form a virtual crystal lattice. This gives

$$\Omega = \lambda \ (\frac{a-b}{a+b})^2 \ ,$$

where λ can be determined from the elastic properties of the
material. Mikkelsen and Boyce [2] have found from EXAFS

measurements, however, that the AC and BC bonds in alloys are within 20 percent of their values, a and b, in the binary compounds, which reduces λ by about 20.

To maintain essentially binary bond lengths, a and b, in a virtual crystal alloy the bond _angles_ must also be distorted so that the factor of 20 reduction above is an under estimate of λ. Mikkelson [3] has taken into account both bond _length_ and _angle_ distortions to obtain values of Ω in good agreement with experimental values of Ω from pseudo-binary phase diagrams. Although Muller [4] has shown that bond distortion should reduce disorder below that expected for a random cation distribution of A and B, all elastic models necessarily result in a positive heat of mixing since strain energy is positive definite.

Zunger _et al_. [5] have included charge transfer effects with bond distortion in their model of semiconductor alloy formation. They find that, although the negative excess energy from charge transfer is small in comparison to the positive excess heat of mixing from bond distortion, the chemical charge transfer provides a means of stabilizing long range order and compound formation. This is because ordered alloys or compounds can accomodate bond distortion with less strain energy than disordered alloys with large strain energy associated with random cation distribution.

As an example, for the alloy $In_{0.5}Ga_{0.5}P$ they obtain $\Omega = +0.11eV/atom$-pair which is the same as obtained by Mikkelsen. For the compound $InGaP_2$ Zunger et al. obtain an equivalent excess energy parameter $\Omega_E = -0.047eV/atom$-pair. On this basis we can qualitatively compare alloys with In and Ga cations to those with Al and Ga cations. That is, alloys with In and Ga cations are expected to have relatively large bond distortion (atomic size differences) and large charge transfer (electro-negativity differences) compared to alloys with Al and Ga cations. Thus, the small positive or zero heat of mixing in alloys with Al and Ga cations is proportionally offset by small negative or zero excess energy due to chemical interaction.

10.2 X-RAY MEASUREMENTS

As mentioned in our last annual report [6] we have obtained some evidence for long range ordering in $In_xGa_{1-x}P$ grown on GaAs by liquid phase epitaxy. This is indicated in Figure 1 where we show back-reflection Laue photographs for (a) a {211} Ga oriented GaAs substrate and (b) an $In_{0.49}Ga_{0.51}P$ lattice-matched epitaxial layer using a Cu target. In these measurements additional spots in the photograph for the epitaxial layer could easily be interpreted as evidence for long range order. What we see instead are enhanced intensity $0\bar{4}\bar{6}$ and $0\bar{6}\bar{4}$ spots. These enhanced intensity spots were also observed in about eight other $In_xGa_{1-x}P$ layers with x between 0.49 and 0.52, but were not observed in one $Al_{0.4}Ga_{0.6}As$ layer we measured. When Laue photographs for an $In_{0.49}Ga_{0.51}P$ layer were taken with a

(a)

(b)
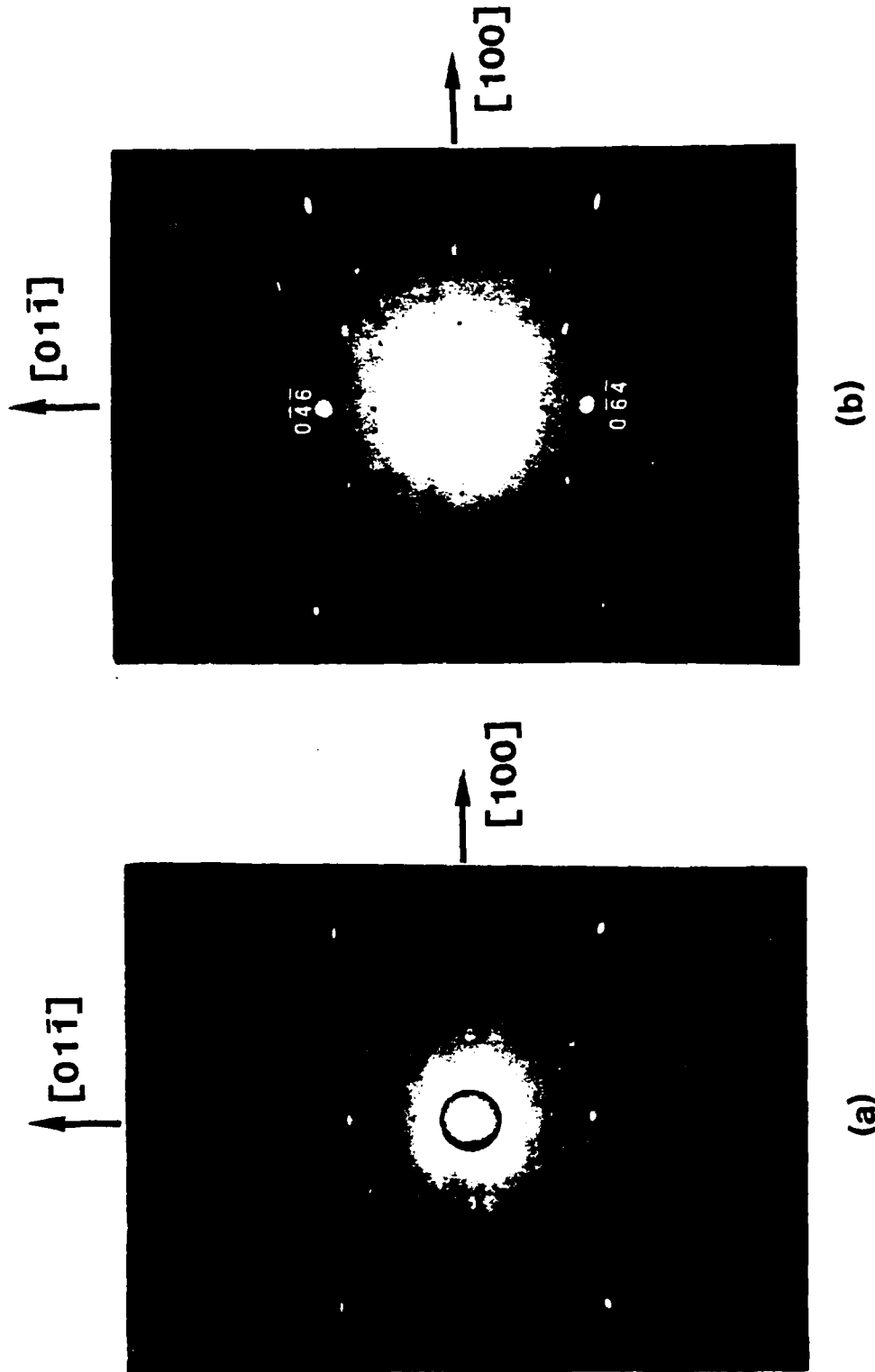
Figure 1 Back-reflection Laue photographs for (a) a {211}Ga orientated
GaAs substrate and (b) an $In_{0.49}Ga_{0.51}P$ lattice-matched
epitaxial layer. The primary X-ray beam from a Cu target
is in the [011] direction.

Mo target, the $0\bar{4}\bar{6}$ and $0\bar{6}\bar{4}$ spots were not enhanced but additional $\bar{2}\,\underline{\bar{10}}\,\underline{\bar{12}}$, $2\,\underline{\bar{10}}\,\underline{\bar{12}}$, $\bar{2}\,\underline{\bar{12}}\,\underline{\bar{10}}$, and $2\,\underline{\bar{12}}\,\underline{\bar{10}}$ were observed.

Table I. Reflections which satisfy the Bragg condition for characteristic Kα lines near the lattice constant of $In_{0.5}Ga_{0.5}P$.

Equivalent Cubic Reflection	Structure Factors			Characteristic Bragg Condition
	Sphalerite	Chalcopyrite	Layered	
032	0	0	$f_{In}-f_{Ga}$	2nd Order Cu Kα
064	$f_{In}+f_{Ga}-2f_{p}$	$f_{In}+f_{Ga}-2f_{p}$	$f_{In}+f_{Ga}-2f_{p}$	1st Order Cu Kα
165	0	0	$f_{In}-f_{Ga}$	2nd Order Mo Kα
$2\underline{12}\,10$	$f_{In}+f_{Ga}+2f_{p}$	$f_{In}+f_{Ga}+2f_{p}$	$f_{In}+f_{Ga}+2f_{p}$	1st Order Mo Kα
$2\underline{12}7$	0	$f_{In}-f_{Ga}$	0	1st Order Cu Kα
$4\underline{10}9$	0	$f_{In}-f_{Ga}$	0	1st Order Cu Kα

In Table I we compare the structure factors for several reflections in the sphalerite structure and two of the most likely ordered structures for $InGaP_2$, chalcopyrite (space group $I\bar{4}2d$) and primitive layered (space group $P\bar{4}2m$) structures. First, note that superlattice structure factors are small $(f_{In}-f_{Ga})$ and will be observed only when they satisfy the

Bragg condition, $2d_{nkl} \sin \theta = n \lambda$, for one of the high intensity characteristic x-ray lines. For example, the 2 12 7 and 4 10 9 (equivalent cubic notation) chalcopyrite reflections satisfy the Bragg condition in 1st order for Cu Kα ($\lambda = 1.5418$Å) lines near the lattice constant of GaAs (5.6532Å). Since we easily observe these reflections in our chalcopyrite ZnSnP$_2$ (5.6407Å) epitaxially grown on GaAs, we conclude that the In$_x$Ga$_{1-x}$P is not ordering in a chalcopyrite structure.

Second, notice that the 064 set of reflections are allowed in all three crystal structures and satisfy the Bragg condition in 1st order for Cu Kα. If the In$_x$Ga$_{1-x}$P has a layered structure, these 064 reflections could be enhanced by 032 reflections, which satisfy the Bragg condition in 2nd order for Cu Kα. In a similar manner the 2 12 10 reflections, which satisfy the Bragg condition in 1st order for Mo Kα ($\lambda = 0.7107$Å), could be enhanced by 165 reflections, which satisfy the Bragg condition in 2nd order for Mo Kα.

Using tabulated atomic scattering factors [7] we can calculate the intensity of the 064 Laue spots that would be expected with different materials and crystal structures. Taking into account 032, 064, 096, and 0 12 8 reflections, the following reflected intensity ratios are obtained.

$\dfrac{\text{InGaP}_2}{\text{In}_{0.5}\text{Ga}_{0.5}\text{P}}$	$\dfrac{\text{In}_{0.5}\text{Ga}_{0.5}\text{P}}{\text{GaAs}}$	$\dfrac{\text{InGaP}_2}{\text{GaAs}}$
3.5	60	220

Although this calculation neglects absorption and secondary extinction, it shows that the 064 enhancement shown in

Figure 1 could be simply due to the difference between

sphalerite $In_{0.5}Ga_{0.5}P$ and GaAs and not layered $InGaP_2$

and GaAs.

10.3 LAYERED STRUCTURE

Recently, Kuan, Kuech and co-workers[8] have reported

long-range order in $Al_xGa_{1-x}As$. They claim to see the most

pronounced evidence for ordering from $Al_{0.75}Ga_{0.25}As$ grown

on {110}GaAs at 700°C by organo-metallic vapor phase epitaxy.

Electron diffraction measurements, which are sensitive to

surface structure, were used to indicate the presence of

a layered crystal structure (the $P\bar{4}2m$ space group discussed

above) with c-axes orientations in the growth plane. No

significantly different physical properties, however, were

obtained for this material.

A fairly definitive x-ray experiment which would indicate

the presence of a layered crystal structure is shown schematic-

ally in Figure 2. The geometry of the experiment is the

same as that used to obtain the back-reflection Laue photographs

shown in Figure 1. The layered face centered cubic cation

sublattice with cations as open and closed circles and [001]

c-axes is shown as observed in the [$\bar{1}$00] direction. Figure 2 (a)

shows that for this c-axis orientation reflections from the

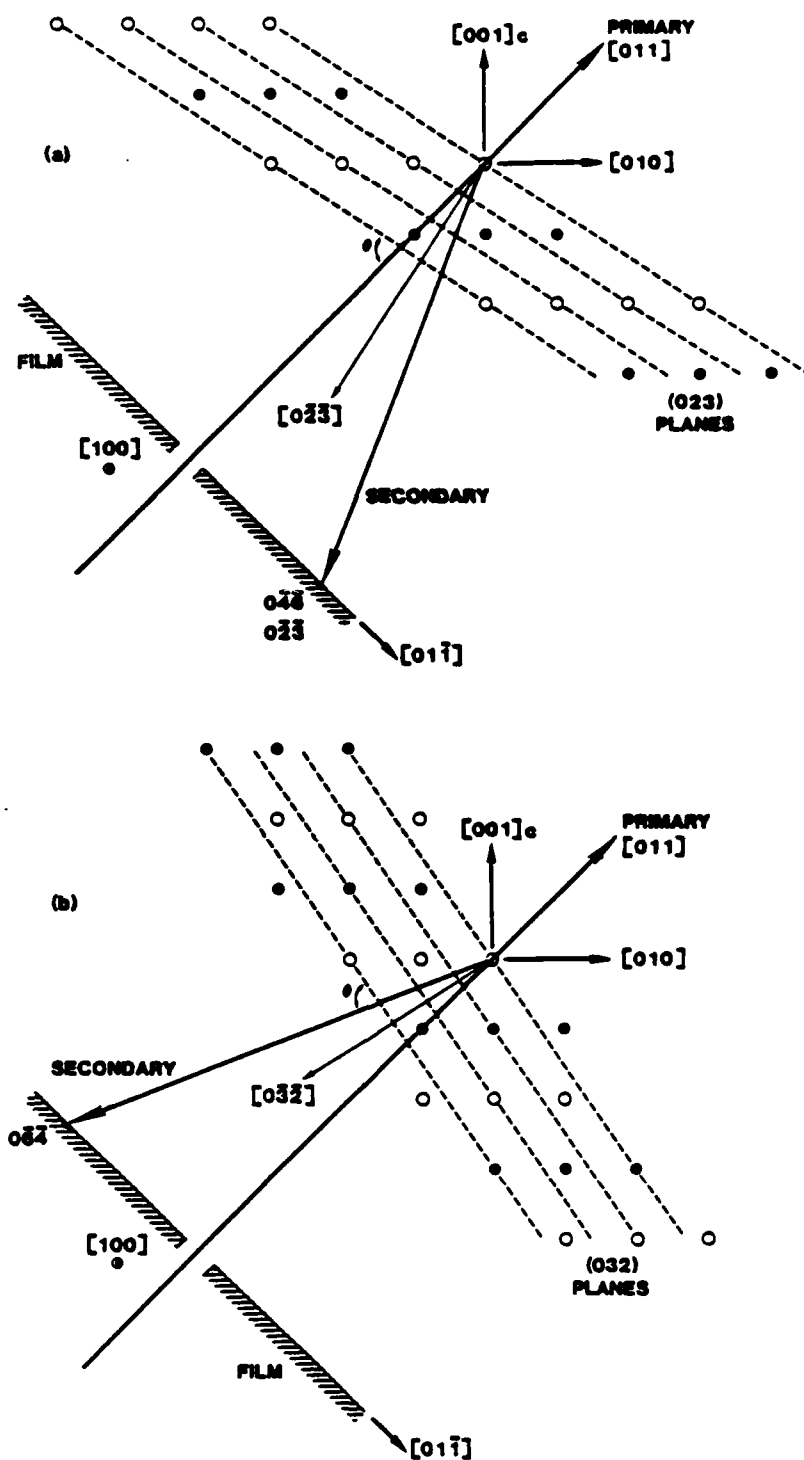(046) planes between the (023) planes do not cancel out (023)

Figure 2 Schematic of a back-reflection Laue measurement which would indicate the presence of a layered crystal structure. The orientation of the experiment is the same as that used to obtain the photographs in Figure 1.

reflections. Thus, both $0\bar{4}\bar{6}$ and $0\bar{2}\bar{3}$ superimpose on the bottom of the film. Figure 2 (b) shows, however, that for the same c-axis orientation reflections from the (064) planes cancel out reflections from the (032) planes. Thus, only $0\bar{6}\bar{4}$ is observed on the top of the film. A significant difference in intensity of these spots on the film (we calculate 3.5 for In and Ga cations), therefore, would indicate a layered structure with one c-axis.

If the c-axis in Figure 2 were in the [010] direction, one can see that the $0\bar{6}\bar{4}$ and $0\bar{3}\bar{2}$ at the top of the film would superimpose while the $0\bar{2}\bar{3}$ reflection would be cancelled by $0\bar{6}\bar{4}$ at the bottom. For the c-axis in the [100] direction both $0\bar{3}\bar{2}$ and $0\bar{2}\bar{3}$ reflections would be cancelled, since the layered structure looks like a sphalerite structure to an [011] x-ray beam orthogonal to the c-axis. The examination of a tetragonal structure with fixed primary x-ray beam orientation and three c-axis orientations is equivalent to the examination of a tetragonal structure with fixed c-axis orientation and three primary x-ray beam orientations. The latter, of course, is experimentally achievable and we summarize potential observations in Table II.

Table II   Summary of conclusions that can be obtained from Laue measurements with primary beam in three <110> directions.

Beam Directions	Enhanced 0 6 4 Spots		$P\bar{4}\bar{2}m$ c-axes
[011]	$0\,\bar{4}\,\bar{6}$	—	
[101]	—	$\bar{4}\,0\,\bar{6}$	[001]
[110]	—	—	
[011]	$0\,\bar{4}\,\bar{6}$	$0\,\bar{6}\,\bar{4}$	[001]
[101]	—	$\bar{4}\,0\,\bar{6}$	and
[110]	$\bar{4}\,\bar{6}\,0$	—	[010]
[011]	$0\,\bar{4}\,\bar{6}$	$0\,\bar{6}\,\bar{4}$	[001]
[101]	$\bar{6}\,0\,\bar{4}$	$\bar{4}\,0\,\bar{6}$	[010] and [100]
[110]	$\bar{6}\,\bar{4}\,0$	$4\,\bar{6}\,0$	

The salient feature of the experiments indicated in Table II is that, to determine the number of c-axes in a layered sample, x-ray measurements must be taken with the primary beam in at _least_ two of the <110> directions indicated. At the present time we have looked at our $In_xGa_{1-x}P$ samples with the primary beam in only one <110> direction. For these samples no asymmetry in 064 spot intensity has been observed which could not be attributed to slight misorientation of the primary beam.

10.4 CONCLUSIONS

From the discussion above we conclude that charge transfer effects in III-V alloys may provide a mechanism for stabilizing equilibrium long range order and compound formation. The resulting total negative excess energy involved, however, appears to be sufficiently small that low growth temperatures and kinetic effects, such as substrate orientation, may be critical factors. This appears to be the case for the recently reported ordering in $Al_xGa_{1-x}As$ and should also be true for alloys with larger atomic size and electronegativity differences. We are now in the process of constructing an OMVPE reactor to examine these effects.

10.5 REFERENCES

1. P.A. Fedders and M.W. Muller, J. Phys. Chem. Solids 45, 685 (1984).

2. J.C. Mikkelsen, Jr. and J.B. Boyce, Phys. Rev. Lett. 49, 1412 (1982).

3. J.C. Mikkelsen, Jr., J. Electrochem. Soc 132, 500 (1985).

4. M.W. Muller, Phys. Rev. B 30, 6196 (1984).

5. A. Zunger et al., Electronic Materials Conference, June 1985.

6. C.M. Wolfe et al., "Clustering and Ordering in III-V Alloys", Annual Scientific Report No. WU/SRL-59583A-3, 31 July 1984.

7. International Tables for X-Ray Crystallography, Vol. 3 (Kynoch Press, Birmingham, 1968).

8. T.S. Kuan et al., Phys. Rev. Lett. 54, 201 (1985); T.F. Kuech et al., Electronic Materials Conference, June 1985.

11. PERSONNEL

The personnel who worked on this grant were as follows:

Prof. C.M. Wolfe, Principal Investigator,

Prof. M.W. Muller, Faculty Associate,

Mr. Gary A. Davis, Research Assistant,

Ms. S. Julie Hsieh, Research Assistant,

Ms. Elizabeth A. Patten, Research Assistant,

Mr. Patrick Roblin, Research Assistant,

Mr. Keith A. Salzman, Research Assistant.

The students who completed requirements for advanced degrees on this grant were:

May 1983, Gary A. Davis, Doctor of Science, "Preparation and Properties of $Zn_xCd_{1-x}SnP_2$ Epitaxially Grown on InP and GaAs";

August 1984, Patrick Roblin, Doctor of Science, "Electron States in Submicron Semiconductor Heterostructures" (partial support);

August 1985, S. Julie Hsieh, Doctor of Science, "$In_{1-x}Ga_xP$-GaAs Heterojunctions";

August 1985, Elizabeth A. Patten, Doctor of Science, "Below Bandgap Emission and Absorption in Staggered Lineup Heterojunctions" ;

May 1986, Keith A. Salzman, Master of Science, "Free Carrier Faraday Rotation Measurements of Effective Mass".

12. PUBLICATIONS

1. G.A. Davis and C.M. Wolfe, "Liquid Phase Epitaxial Growth of $ZnSnP_2$ on GaAs", J. Electrochem. Soc. <u>130</u>, 1408 (1983).

2. G.A. Davis, M.W. Muller, and C.M. Wolfe, "Antiphase Domain Boundary Suppression in Chalcopyrite-on-Sphalerite Epitaxy", J. Crystal Growth <u>69</u>, 141 (1984).

3. P.A. Fedders and M.W. Muller, "Mixing Enthalpy and Composition Fluctuations in Ternary III-V Semiconductor Alloys", J. Phys. Chem. Solids <u>45</u>, 685 (1984).

4. M.W. Muller, "Composition Correlations in Ternary Semiconductor Alloys", Phys. Rev. <u>B 30</u>, 6196 (1984).

5. S. Julie Hsieh, Elizabeth A. Patten, and C.M. Wolfe, "Below Bandgap Photoresponse of $In_{1-x}Ga_xP$-GaAs Hetero-junctions", Appl. Phys. Letters <u>45</u>, 1125 (1984).

6. E.A. Patten, G.A. Davis, S.J. Hsieh, and C.M. Wolfe, "Below Bandgap Emission and Absorption in $ZnSnP_2$/GaAs Heterojunctions", IEEE Electron Device Letters <u>6</u>, 60 (1985).

7. P. Roblin and M.W. Muller, "Spatially Varying Band Structures", Phys. Rev. <u>B32</u>, 5222 (1985).

8. E.A. Patten, S.J. Hsieh, G.A. Davis, and C.M. Wolfe, "Below Bandgap Emission and Absorption in Staggered Lineup Heterojunctions", <u>Microelectronics--Photonics</u>, <u>Materials</u>, <u>Sensors</u> <u>and</u> <u>Technology</u>, <u>Vol</u>. <u>8</u> (SRI International, Menlo Park, Calif., 1986).

9. G.A. Davis, "Chalcopyrite-Sphalerite Heteroepitaxial Growth", <u>Proc</u>. <u>7th</u> <u>Intern</u>. <u>Conf</u>. <u>Ternary</u> <u>and</u> <u>Multinary</u> Compounds (Snowmass, Colo., Sept. 1986), to be published.

13. TALKS

1. G.A. Davis, "Preparation and Properties of $Zn_xCd_{1-x}SnP_2$ Epitaxially Grown on InP and GaAs", Seminar, M.I.T. Lincoln Laboratory, Lexington, Mass., 1 April 1983.

2. —————, IBM Research, Yorktown Heights, N.Y., 4 April 1983.

3. —————, General Motors Research Laboratory, Detroit, Mich., 8 April 1983.

4. —————, Varian Associates, Palo Alto, Calif., 11 April 1983.

5. M.W. Muller, "Mixing Enthalpy and Composition Fluctuations in Ternary III-V Semiconductor Alloys", Seminar, SRI International, Menlo Park, Calif., 20 December 1983.

6. S. Julie Hsieh, "$In_{1-x}Ga_xP$-GaAs Heterostructures", Seminar, Hewlett Packard, Palo Alto, Calif., 7 November 1984.

7. —————, Texas Instruments, Dallas, Tex., 17 December 1984.

8. —————, GTE Laboratories, Waltham, Mass., 20 December 1984.

9. —————, AT&T Bell Laboratories, Murray Hill, N.J., 14 February 1985.

10. —————, Universal Energy Systems, Dayton, Ohio, 5 March 1985.

11. —————, AT&T Bell Laboratories, Murray Hill, N.J., 19 March 1985.

12. —————, RCA Laboratories, Princeton, N.J.,
    20 March 1985.

13. Elizabeth A. Patten, "Below Bandgap Emission and
    Absorption in Staggered Lineup Heterojunctions",
    Seminar, AT&T Bell Laboratories, Murray Hill, N.J.,
    1 April 1985.

14. —————, Santa Barbara Research Center, Goleta,
    Calif., 9 April 1985.

15. —————, SRI International, Menlo Park, Calif.,
    12 April 1985.

16. —————, TRW, El Segundo, Calif., 29 April 1985.

17. —————, M.I.T. Lincoln Laboratory, Lexington, Mass.,
    6 May 1985.

18. Gary A. Davis, "Chalcopyrite-Sphalerite Heteroepitaxial
    Growth", 7th Intern. Conf. Ternary and Multinary Compounds,
    Snowmass, Colo., 10 September 1986.

END

6 – 81

DTIC